The Dissertation Committee for Andrea Nolting Certifies that this is the approved version of the following dissertation:

Syndepositional Deformation in Steep-Walled Carbonate Margins: Insights from Outcrop and Numerical Modeling of Carbonate Platforms in the Recent and Ancient Rock Record

Committee:

Charles Kerans, Supervisor

Christopher K. Zahm, Co-Supervisor

Maria A. Nikolinakou

Peter B. Flemings

David Mohrig

Syndepositional Deformation in Steep-Walled Carbonate Margins: Insights from Outcrop and Numerical Modeling of Carbonate Platforms in the Recent and Ancient Rock Record

By

Andrea Nolting

Dissertation

Presented to the Faculty of the Graduate School of

The University of Texas at Austin

in Partial Fulfillment

of the Requirements

for the Degree of

Doctor of Philosophy

The University of Texas at Austin

December 2017

Dedication

I dedicate this work to my parents, family, and friends who have supported me endlessly.

Acknowledgements

I owe a great deal to Dr. Chris Zahm and Dr. Charles Kerans, for not only the past four and half years, but for the opportunities and experiences that I've had that continue to impact my life daily. I would like to express my gratitude to Dr. Chris Zahm for his constant support, guidance, and the will to push me to be the best version of myself and the best scientist possible, without which this work would not have been possible. The opportunity to be taught by and learn from Charlie Kerans will forever be an invaluable experience and a highlight of my geological career. I could never have imagined how rewarding, thrilling, and fulfilling my graduate degree would be, and it would not have been so without Charlie and Chris. Thank you to Laura Zahm for always being my cheerleader and advocate, to Dr. Maria Nikolinakou for her support and help with the ever frustrating ELFEN, and to Dr. John Humphrey for opening my eyes to the wonderful world of carbonate geology.

Funding for this work was provided by the Jackson School of Geosciences, The University of Texas at Austin, The Houston Geological Society, and American Association of Petroleum Geologists. This work benefited greatly from contributions and discussions with Yaser Alzayer, Ben Smith, Kelly Hattori, and Jeffrey Sitgreaves. Many thanks to all the friends I have had the opportunity to make in graduate school and in Austin.

Lastly, my family is thanked for their endless support and guidance. For their enduring belief that I am capable. They are the real MVP, for without them none of this would have ever been possible.

Syndepositional Deformation in Steep-Walled Carbonate Margins: Insights from Outcrop and Numerical Modeling of Carbonate Platforms in the Recent and Ancient Rock Record

Andrea Nolting, Ph.D.

The University of Texas at Austin, 2017

Supervisor: Charles Kerans

Co-Supervisor: Christopher K. Zahm

Syndepositional deformation is common in steep-walled carbonate platforms and is typically manifested as large, open-mode fractures and normal faults. Despite the recognition of syndepositional features and their importance in steep-walled carbonate platform systems worldwide, the controls behind the development and the distribution of early-formed deformation are still poorly understood. There remains a gap in knowledge with regards to the relationships between mechanical properties of carbonate rocks and facies type, age and early diagenesis, which hinders our ability to systematically test and evaluate potentials controls on the development of early deformation. This work investigates (1) how facies type, depositional setting, diagenetic alteration, and age affect rock strength in Pleistocene carbonate rocks; (2) how carbonate platform geometry impacts the development of early deformation; and (3) the control that progradation to aggradation (P/A) ratio and carbonate rock property heterogeneities has on the development of syndepositional deformation. This research utilizes a combination of outcrop-based work

and numerical modeling of steep-walled carbonate platforms to aid in identifying and evaluating the controls on the development of early-formed deformation.

Mechanical rock properties tied to key facies, depositional setting, age, and diagenetic alteration were characterized from field measurements and laboratory analysis on samples collected from the Island of West Caicos on the Turks and Caicos platform,. Results suggest that rock strength in unburied Pleistocene carbonate rocks is controlled by cement percentage and, to a lesser extent, facies type, where reef facies are stronger than grain dominated facies. Increases in cementation tied to subaerial exposure and calichification is strongly tied to increases in unconfined compressive strength (UCS). Our observations on West Caicos are best explained by periods of long repeated subaerial exposure (and ensuing cementation from early meteoric diagenesis) and brief marine inundation consistent with the climatic conditions of the Pleistocene Epoch, when high-frequency, high-amplitude sea-level oscillations occurred.

The observations and rock properties collected on West Caicos were used to populate the material database within the numerical models, allowing for realistic simulation of syndepositional deformation. Numerical models were constructed using ELFEN®, a finite element modeling program that allows for the development of discrete fracture and fault development. Our numerical modeling results suggest that platform geometry, specifically the presence of a high-relief vertical reef wall, and changes in P/A ratio are primarily controls on the development of early-formed deformation. To a lesser extent, facies partitioning and juxtaposition control the intensity, distribution and propagation of deformation. The development of syndepositional deformation in steep walled carbonate platforms is largely a byproduct of the lack of a confining stress in the seaward direction. This leads to the development of a tensile stress state that is prone to failure by open-mode fractures and faults. These deformation features form under the sole

application of gravity, in the absence of differential compaction of basinal sediments or external perturbations (e.g. regional tectonics, active faults, etc.), highlighting the syndepositional origin of deformation. Results demonstrate that carbonate platforms that have a vertical to near vertical reef wall and steep angle slopes are routinely modified by syndepositional deformation. These parameters are thus primary controls on platform architecture, stratal geometries through time, and development of preferred failure and fluid flow pathways.

Table of Contents

List of Tables

List of Figures

Chapter 1: Introduction

Syndepositional deformation is a common phenomenon in steep-walled carbonate platforms such as those found in the Devonian of Western Australia (Playford et al., 1984; George et al., 1995; Frost and Kerans, 2009, 2010), the Carboniferous of Kazakhstan (Carpenter et al., 2006; Collins et al., 2006; Narr et al., 2008), the Permian of West Texas and New Mexico (King, 1948; Hunt and Fitchen, 1999; Kerans and Tinker, 1999; Hunt et al., 2003; Koša and Hunt, 2005; Rush and Kerans, 2010; Hunt et al., 2012), and the Pleistocene of British West Indies (Wanless and Dravis, 1989; Guidry et al., 2007; Kerans et al., 2016). The occurrence, distribution, and fault and fracture characteristics related to syndepositional deformation have been documented (Frost and Kerans, 2009, 2010). Despite the large body of evidence emphasizing the importance of syndepositional features to steep-walled carbonate platforms, little work has been done to pinpoint the exact drivers and their contribution to the development of early deformation. Additionally, there is very little published material on the mechanical properties of young, unburied carbonates rock tied to facies, age, and depositional setting. This dissertation addresses these gaps in knowledge by evaluating and testing the mechanisms responsible for the development of syndepositional deformation.

In an effort to address the gaps in understanding the mechanisms behind the development of early-formed deformation, a combination of outcrop-based work and numerical models was used. The compilation of rock properties comprises both field measurements via Schmidt hammer and laboratory testing of collected samples from the Pleistocene Island of West Caicos B.W.I. Field measurements and sample locations were chosen based upon known, established facies types, stratigraphic relationships, and age dates. The Schmidt hammer was used to collect unconfined compressive strength (UCS)

measurements to capture the variability in rock strength related to facies, age, depositional environment, and early diagenetic overprinting. Schmidt hammer measurements were compared against laboratory measured UCS via triaxial compression test for collected samples. All measurements were tied to the island's stratigraphy to identify how facies type, age, depositional environments and diagenetic alteration affect the mechanical properties of carbonate rocks. Rock properties were collected and used from this locality because it represents a young, unburied carbonate platform system that lacks significant diagenetic overprinting. The rock properties collected were then used to populate the material database in numerical models that were constructed to evaluate the mechanisms behind early deformation.

Numerical models were used to investigate the impact that (1) platform geometry, (2) progradation to aggradation (P/A) ratio, and (3) rock property heterogeneity has on the development of syndepositional deformation. 2D finite-element numerical models were constructed in a software called ELFEN®, using both continuum and discontinuum analysis methods. Discontinuum analysis allows for the realistic simulation of deformation via the development of discrete fractures and faults, dissipation of stress following failure, and tracking deformation throughout the model duration. An inelastic Mohr-Coulomb with a Rankine rotating crack modification constitutive law was used because it allows for the simulation of brittle tensile failure, i.e. open-mode fracturing and faulting. Each model was set up to simulate conditions under gravity, where the gravitational load is applied gradually over a specified number of time steps. All models had the same boundary conditions (e.g. pore pressure distribution, length of the model runs, number of time step, etc.) to isolate the effects of the different model scenarios upon deformation. This combined approach utilizes first order principles which allows for the isolation of

individual variables and the ability to directly determine the impact each variable has on the development of syndepositional deformation.

This work represents one of the first studies to identify primary and secondary controls on the development of syndepositional deformation in steep-walled carbonate systems using a numerical modeling approach where discrete fractures and faults can develop. Results from numerical modeling demonstrate that carbonate platform geometry and P/A ratio are primary controls on the development of syndepositional deformation. To a lesser extent, variations in and the juxtaposition of rock properties tied to different facies control the intensity, distribution and propagation of deformation in carbonate platform systems. Much of the previous work characterizing and investigating the manifestation of syndepositional deformation has speculated that the differential compaction of mud-rich, basinal sediments is the primary mechanism of syndepositional deformation (Hunt et al., 1995; Hunt et al., 1996; Saller, 1996; Hunt and Fitchen, 1999; Longley, 1999; Hunt et al., 2002; Koša and Hunt, 2005; Rush and Kerans, 2010). However, this work suggests otherwise. Modeling results suggest that carbonate platforms that are characterized by high relief, vertical reef walls are predisposed to gravitational failure under a tensile stress state from the lack of lateral confining stress. The lack of a lithostatic confining stress in the basinward direction promotes the development of a tensile stress state, where volumes of rock are susceptible to mobilization, fracturing and faulting. These deformation features develop under the sole application of a gravitational load, highlighting their syndepositional nature. This work demonstrates that syndepositional deformation can and likely does form in the absence of differential compaction, suggesting that the compaction of mud-rich basinal sediments is not necessary for syndepositional deformation to develop in steep-walled carbonate platform systems.

This study and its findings has important implications for the recognition and characterization of syndepositional deformation in the subsurface. Syndepositional fractures and faults have been previously identified as being important features in hydrocarbon reservoirs (Carpenter et al., 2006; Narr et al., 2008), where they commonly serve as fluid flow conduits, not only for hydrocarbons, but also for early and late diagenetic fluid flow (Frost and Kerans, 2010; Budd et al., 2013). These features have the ability to impact well performance and can cause reservoir heterogeneity (Carpenter et al., 2006; Jones and Xiao, 2006; Narr et al., 2008; Ronchi et al., 2010; Frost et al., 2012). Despite the clear importance of syndepositional fractures to hydrocarbon reservoirs, it is often overlooked because it is difficult to distinguish syndepositional deformation from other deformation features in the subsurface (Frost et al., 2012). This work provides a newfound appreciation on what controls the development and intensity of early deformation in carbonate platform settings, where it most commonly occurs, and an understanding into the stress conditions that leads to its development.

This research also has significant implications for future work in studying steep-walled carbonate shelf margin systems. Model results illustrate that zones characterized by a lack of lateral confining stress can develop a tensile stress state that can then result in brittle, tensile failure, which is a critical element of steep-walled carbonate platform systems. Syndepositional deformation has the ability to alter depositional dips, transport debris and spalled blocks down slope, alter platform architecture, stratal geometries, and facies thickness and distribution. Thus, syndepositional deformation must be considered when studying shelf margin systems and carrying out detailed sequence stratigraphic interpretations.

In this dissertation, all three chapters are written as self-contained journal style papers. Chapter two details how cementation tied to early diagenesis affects the spatial and

temporal evolution of mechanical rock properties from the Pleistocene. Chapter three examines how differences in platform geometry control the location and distribution of syndepositional fractures. Chapter four investigates how variable P/A ratio and rock property heterogeneity of steep-walled carbonate platforms affect the development of syndepositional deformation features. Finally, chapter five provides the key findings and conclusions of this dissertation.

Chapter 2: Early-Formed Rock Strength Heterogeneity in Pleistocene Carbonates: The Significance of Cementation

INTRODUCTION

A firm grasp on the evolution of mechanical properties of steep-rimmed carbonate platforms is as essential to understanding the structural evolution and subsequent failure of carbonate platform as is understanding carbonate platform genesis, stratigraphic architecture, and reef growth patterns. The evolution of mechanical rock properties of steep-rimmed carbonate margins is typically attributed to early lithification via early marine cementation (Ginsburg, 1957; James et al., 1976; Land and Moore, 1977; Grammer et al., 1993a; Grammer et al., 1993b; Grammer et al., 1999). While early marine cementation has been commonly documented it is not the only process that leads to the evolution of mechanical rock properties in carbonates (Fig. 2.1). The effect of burial and mechanical compaction on porosity has also been well documented (e.g. Schmoker and Halley, 1982; Anselmetti and Eberli, 1993; Goldhammer, 1997; Incze, 1998; Anselmetti and Eberli, 1999; Eberli et al., 2003).

Numerous studies have recognized the relationship between porosity, unconfined compressive strength (UCS), and predominant mineralogy, grain type, and size (Kowalski, 1966; Hugman and Friedman, 1979; Hatzor and Palchik, 1997; Palchik, 1999; Palchik and Hatzor, 2004). However, these studies lack specific information about facies type, depositional setting, diagenetic alteration, and age. This gap in knowledge hinders our

ability to evaluate the factors that affect the evolution of carbonate rock properties. This study aims to fill that gap by examining the impact that age, facies, and cementation from early meteoric digenesis has on mechanical rock properties of carbonates.

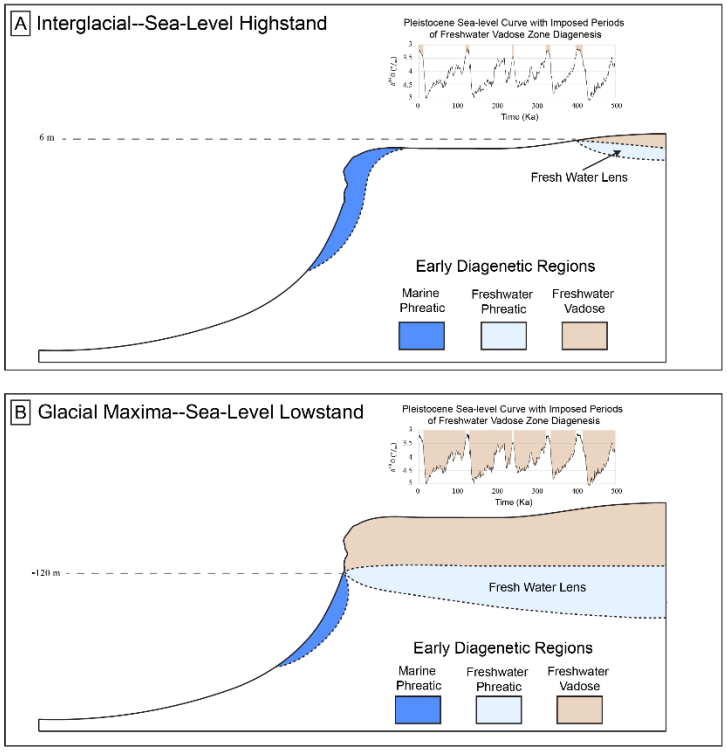

Figure 2.1. Schematic diagram illustrating a steep-walled carbonate platform with likely development of early-formed fractures and different early diagenetic regions tied to A) sea-level highstands and B) sea-level lowstands.

Pleistocene carbonates of the Bahamian Archipelago are a type example of the integration of early-formed and highly variable meteoric dissolution and cementation processes (Matthews, 1968; Gavish and Friedman, 1969; Land, 1970; Steinen and Matthews, 1973; Matthews, 1974; Steinen, 1974; Harrison, 1975; Walls et al., 1975; Harrison, 1977; Harrison and Steinen, 1978; Reeckman and Gill, 1981; Beach, 1982; James

and Choquette, 1984; Pierson and Shinn, 1985; Humphrey and Kimbell, 1990; Beach, 1995; Dravis, 1996; Budd, 2002). Subaerially exposed carbonates of the Pleistocene island of West Caicos offer a natural laboratory that can be used to document the early evolution of rock strength as a function of facies, cementation from early diagenesis, and age. This study couples field measurements of unconfined compressive strength (UCS) with laboratory testing of four collected samples to characterize mechanical and physical properties of the recognized Pleistocene units on the island. The combination of field-measured UCS and laboratory analyses allows us to interrogate the controls on the spatial and temporal changes in rock properties within strata that have undergone less than 10 m of burial. The controls investigated include facies type (predominant grain type and composition), porosity, and early meteoric diagenetic features such as crystalline cements, secondary pores, and micritized rock (caliche). Here we show that early meteoric diagenesis is a first order control on mechanical rock properties, and that subaerial exposure from moderate- to high-amplitude eustatic variations can lead to the development of drastic changes in rock strength through time.

GEOLOGIC BACKGROUND

The Caicos platform is located in the southeastern portion of the Bahama Archipelago, roughly 850 km southeast of Florida and 150 km north of Hispaniola (Fig. 2.2A). The Caicos platform comprises Holocene- and Pleistocene-aged deposits, with islands rimming the northwest, north, and northeast sides of the platform (Fig. 2.2B). The island of West Caicos is located on the most western (leeward) edge of the Caicos platform

and experiences trade winds from the east as well as open ocean swell from the west. The island is just over 9 km long and 3 km wide at its widest section, with a maximum elevation of 18 m above sea-level. West Caicos is characterized by a semiarid climate, receiving an annual rainfall of 500–700 mm/yr. Much of the rainfall occurs between September and December, such that West Caicos alternates between periods of net precipitation and evaporation (Sealey, 2006). Pleistocene/Holocene strata of West Caicos represent a wide variety of depositional environments and their associated facies assemblages—from fringing reefs to oolitic eolian dunes to evaporite salinas (Waltz, 1988; Wanless and Dravis, 1989; Simo et al., 2008; Kerans et al., 2016)—make it an ideal location to test the control that facies type imparts on rock strength.

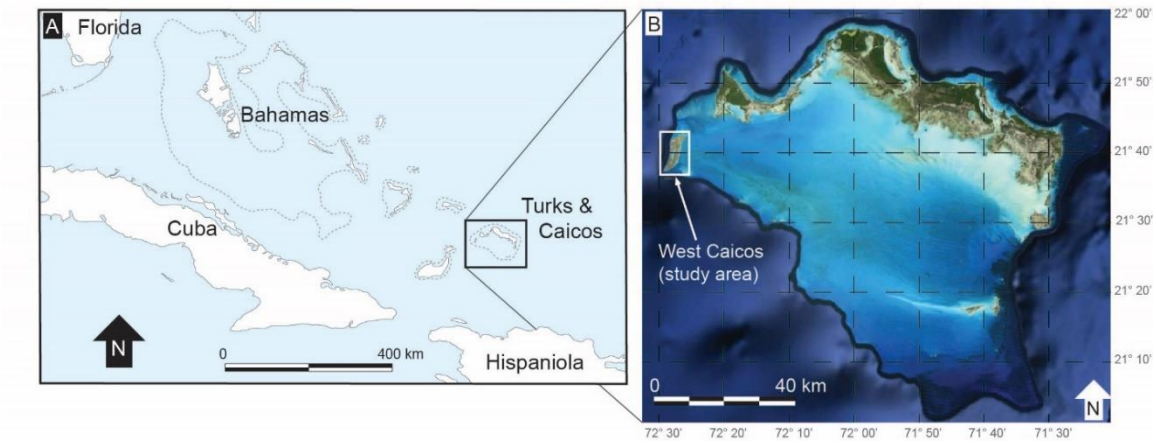

Figure 2.2. (A) Large location map of Caribbean, with Turks and Caicos platform highlighted. (B) Satellite image of Turks and Caicos platform. West Caicos Island (study area) is located on leeward side of platform.

The strata of West Caicos also record a complex eustatic signal through the middle to upper Pleistocene, including four major glacial–interglacial sea-level fluctuations. The composite sea-level curve illustrates that marine isotope stages (MIS) 5 and 9/11 resulted

in higher relative mean sea-level (RMS) compared to present-day (Waelbroeck et al., 2002). Higher RMS promoted deposition and possible preservation of sediments. During times when the RMS curve was lower than present-day levels, West Caicos experienced subaerial exposure, weathering/erosion, and meteoric diagenesis.

Detailed published stratigraphy, sedimentology, and geochronology of West Caicos Island provide the geologic foundation for this work (Fig. 2.3A & B) (Lloyd et al., 1987; Wanless and Dravis, 1989; Iannello et al., 2006; Simo et al., 2008; Kerans et al., 2016). Most recently, detailed high resolution mapping by Kerans et al. (2016) identified a portion of the southern tip of West Caicos as MIS 9/11–aged (340 ≥ 440 Ka) deposits. This work followed that of Simo et al. (2008), who constrained the prominent north–south trending dune (closest to Lake Catherine) ridge as MIS 7 (219 Ka), and the second dune (west of the Great Salina) as early MIS 5e (136 Ka) (Fig. 2.3A). Outcrops exposed along the entire western coast of the island are dated as MIS 5e deposits (120–130 Ka) (Wanless and Dravis, 1989; Simo et al., 2008) (Fig. 2.3A), while the oldest of the Holocene dune ridges on the east side of the island is dated at 3450 ybp, decreasing in age eastward toward the platform interior. The beach dates at 790 ybp (Fig. 2.3A) (Lloyd et al., 1987). A geologic map tying stratigraphic units to MIS events was constructed using previously established ages (Fig. 2.3A) and the high-resolution mapping conducted by Kerans et al (2016).

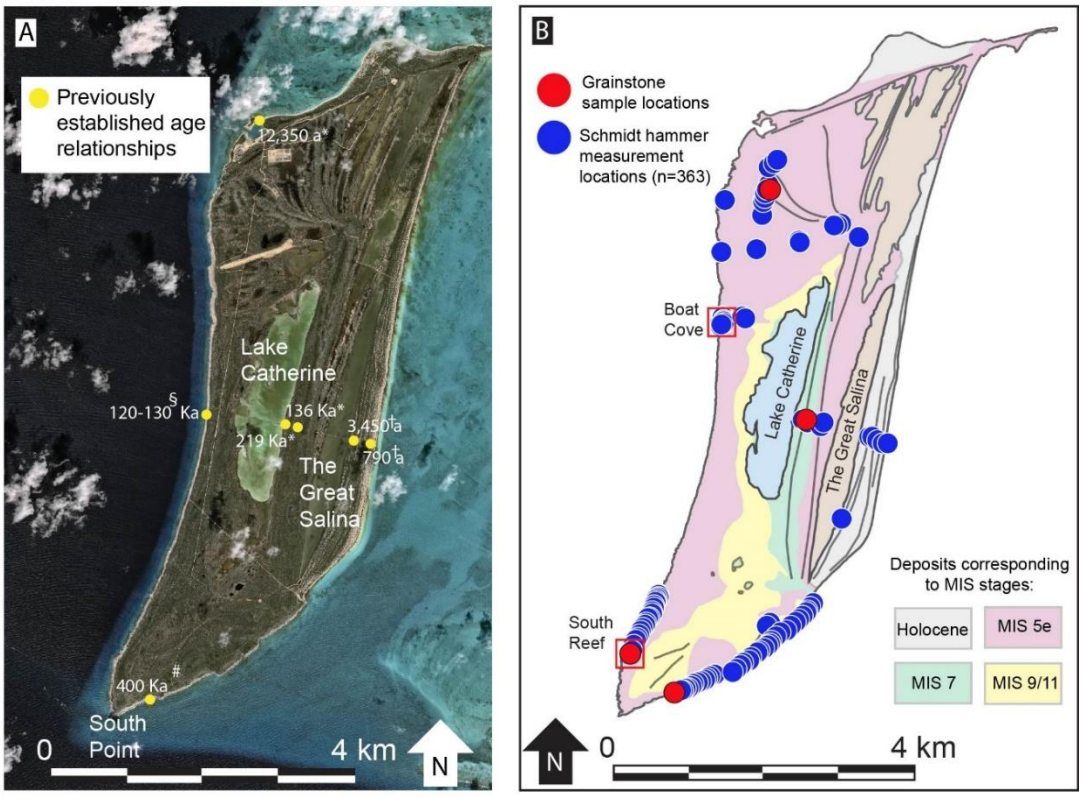

Figure 2.3. (A) QuickBird satellite image of West Caicos Island with key locations and previously published age dates. The southern tip of the Island is dated at 400 Ka (# Kerans et al., 2016). The westernmost dune on the interior of the island is age dated at 219 Ka while the dune closest to the Great Salina is age dated at 136 Ka (* Simo et al., 2008).The west coast of West Caicos is dated at 120-130 Ka (§ Wanless and Dravis, 1989). The most recent (Holocene) dune closest to the Caicos platform interior range from 3,450 a to 790 a († Lloyd et al., 1987). (B) Simplified map of West Caicos with sample locations (red dots), and field Schmidt hammer measurements (blue dots) and the distribution of deposits corresponding to each MIS stage (from Kerans et al., 2016).

Following compilation of the map, caliche crusts and other evidence of sea-level lowstands were superimposed on the strata as they are preserved today. Including this additional data is of critical importance because most diagenesis of carbonate platforms occurs during periods of low sea-level or exposure. The mineralogically unstable nature of

carbonate rocks often makes them susceptible to early diagenetic alteration from marine and meteoric fluids (James and Choquette, 1984). The Boat Cove locale on West Caicos has been previously studied by Jones et al (2008) to evaluate the paragenetic sequences associated with the various grainstone facies present. The workers showed that blocky calcite cement, which is indicative of a meteoric phreatic environment, is the dominant diagenetic byproduct present. Needle fiber and isopachous rim cements, representative of vadose and marine environments respectively, are also present but to a lesser extent.

Caliche crusts, which commonly develop in response to subaerial exposure caused by sea- level lows (Matthews, 1968, 1974; Harrison, 1977; Harrison and Steinen, 1978; Esteban and Klappa, 1983), are common across West Caicos. The caliche fabric is a reflection of near-surface diagenetic processes, where crusts commonly form at the sediment-air-water interface by evaporation and microbial processes that precipitate micrite and drive recrystallization (James, 1972; Jones, 1988; Wright, 1994; Zhou and Chafetz, 2009; Alonso-Zarza and Wright, 2010). The distribution and thickness of caliche can be highly variable, dependent upon the humidity of the climate, the source of calcium carbonate, and the porosity and permeability of the host rock (Matthews, 1968; Gavish and Friedman, 1969; Land, 1970; Steinen and Matthews, 1973; Reeves, 1976; Reeckman and Gill, 1981; Esteban and Klappa, 1983; James and Choquette, 1984; Pierson and Shinn, 1985; Wright, 1994; Alonso-Zarza and Wright, 2010). Because caliche crusts form under specific arid to semi-arid climatic conditions, most commonly during subaerial exposure, they can be valuable indicators of past sea-level changes and paleoclimates (James, 1972;

Reeves, 1976; Esteban and Klappa, 1983; James and Choquette, 1984; Zhou and Chafetz, 2009; Li and Jones, 2014).

Caliche crusts have been previously documented across the island of West Caicos (Rossinsky and Wanless, 1992). Many of the crusts on West Caicos form as distinct layers, with heavily micritized host rock above and relatively unaltered host rock below. The caliche crusts are found at various depths and separate the three stratigraphic packages present on the island, corresponding to the sea-level lowstands following the MIS 5e, 7, and 9/11 events (Rossinsky and Wanless, 1992). The crusts are easy to recognize in the field due to their red to reddish-brown appearance, a color thought to come from the red (likely iron-rich) soils that accumulate in low-lying areas across the island (Rossinsky and Wanless, 1992).

On West Caicos, caliche surfaces are most commonly found on top of eolianite and foreshore deposits (Fig. 2.4A); they often exhibit bulbous and/or laminated to non-laminated massive growth habits (Fig. 2.4B). Caliche-surface thickness—ranging from 5.0 mm to over 15 cm, with an average between 1.0 and 3.0 cm—varies greatly across short distances and often exhibits a laminated habit containing nodules of host rock (Fig. 2.4C). In cross section, caliche surfaces most often exhibit two distinct habits. The first is a clearly defined surface, with unaltered, intact carbonate grainstone below and altered host rock above (Fig. 2.4D). The second is a more diffuse surface that forms thin stringers through the lightly altered host rock. The stringers anastomose within the host rock and are often several millimeters in thickness. Both caliche morphologies are common and often occur near one another. In map view, the two different caliche morphologies cannot be

differentiated; however, thin section analysis reveals the complexity of this diagenetic byproduct. In thin section, caliche crust is dominated by micrite with intact host rock below (Fig. 2.4E). Pores and outlines of grains can often be seen within the calichified region. While it has been previously documented that the weathering of carbonate rocks affects UCS (e.g. Tuğrul and Zarif, 2000; Tuğrul, 2004), little work has pinpointed the exact impact the development of caliche crusts has on rock strength, despite the clear heterogeneity developed around and within them.

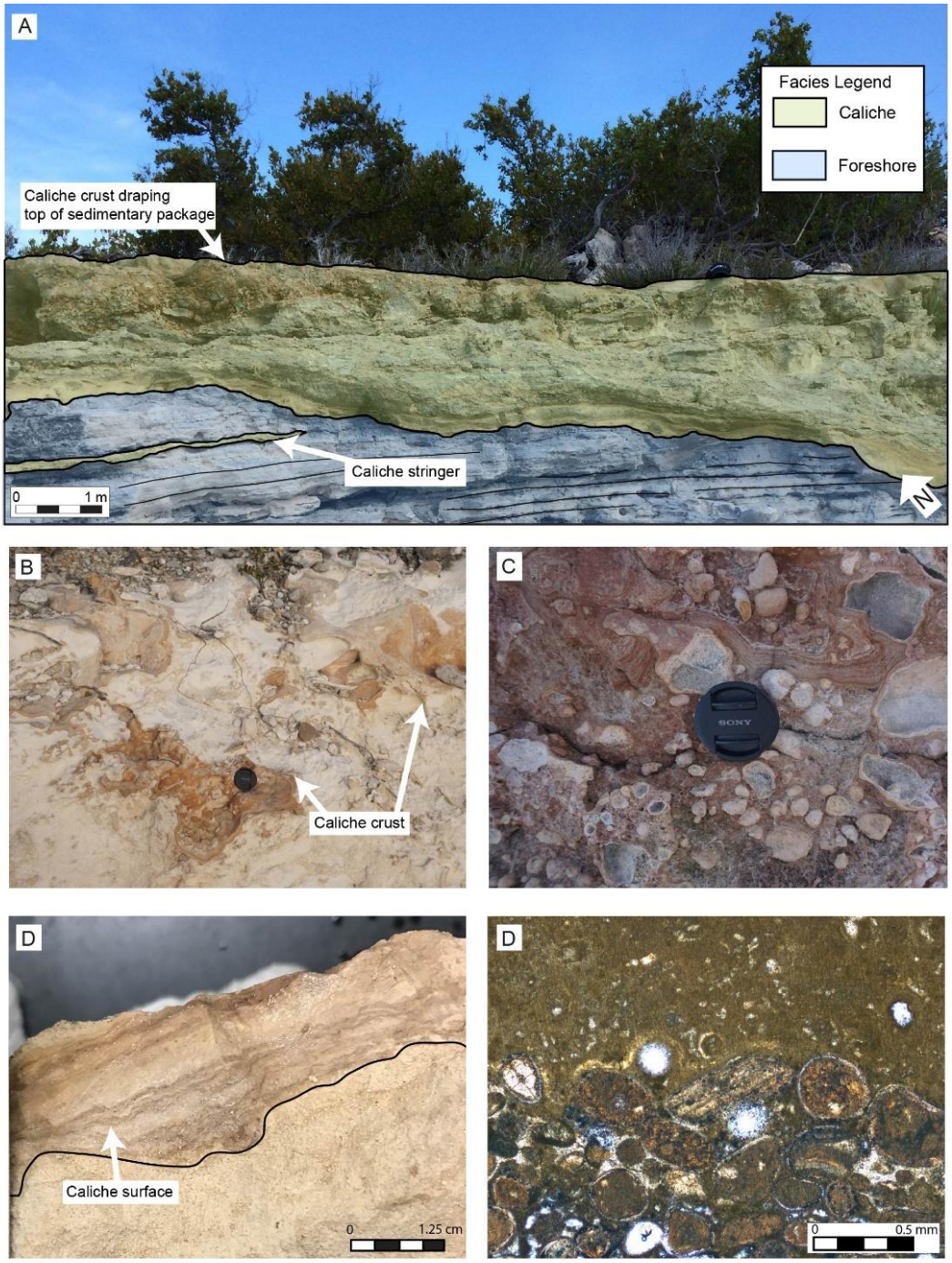
A
Facies Legend
Caliche
Foreshore
Caliche crust draping
top of sedimentary package
Caliche stringer
0
1 m
N
B
Caliche crust
C
D
Caliche surface
0
1.25 cm
D
0
0.5 mm

Figure 2.4.

Figure 2.4. Field, hand-sample, and thin section photographs of caliche crusts occurring on West Caicos. (A) Field photograph of caliche horizon(s) on west coast of West Caicos. Photograph illustrates two caliche horizons. Uppermost horizon drapes MIS 5e sedimentary package; second horizon anastomoses through middle of sedimentary packages, cutting across multiple facies. (B) Field photograph of caliche horizon on top of MIS 5e deposits. Horizon is well defined, with unaltered sediments below. Caliche horizons are well-cemented layers often red to reddish-brown in appearance. (C) Field photograph of caliche horizon in MIS 5e deposit. Photo highlights irregular nature of caliche horizon, which often drapes underlying sediments and contains nodules. (D) Photograph of hand sample collected on West Caicos from within caliche horizon, illustrating clearly defined laminations of crust above relatively unaltered host rock. (E) Photomicrograph of a caliche horizon, illustrating irregular nature and of the horizon. Micritized host rock above caliche surface and intact host rock below.

In addition to calichification, locally abundant opening-mode fractures have been documented along the western coastline of West Caicos (Wanless and Dravis, 1989; Guidry et al., 2007). They occur within foreshore and upper shoreface strata that run parallel to the shelf margin (which is characterized as a steep-rimmed margin) and are often vertical to subvertical in dip (Wanless and Dravis, 1989; Guidry et al., 2007). These fractures compose a complex network, often forming *en echelon* ladder structures (Zahm, 2015). Guidry et al. (2007) noted that fracture networks of the Caicos platform developed early in its history prior to mineral stabilization, often during subaerial exposure, forming fluid conduits for diagenetic alteration. The exact origin of the fractures present on West Caicos is unknown; though the Bahama Archipelago has been tectonically active since the Miocene (Mullins et al., 1992; Dolan et al., 1998), there is little evidence on West Caicos to suggest a tectonic origin for fracturing despite the island's close proximity to the active tectonic margin.

METHODOLOGY

This study utilizes two primary avenues for characterization of rock strength: field measurements and laboratory testing of collected samples. Field measurements and sample locations were chosen based upon known established facies types, stratigraphic relationships, and age dates. A Schmidt hammer was used to gather UCS measurements in the field to capture the variability in carbonate rock strength. The Schmidt hammer is a quick, nondestructive, reliable tool that provides instant feedback about rock strength. It uses a spring-loaded piston, which, when pressed to the rock surface, releases a plunger.

The height of the rebounded piston is a measure of the hardness (Aydin and Basu, 2005), which can be reliably empirically related to UCS (Sachpazis, 1990; Chang et al., 2006). The ASTM D5873-14 standard test method was used for all Schmidt hammer measurements (ASTM, 2014). On West Caicos, 363 field Schmidt hammer measurements were taken at two locations to capture the diversity in facies type; measurements were tied to depositional and diagenetic facies type and relative age to characterize their mechanical behavior (Fig. 2.3B). Of the two locations, Boat Cove is predominantly composed of grainstone facies (FS, USF, and BRC facies described below), while reef facies dominate the South Reef location. Reef and subtidal facies were exclusively measured for rock strength using the Schmidt hammer and were not otherwise sampled for laboratory analysis due to their friable nature and unsuitability for transport.

Four samples were collected from localities where age (MIS event), stratigraphic relationship, and facies type had been previously established. A calichified MIS 5e grainstone sample was taken to compare its petrophysical properties with its unaltered counterpart, and to document the variability in cementation. The other three samples represent each MIS event (5e, 7, and 9/11), and were collected from grainstone facies across the island to determine possible temporal effects on rock strength within a similar facies type. The three unaltered grainstone samples were cored into multiple 1-inch diameter by 2-inch-long plugs, each of which underwent laboratory measurements of UCS via uniaxial compressive tests to provide a more rigorous cross-check of the field-measured UCS values. By performing a uniaxial compressive test on multiple plugs from a single sample, we constrain the UCS for a given sample more rigorously and simultaneously

capture variability in rock strength. Tests were performed on the plugs using a CGCS RTR-100 rapid triaxial rock-testing system to determine laboratory-derived UCS values, though testing was limited to grainstone facies because they are well-lithified and remained consolidated throughout the slabbing and coring procedure.

In all uniaxial tests, confining pressure was absent while a load was applied incrementally in the axial direction until failure occurred (Jaeger et al., 2007). Failure marks the yield point, or UCS, of the sample. The International Society for Rock Mechanics (ISRM) standard test method was used for all uniaxial tests (Bieniawski and Bernede, 1979b, a). Additionally, thin sections were made for each of the four samples collected. A total of 16 end trims from the four collected samples were taken to document the petrophysical variability within each sample at a centimeter scale. Plugs from each sample were sent to Weatherford Laboratories for porosity and permeability testing.

RESULTS

Facies Descriptions and Thin Section Analysis

Reef (R). Various types of reef deposits are found across the island; however, for the purposes of this work, they have been combined into one representative unit. Reef facies are characterized by *in situ* branching corals (*Acropora palmata* and lesser *Acropora cervicornis*), head corals (*Diploria sp*. and *Montastrea sp.*), finger corals (*Porites*), and coral fragments/debris typically contained within a grain-rich matrix (Fig. 2.5A). The grain-rich fill in and around the reef is a grainstone composed of ooids, red algae fragments, peloids and skeletal fragments. The reef crest, where a pavement-like surface has

developed, is formed by encrusting red algae, *Goniolithon.* Thickness of the exposed reef section varies between 0.75-1.25 meters.

Coral conglomerate (CC). CC is composed of rounded coral fragments/debris, conch shells, and minor amounts of *Goniolithon*. Pieces range in size from 5.0 cm to 30 cm, and average bed thickness ranges from 0.25 to 1.0 meters. On the southwest portion of the island (Fig. 2.5B), CC exhibits multiple outcrop expressions, from continuous beds beneath foreshore deposits to massive discontinuous deposits scattered within topographic lows. CC has a fine-grained, ooid-skeletal-rich grainstone to grain dominated packstone matrix.

Burrowed upper shoreface (B). Burrowed upper shoreface is characterized by a burrowed composite-grain/ooid-skeletal-grain-dominated packstone. This facies contains abundant ichnofacies, including *Ophiomorpha* and rare *Diplocraterion* burrows. Trough cross-bedding is present within this facies but has been heavily reworked by bioturbation (Fig. 2.5C). Thickness of the burrowed upper shoreface ranges from 0.25-0.5 meters

Upper shoreface (USF). USF is composed of skeletal fragments, composite grains, peloids, and ooids and is characterized as a skeletal grapestone ooid grainstone (Fig. 2.5D). Individual grains range from 0.25 to 0.75 mm. USF is trough cross-stratified in cross section, with individual trough sets ranging in size from 0.1 to 0.5 m, with a total thickness of 0.5-0.75 meters. Troughs have a south-southwest paleoflow orientation, indicating a south paleocurrent direction. USF often exhibits differential cementation within individual laminae of cross-bed sets.

Beach rock conglomerate (BRC). BRC is often found along the island's west coast in discontinuous pockets within USF deposits, ranging in thickness from 0.5- 1.0 meters. BRC is composed of rounded to subrounded boulders of foreshore deposits. Boulders range in size from 0.2 to 1 m in size (Fig. 2.5E). Coral conglomerate is distinguished from the beach rock conglomerate by the presence and high concentration of coral fragments and conch shells within a grain-rich matrix. The beach rock conglomerate is composed of foreshore boulders and lacks the presence of coral/conch fragments.

Foreshore (FS). FS is a fine- to medium-grained grapestone-ooid to ooid grainstone. Ooids display concentric laminations and are most commonly 0.15–0.3 mm in diameter. FS deposits display fine to coarse laminations that often exhibit differential cementation (Fig. 2.5F), along with common parting lineations and keystone vugs. FS deposits exhibit low-angle (3°–5°) seaward-dipping beds and often have shingled bedding geometries. FS deposits, which occur extensively on the west coast of the island, are 0.5-0.75 m thick and are often capped or draped by the development of a caliche crust.

Eolianite (E). Eolianite is predominately composed of ooids (0.2–0.7 mm in size), minor skeletal fragments, grapestones, and intraclasts. Dunes on West Caicos range in size but can be up to 5.0 m in thickness. Individual dune bedding planes, which dip up to 20 degrees, often display differential cementation. (Fig. 2.5G). This facies is associated with a high concentration of blocky calcite in and around individual grains, and lesser meniscus and isopachous rimming cements. Eolianite dunes are differentiated from foreshore deposits by the lack of keystone vugs (fenestrae). Eolianite deposits, common across West Caicos, are very often capped by a caliche surface.

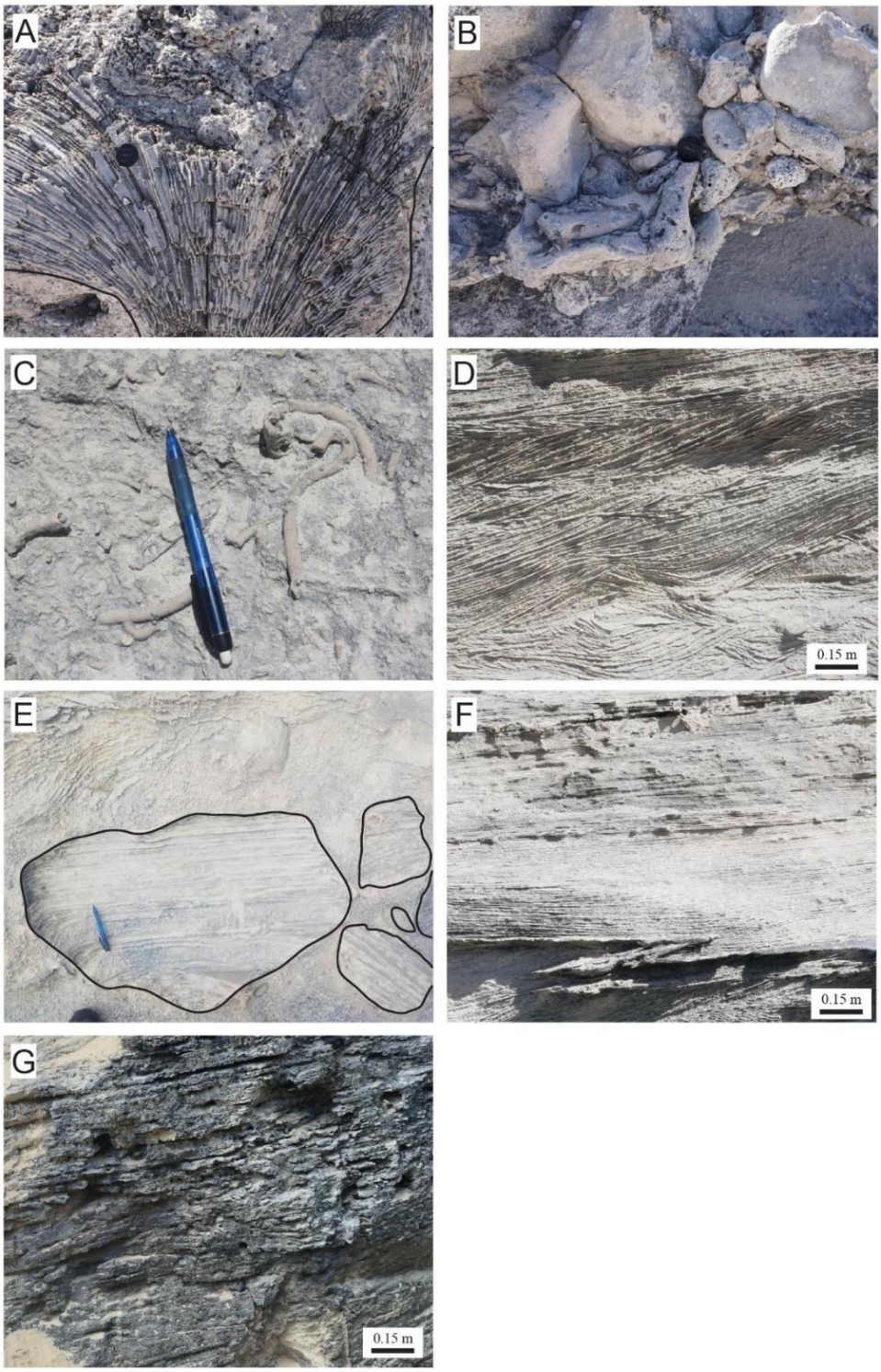

Figure 2.5

Figure 2.5. Field photographs of various facies described and identified to correlate with field UCS measurements. (A) Reef facies is often composed of large brain and hemisphere corals, along with *Acropora palmata* and *Acropora cervicornis*, within a grain-rich matrix. (B) Coral conglomerate facies is composed of coral and conch fragments and occasionally minor foreshore boulders within a grain-rich matrix. (C) Burrowed upper shoreface facies is predominately composed of skeletal fragments, peloids, and ooids. Bioturbation is indicative of this facies. (D) Upper shoreface facies is composed of skeletal fragments, peloids, and a high concentrations of ooids. Trough cross-bedding is common throughout. (E) Beach rock conglomerate is characterized by blocks of foreshore beach rock contained within homogenized (highly burrowed) upper shoreface sands. (F) Foreshore facies is composed of predominately peloid, skeletal fragments and ooids with low-angle seaward-dipping beds. (G) Eolianite facies, characterized by low-angle beds, is predominately composed of ooids.

Thin section analysis of each facies (Figs. 2.6 and 2.7) reveals a trend where grain type, porosity, cement type, and cement percentages change with age. The sample associated with MIS 9/11 (Fig. 2.6B) is predominantly composed of ooids with high concentrations of oomoldic porosity caused by the dissolution of ooids and blocky calcite cement filling interstitial pore space. Younger rocks show a greater grain diversity, more interparticle pore space, and less cement (Fig. 2.6C and D). Cement type also changes with age. The sample associated with MIS 5e contains blocky calcite cement similar to that of the sample from MIS 9/11; however, the former also has early cements (meniscus and rimming) that are not present in the older (MIS 9/11) sample.

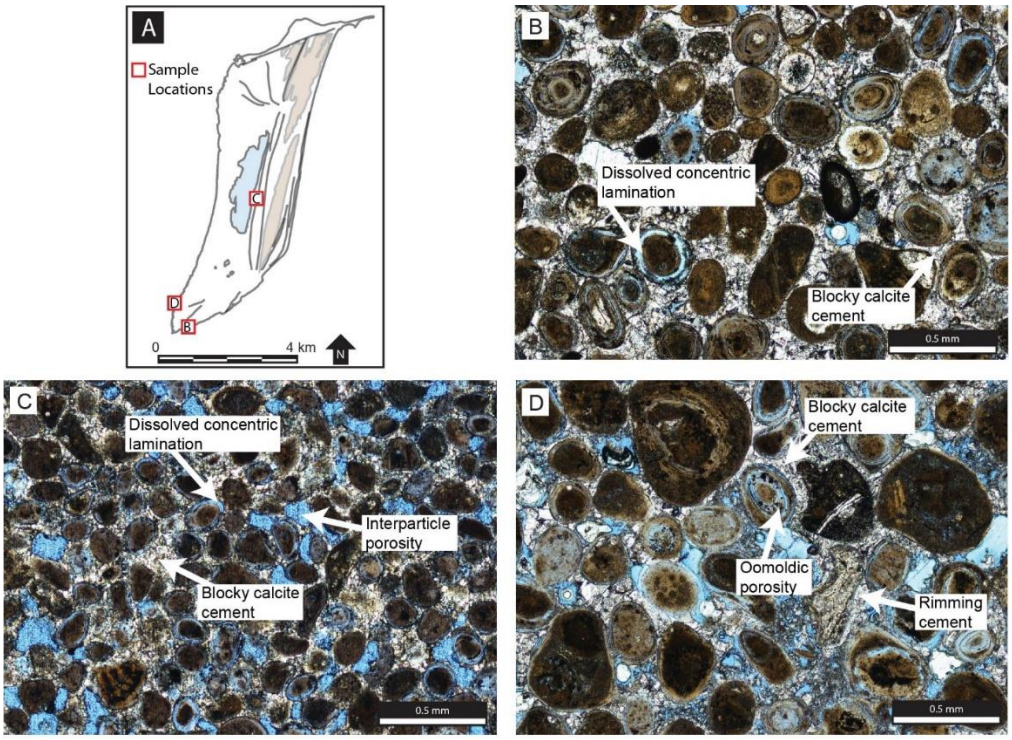

Figure 2.6. Thin-section photomicrographs of samples from West Caicos. (A) Simple outline drawing of West Caicos with sample locations highlighted. (B) Sample of MIS 9/11 grainstone. Sample is composed of ooids, with minor amounts of interparticle porosity. Sample contains a high percentage of blocky calcite cement and exhibits dissolution of concentric laminations of individual ooids. (C) Grainstone sample from MIS 7, contains a wider diversity of grain types, with ooids, peloids, skeletal fragments, and grapestones. Sample has interparticle porosity and contains a high concentration of blocky calcite, with minor dissolution of ooid laminations. (D) MIS 5E grainstone sample exhibits higher porosity than MIS 7 and MIS 9/11 grainstone samples. Sample is predominately composed of skeletal fragments, intraclasts, grapestones, and ooids and has minor amounts of oomoldic porosity present. Photomicrograph illustrates the presence of blocky calcite cement, suggestive of meteoric diagenesis.

Thin section observations on various caliche crusts reveal that their features vary greatly from sample to sample. The contact of caliche crust with host rock ranges from (1) a clearly defined surface where host rock is highly altered by the precipitation of micrite

with unaltered grainstone below (Fig. 2.7B), to (2) a diffuse zone containing evidence of the original depositional fabric with individual grains intact within the caliche crust but encompassed within a fine-grained matrix of micrite (Fig. 2.7C). In some portions of caliche alteration halo, the extensive alteration leaves little to no evidence of original depositional fabric or original porosity (Fig. 2.7D).

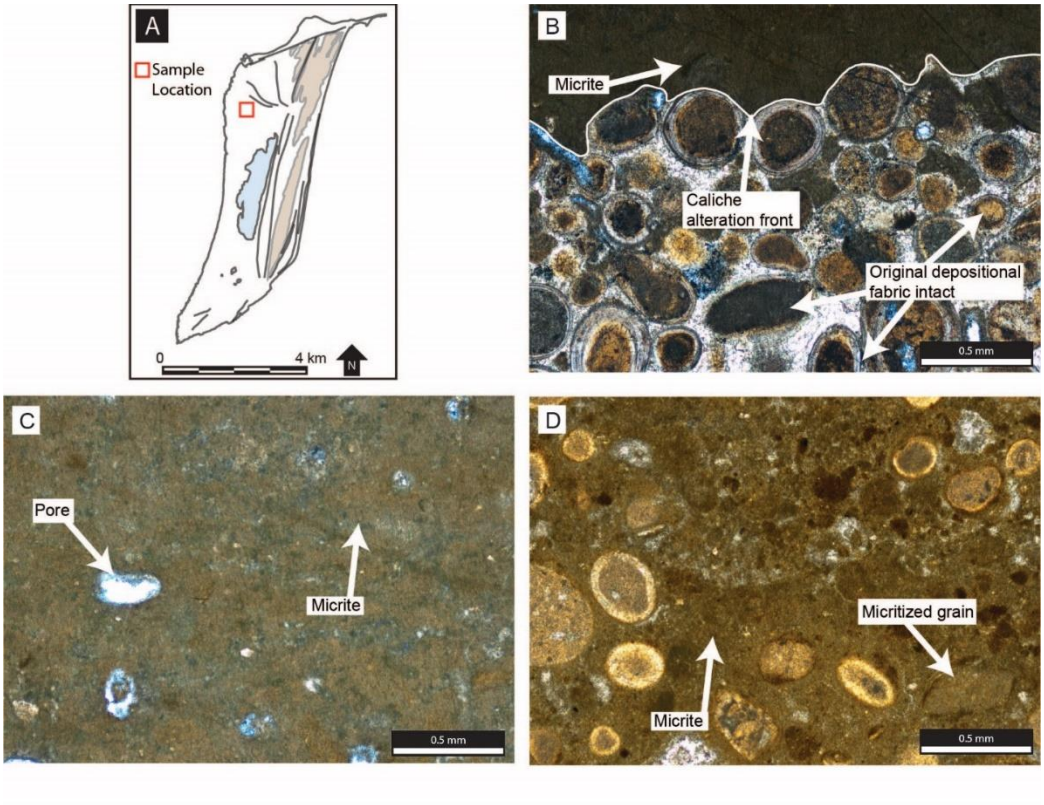

Figure 2.7. Photomicrographs of caliche sample. (A) Simple outline drawing of West Caicos with sample location highlighted. (B) Photomicrograph from caliche surface that has developed in MIS 5e grainstone. Photomicrograph clearly illustrates distinctive caliche horizon, where altered host rock lies above and relatively unaltered host rock lies below. (C) Photomicrograph taken within altered host rock of caliche horizon within MIS 5e grainstone. Thin section highlights high concentration of very fine grained micrite precipitated. (D) Thin section made from caliche surface that has developed within MIS 5e foreshore deposits on west coast of West Caicos. Photomicrograph illustrates variability in alteration of host rock, where evidence of original depositional fabric and grain type is present.

Rock Strength

Outcrop UCS Data.---UCS variability is observed both across facies and through time. Changes in UCS by grainstone facies type are best highlighted at the Boat Cove location (Fig. 2.8). Schmidt hammer measurements were performed at the same spot, multiple times to ensure reproducibility and reliability of measurements. Overall, all grainstone facies (FS, USF, and BRC) exhibit low-UCS values (median of 8 MPa), while the caliche crust draping the FS deposits displays a fourfold increase in UCS values (median of 34 MPa). This illustrates that early meteoric diagenesis of grainstone facies by the development of a caliche crust (precipitation of micrite) has the ability to greatly increase UCS values. Recorded UCS values for the Boat Cove location also highlight the lateral variability within a grainstone facies, where unaltered foreshore deposits (UCS = 9 MPa) are juxtaposed against a caliche crust (UCS = 36 MPa). The oblique cross section through Boat Cove (Fig. 2.9) illustrates changes in UCS with depth. UCS is highest stratigraphically within the FS caliche and decreases downward away from the caliche surface. Burrowed upper shoreface and upper shoreface facies exhibit the lowest UCS values. The Boat Cove exhibits a similar trend when the measured section is tied to point counted cement percentages for the various facies. Cementation is greatest at the caliche surface and decreases in the facies underlying the exposure surface. A thorough evaluation of the diagenetic paragenetic sequences has been previously carried out for Boat Cove out by Jones et al. (2008) and therefore is not included in this study.

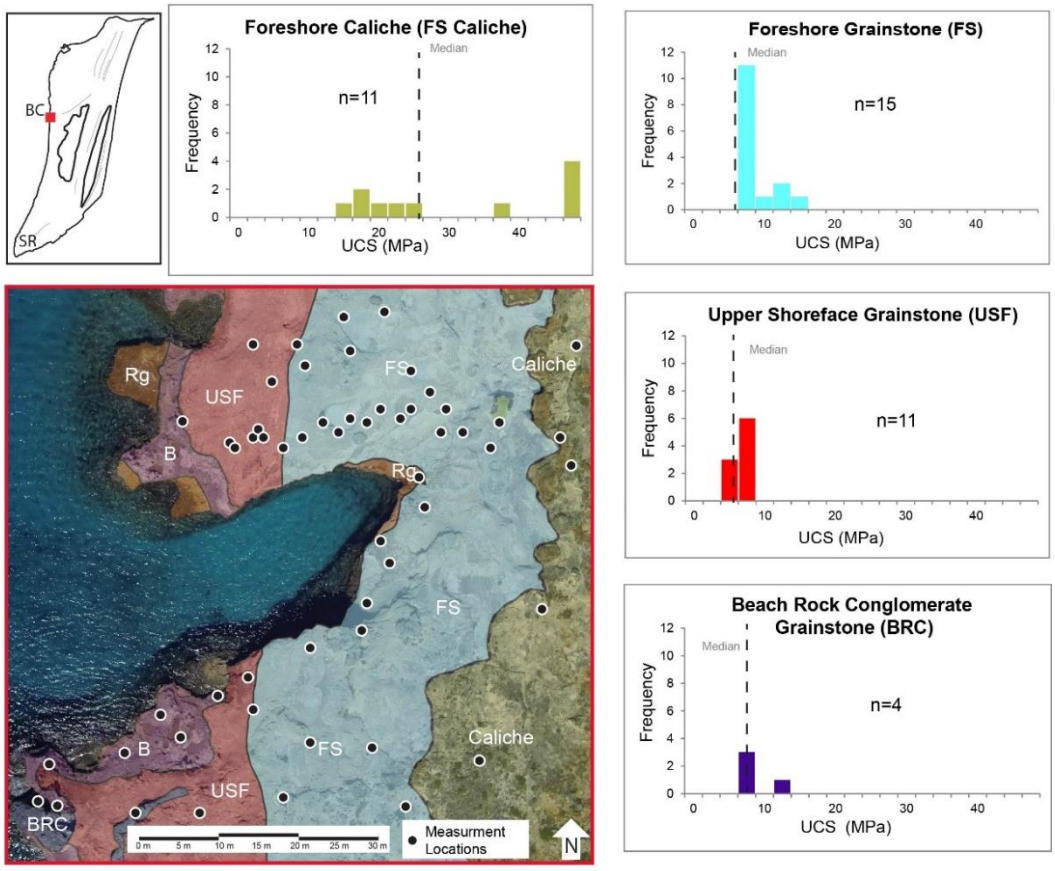

Figure 2.8. Map view of Boat Cove location with mapped facies. UCS distribution by frequency per facies type. Grainstone facies (FS, USF, and BRC) mechanically behave the most weakly of mapped facies at Boat Cove. Caliche surface that developed on foreshore exhibits highest mapped UCS. Facies key: C = caliche, E = eolianite, FS = foreshore, USF = upper shoreface, BRC = beach rock conglomerate, B = burrowed upper shoreface, Rg = reef-crest coral-*goniolithon* boundstone. Located at 21.673264 N., 72.467258 W (center of the image).

Figure 2.9.

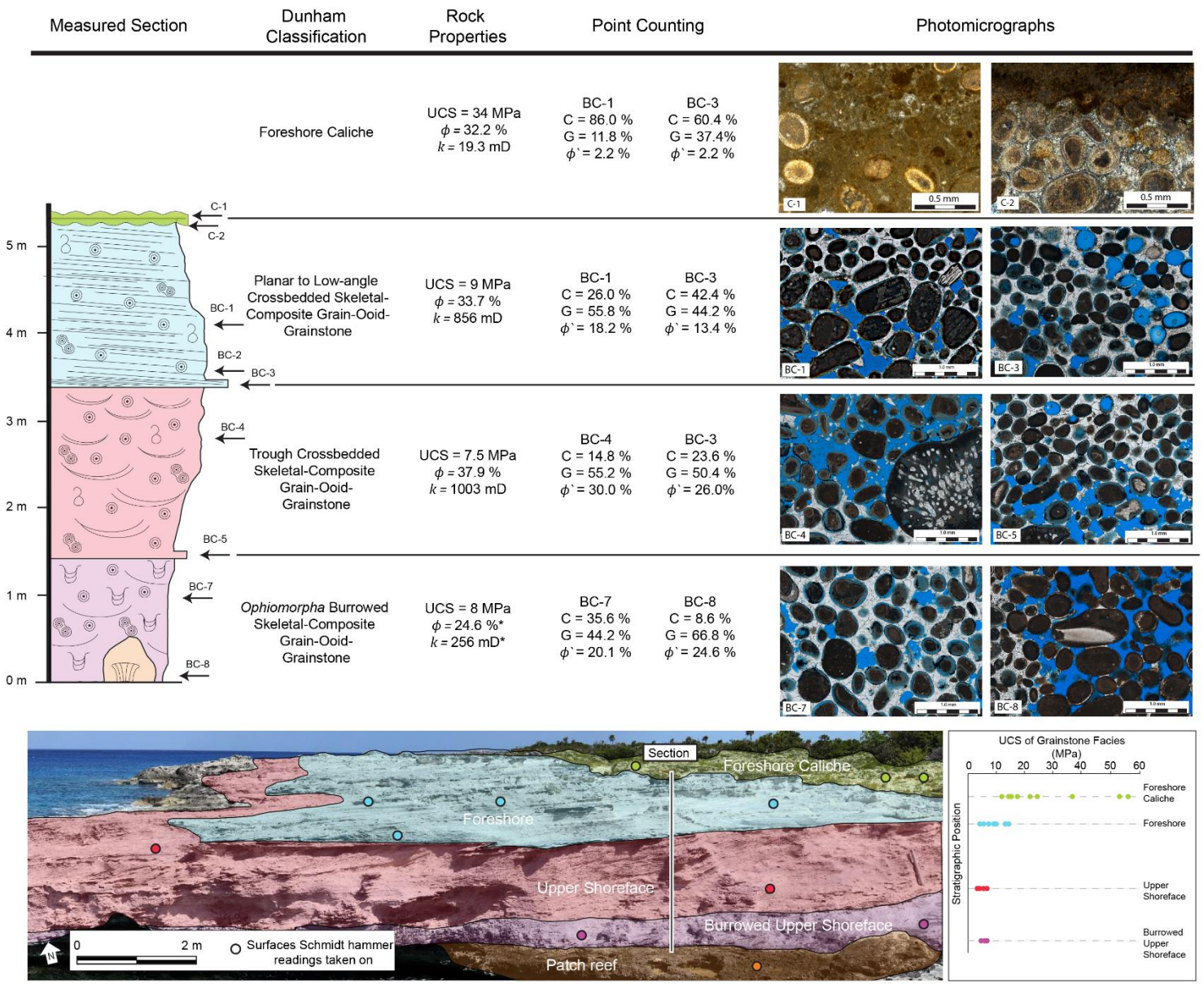
Measured Section
Dunham Classification
Rock Properties
Point Counting
Photomicrographs
Foreshore Caliche
UCS = 34 MPa
ϕ = 32.2 %
k = 19.3 mD
BC-1
C = 86.0 %
G = 11.8 %
ϕ` = 2.2 %
BC-3
C = 60.4 %
G = 37.4%
ϕ` = 2.2 %
C-1
C-2
0.5 mm
5 m
4 m
3 m
2 m
1 m
0 m
Planar to Low-angle Crossbedded Skeletal-Composite Grain-Ooid-Grainstone
UCS = 9 MPa
ϕ = 33.7 %
k = 856 mD
BC-1
C = 26.0 %
G = 55.8 %
ϕ` = 18.2 %
BC-3
C = 42.4 %
G = 44.2 %
ϕ` = 13.4 %
BC-1
BC-2
BC-3
Trough Crossbedded Skeletal-Composite Grain-Ooid-Grainstone
UCS = 7.5 MPa
ϕ = 37.9 %
k = 1003 mD
BC-4
C = 14.8 %
G = 55.2 %
ϕ` = 30.0 %
BC-3
C = 23.6 %
G = 50.4 %
ϕ` = 26.0%
BC-4
BC-5
Ophiomorpha Burrowed Skeletal-Composite Grain-Ooid-Grainstone
UCS = 8 MPa
ϕ = 24.6 %*
k = 256 mD*
BC-7
C = 35.6 %
G = 44.2 %
ϕ` = 20.1 %
BC-8
C = 8.6 %
G = 66.8 %
ϕ` = 24.6 %
BC-7
BC-8
Section
Foreshore Caliche
Foreshore
Upper Shoreface
Burrowed Upper Shoreface
Patch reef
0
2 m
Surfaces Schmidt hammer readings taken on
UCS of Grainstone Facies (MPa)
0
10
20
30
40
50
60
Stratigraphic Position
Foreshore Caliche
Foreshore
Upper Shoreface
Burrowed Upper Shoreface

Figure 2.9. Oblique cross section at Boat Cove location. Photograph interpreted by facies type (and colored according to Fig. 6), representing a typical cycle succession from burrowed upper shoreface to caliche-capped foreshore. Examples of locations where Schmidt hammer measurements were taken are highlighted by colored dots. UCS distributions for given facies are detailed on the right; the development of a caliche crust on foreshore deposits exhibits highest UCS values, which decrease downward (stratigraphically), away from exposure surface. Measured section of Boat Cove with corresponding Dunham classification, rock properties, and point counting results. UCS = Unconfined compressive strength, ϕ = porosity, k = permeability. Point counting completed for photomicrographs, with C = cement percentage, G = percent of grain, ϕ` = porosity. *Value from Jones et al. (2008). Located at 21.673264 N., 72.467258 W (center of the image).

Comparatively, the South Reef location (Fig. 2.10) best highlights the variability in recorded UCS values between grain-rich fill (matrix) and reef facies. The grain-rich fill in and around the reef and coral conglomerate demonstrates mechanical weakness, with a median UCS value of 14.3 MPa. Schmidt hammer readings taken directly on coral heads or large coral fragments demonstrate that intact corals are mechanically much stronger, with a median UCS of 27.5 MPa.

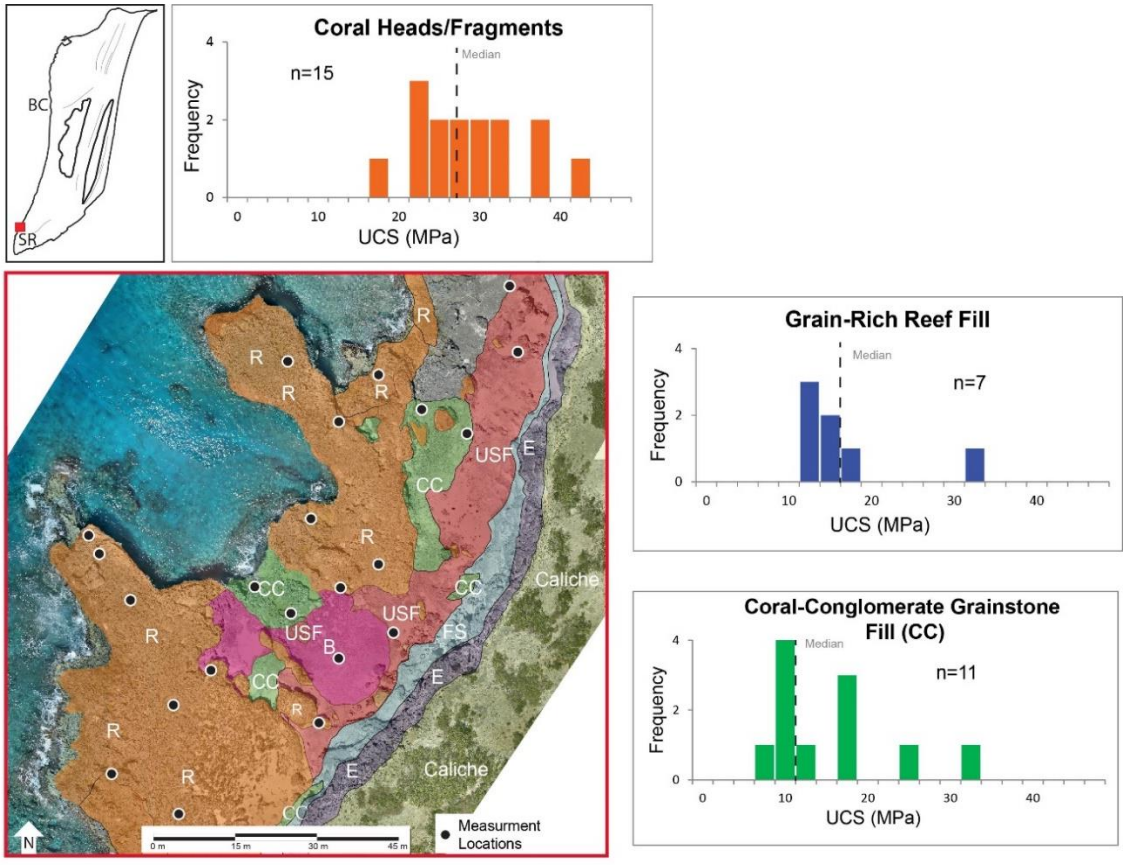

Figure 2.10. Map view of South Reef location with mapped facies. UCS distribution by frequency per facies type. Grain-rich fill in and around reef and coral conglomerate exhibits weakest UCS; readings taken on coral heads/fragments exhibit higher UCS values. Facies key: C = caliche, E = eolianite, FS = foreshore, USF = upper shoreface, B = burrowed upper shoreface, Rg = reef-crest coral-*goniolithon* boundstone, CC = coral conglomerate. Located at 21.631064 N., 72.480656 W (center of the image).

When analyzed together as MIS 5e strata, UCS relationships for all facies at Boat Cove and South Reef hold as described above (Fig. 2.11). The box plot highlights three predominant facies groupings (grainstone, reef, and caliche) and their variations in recorded UCS values. Grain-supported facies are the weakest of all recorded UCS values for MIS 5e deposits on West Caicos, with a median UCS of 8.0 MPa. UCS measurements taken on reef and coral heads/fragments fall into the middle of recorded UCS values, with a median UCS of 19.3 MPa. However, because the coral heads/fragments are often contained within a grain-rich matrix, the overall unit may be mechanically weak due to the bimodal distribution of mechanical properties. Caliche crusts have a median UCS of 34.1 MPa.

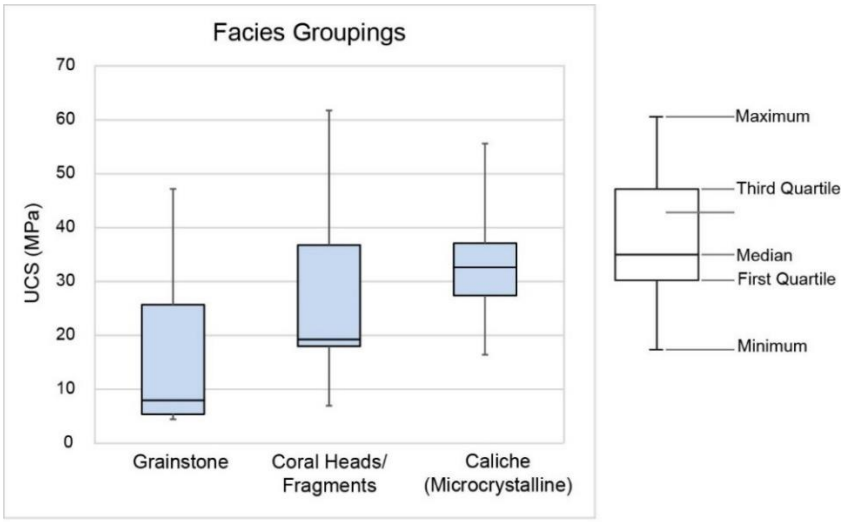

Figure 2.11. Box-and-whisker plot of field Schmidt hammer measurements for MIS 5e deposits. Measurements have been grouped based on their Dunham classification, where predominant composition and grain type exert a control over rock strength. Grainstone facies (including grainstone facies and grainstone matrix within the reef facies) mechanically behave the most weakly of mapped facies, with a median UCS of 8.0 MPa. UCS measurements taken on boundstone/framestone illustrate that reef deposits behave much more strongly, with a median UCS of 19.3 MPa. Of mapped facies, development of a caliche surface, composed of microcrystalline carbonate material, exhibits highest median UCS values (34.1 MPa). While facies-grouping details change in overall average of measured UCS values, a wide range of values is reported for each facies.

Temporal variations in all UCS measurements taken on Holocene and Pleistocene grainstone outcrop exposures across West Caicos are illustrated in Figure 2.12. Each stratigraphic package (MIS event) is capped by a caliche surface caused by subaerial exposure, where UCS values are the highest. While UCS is highest on the caliche crust, alteration and precipitation of cements would likely occur below this surface, which may lead to higher UCS values in deposits close to the caliche surface. This relationship is illustrated in Figure 2.12, where MIS 5e eolianite samples below the caliche surface exhibit

a higher median UCS (18.2 MPa) than foreshore deposits farther away from the alteration associated with the development of the caliche surface, which have a median UCS of 14.5 MPa. The larger trend present in the data illustrates that overall UCS increases with increasing age, as exemplified by comparing the caliche crust median UCS value of MIS 5e (34.0 MPa) with the median UCS value of MIS 9/11 deposits (53.5MPa).

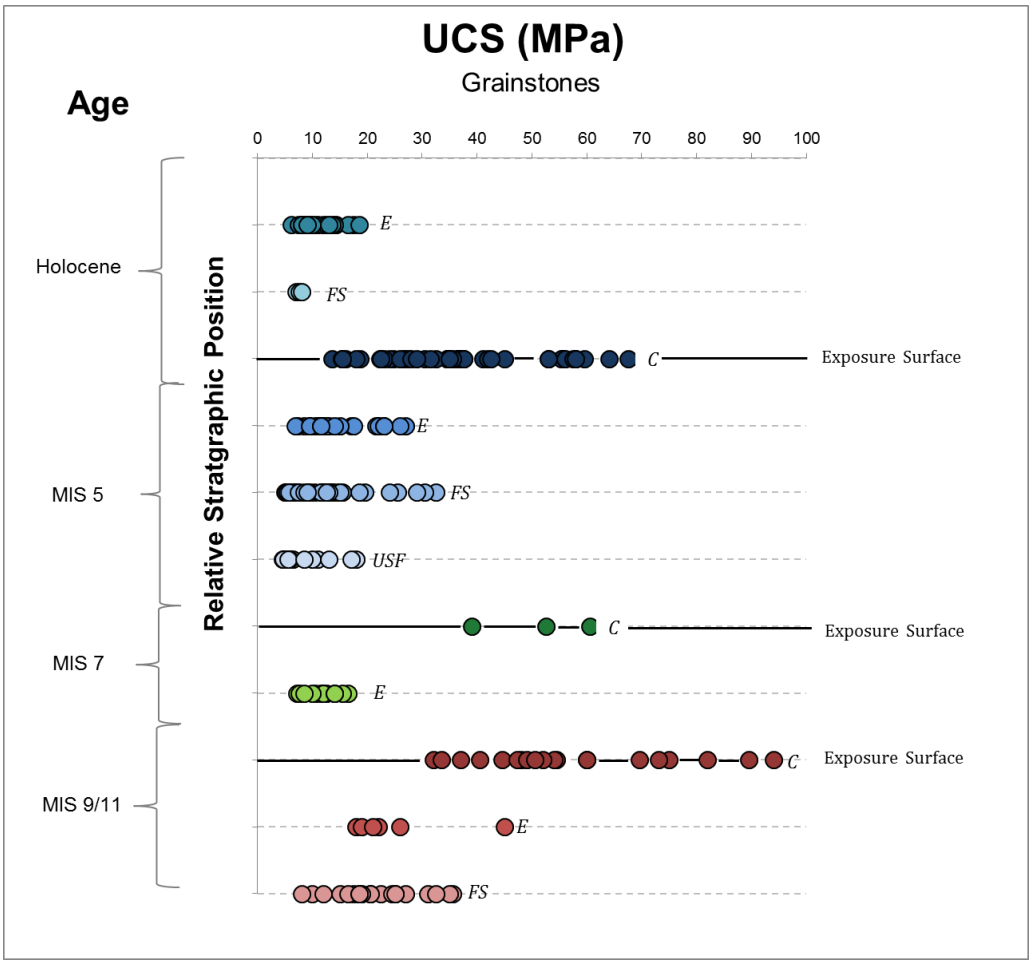

Figure 2.12. Temporal variation for all grainstone Schmidt hammer field measurements. All field measurements were tied to facies type and age by previously established geologic framework. Schmidt hammer field results record two trends in data. First trend is recorded on a scale consistent within each of four stratigraphic packages on West Caicos: exposure surface exhibits highest UCS values; UCS then decreases down and away from surface. Second, larger-scale trend is increasing UCS with increased age. Facies key: C = caliche, E = eolianite, FS = foreshore, USF = upper shoreface.

Laboratory UCS and Porosity Data.--- Results for median values of the uniaxial compression tests on the three large grainstone samples reveal a trend similar to UCS results from field measurements (Table 2.1). The grainstone sample associated with the

MIS 5e event exhibits the weakest UCS, with a median of 4.5 MPa, while the sample associated with the MIS 9/11 event exhibits the highest, with a median UCS of 14.5 MPa.

	MIS 5e Grainstone (WC-ABC-6)	MIS 7 Grainstone (WC-RR2)	MIS 9/11 Grainstone (WC-SE-11-1.2)
Latitude	21° 37' 50.6857" N	21° 39' 34.8049" N	21°37'27.34"N
Longitude	72° 28' 50.3077" W	72° 27' 23.8788" W	72°28'41.91"W
UCS (MPa) (from uniaxial testing)	4.5	5.0	14.0
Porosity (%)	34.0	36.0	27.0
Permeability (mD)	860.0	228.0	0.64
Grain Density (g/cm^3)	2.82	2.79	2.78
Grain Type	Ooids, minor intraclast, and grapestones	Ooids, minor intraclast, skeletal fragments, and grapestones	Intraclasts, grapestones, skeletal fragments, and ooids
Grain Sorting	Poorly sorted	Moderately to well sorted	Very well sorted
Grain Size (mm)	0.25–0.5	0.25–0.5	0.25–1.0
Porosity Type	Inter- and intraparticle	Inter- and intraparticle	Inter- and intraparticle
Cement Percentage (%)	32.0	37.0	40.0
Cement Type	Blocky calcite with minor meniscus and rimming cements	Blocky calcite cement	Blocky calcite cement

Table 2.1. Compilation of laboratory data for the grainstone samples collected on West Caicos. Data includes uniaxial data, petrophysical data, and thin section analysis/ observations.

Nitrogen porosimetry results indicate that with increasing age, overall permeability and porosity decreases (Fig. 2.13).Permeability is more negatively impacted than porosity. The grainstone sample associated with MIS 9/11 has an average porosity of 27.0% and permeability of 0.64 mD; the grainstone sample from MIS 5e has an average porosity of

34.0% and permeability of 860.0 mD. A sample was taken from below the MIS 5e caliche surface to compare the measured porosity/permeability values against the unaltered MIS 5e sample. On average, the diagenetically altered MIS 5e caliche sample has a porosity of 32.5% and permeability of 19.3 mD, both lower values than those associated with the MIS 5e grainstone sample.

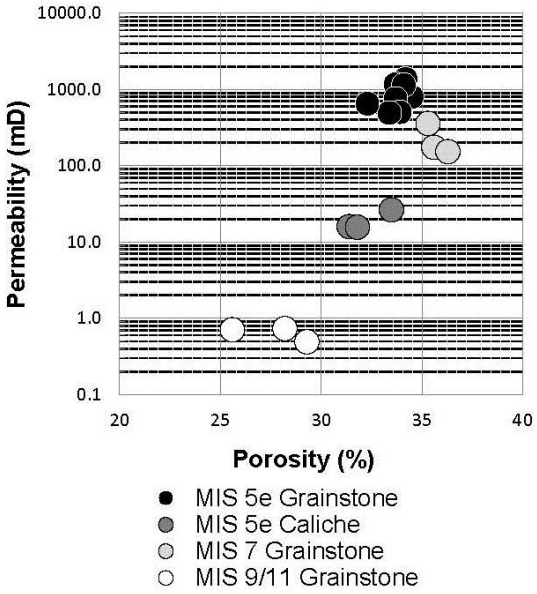

Figure 2.13. Porosity–permeability plot for samples collected on West Caicos. Multiple analysis were run from each 20X40 cm sample. Plot illustrates changes in porosity value with changes in age, where MIS 9/11 grainstone has lowest overall porosity and permeability values. Sample collected from within MIS 5e caliche horizon that developed on top of MIS 5e grainstone illustrates overall lower permeability and porosity than its unaltered counterpart, MIS 5e grainstone.

DISCUSSION

Stratigraphically thin caliche surfaces that formed on exposure horizons demonstrate significant increases in rock strength. UCS measurements on individual coral

heads and/or fragments also exhibit greater rock strength. All other facies, all of which are grain-dominated, are significantly weaker. Variations in rock strength in the weak, grain-dominated facies are dependent on the extent to which the sample is cemented. Cementation tends to increase in proximity to a subaerial exposure surface, and successively older depositional packages accumulate more cement due to repeated exposure to meteoric diagenetic events through time. The resultant vertical profile of strength in stacked packages illustrates an overall increase in UCS with age, within which are nested positive spikes in UCS at the exposure surfaces that rapidly decay through underlying strata (Fig. 2.12). This demonstrates that cementation from early near-surface diagenesis controls rock strength in carbonates more so than facies.

Because rock strength in Pleistocene carbonate rocks is primarily a byproduct of cementation and dissolution processes tied to near surface diagenesis, spatial heterogeneity in UCS across other islands and climate zones is likely significant. However, because porosity covaries with rock strength, it can be empirically related to UCS in the absence of field or laboratory strength data. Through literature review, porosity values for similarly aged Pleistocene rocks (from across the Bahamian Archipelago) where the stratigraphic context has been previously established are empirically related to UCS (Table 2.2). Using a transform established to relate porosity to UCS for carbonate rocks by Moh'd (2009), we are able to plot the broad distribution of UCS for a given MIS event (Fig. 2.14) from 10 locations. The field results data for UCS from this study are shown as a box and whisker plot with the UCS values for other locations overlain demonstrating the spread in UCS values (as determined from porosity) for similarly aged Pleistocene rocks from across the

Caribbean. However, to truly capture the spatial and temporal heterogeneities in rock strength, a similar data set to what is reported in this study is needed for other islands. While one could postulate that overall the UCS values for Pleistocene age rocks are increasing, we are unable to say conclusively what happens within a given MIS event to rock strength (Fig. 2.14). This is a byproduct of the limited number of porosity values for the given location and a lack of information on proximity to a subaerial exposure surface.

Location	Age (MIS Stage)	Facies/composition	Porosity (%)	UCS* (MPa)	Reference
Abaco, Bahamas					
	Holocene	Oolite	24.1	30.2	Kindler and Hearty (1996)
	MIS 5	Oolite	12.5	79.5	
	MIS 7	Bioclastic Calcarenite	24.2	29.9	
	MIS 9	Oolite	15.3	62.9	
Barbados, B.W.I					
	MIS 5	Grainstone	20	42.5	Harrison (1975)
	MIS 7	Grainstone	28	21.8	
	MIS 9/11	Grainstone	23	33.1	
Bermuda	MIS 5	Grainstone	31	17.0	(Land et al. (1967); Hearty (2002))
Cat Island, Bahamas	Holocene	Oolite	14.7	66.1	Kindler and Hearty (1996)
	MIS 5	Oolite	17.9	50.64	
	MIS 7	Bioclastic Calcarenite	29.1	19.9	
	MIS 9	Oolite	8.6	110.0	
Eleuthera, Bahamas	Holocene	Oolite	17.7	51.5	Kindler and Hearty (1996)
	MIS 5	Oolite	18.9	46.6	
	MIS 7	Bio-clastic Calcarenite	29.5	19.2	
	MIS 9	Oolite	12	82.8	
Exhuma, Bahamas	Holocene	Oolite	19	46.2	Kindler and Hearty (1996)
	MIS 5	Oolite	19.6	43.9	
	MIS 7	Bioclastic Calcarenite	40.6	7.62	
Florida, USA	MIS 5	Oolite	16	59.3	Coniglio and Harrison (1983)
	MIS 7	Oolite	12	82.8	

Table 2.2. Data compiled from literature for Pleistocene aged carbonates where composition (grain type and mineralogy) and porosity is reported. Porosity is related to UCS using an empirical relationships established by *Moh'd (2009).

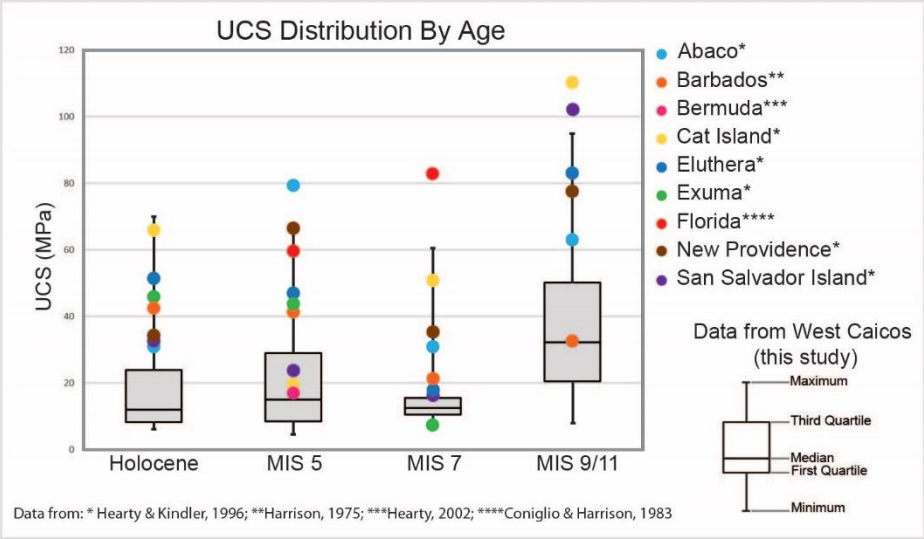

Figure 2.14. Data collected from West Caicos (this study) is plotted by Box and Whisker plot to highlight the spread in recorded UCS values for the various MIS events. Additional data points UCS data points (derived from porosity) for nine locations are overlain. Plot highlights the drastic variability in UCS values for a given MIS event. Without a high resolution data set that is rigorously tied to stratigraphy, but also position within a given stratigraphic package and proximity to subaerial exposure surfaces, one cannot conclusively determine the factors affecting rock strength in Pleistocene carbonates.

Overall, the high resolution data set reported within this study allows for an understanding of how rock strength in carbonates varies with age and cementation tied to near-surface diagenesis. The repetitive process of deposition and subsequent alteration of initial rock properties via near-surface diagenesis is tied to fluctuations in sea-level and can be predicted to continue with each rise and fall in sea-level. In the case of West Caicos, three periods of deposition and subsequent near-surface diagenetic alteration are recorded and represented by the occurrence of three distinct caliche surfaces. Changes in rock properties of young, unburied carbonate rocks are driven by subaerial exposure, during

which early near-surface diagenetic processes drastically alter rock strength (Fig. 2.15) via increased cementation. The alteration of rock properties creates spatial and temporal variability of mechanical behavior for a given sediment package.

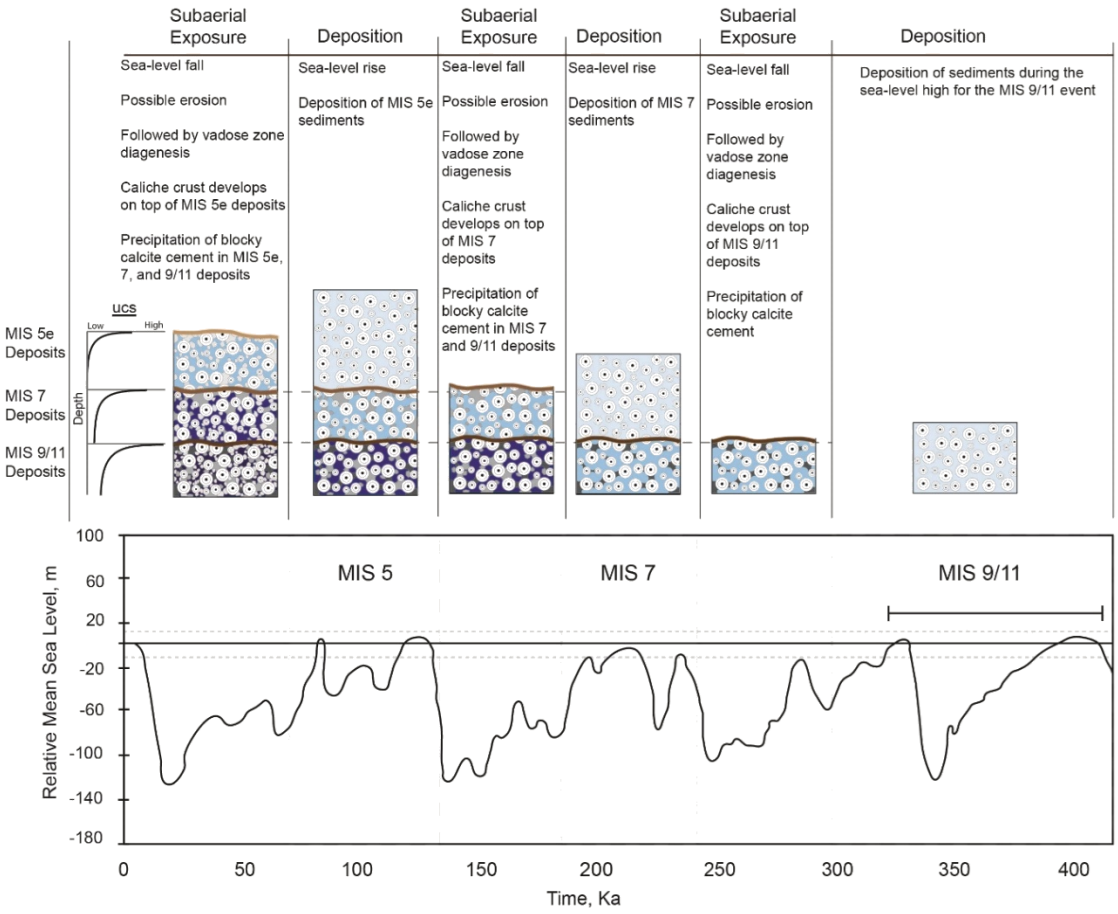

Figure 2.15. Composite sea-level curve is tied to schematic model that details deposition of sediments on West Caicos during sea-level highs, and subsequent subaerial exposure and diagenetic products during sea-level lows. Cyclic weathering process continued for each MIS-related stratigraphic package; sediments previously deposited were subjected to continued diagenesis, with each successive subaerial exposure from sea-level falling. Increases in cementation through time (represented by increased gray shading) led to increase of UCS, represented by change in background color. Light-blue background color is representative of low UCS values; dark blue is representative of high UCS values. Sea-level curve modified after Waelbroeck et al. (2002).

CONCLUSIONS

The island of West Caicos provides the ideal location to test and evaluate factors that affect the strength of young, near-surface carbonate rocks. Field and laboratory measurements show a relationship between rock strength, porosity, and calichification/cementation related to near-surface diagenesis. The development of caliche crusts (marking subaerial exposure during a sea-level low) and increased cementation below the crust is strongly tied to increases in UCS. Caliche surfaces across West Caicos exhibit the highest average UCS values of all measured facies. Facies within close proximity to caliche surfaces also have high UCS values due to increased cementation from the development of the caliche surface. Each stratigraphic package related to each individual MIS event on West Caicos is capped with a caliche surface, and therefore the top of each temporal package shows higher rock strength than the rest of the package beneath it. Older strata not directly overlain by a caliche crust display lesser effects of near-surface diagenesis, leading to decreases in average UCS values. Overall, UCS increases with age, which is the result of increased cementation and overall porosity reduction due to repeated exposure to meteoric near-surface diagenesis through time.

Pleistocene sediments of West Caicos were exposed to periods of long repeated subaerial exposure and brief marine inundation characteristic of the climatic conditions periods of long repeated subaerial exposure and brief marine inundation consistent with the climatic conditions of the Pleistocene Epoch, when high-frequency, high-amplitude sea-level oscillations occurred. Changes in rock properties happening at the high-frequency

depositional-cycle scale are important in predicting how stratigraphic packages influences rock strength, especially in younger carbonate strata, and ultimately how the overall shelf margin behaves mechanically.

Chapter 3: Effect of Carbonate Platform Geometry on Syndepositional Deformation: insights from numerical modeling of carbonate platforms in the recent and ancient rock record

INTRODUCTION

Steep-walled carbonate platforms are ubiquitous throughout Earth's history despite differences in ocean water chemistry and organic binding potential (i.e. different organisms) from the Precambrian to the modern(Read, 1985; Grotzinger, 1989). Steep-walled carbonate platforms have been documented as far back as the Precambrian, where their morphologies and development are very similar to their Phanerozoic counterparts (Grotzinger, 1989). The occurrence of syndepositional and/or early deformation is intrinsic in steep-rimmed carbonate platforms, where early lithification coupled with biological reef growth (Land and Moore, 1977; James and Ginsburg, 1979b; Grammer et al., 1993b; Grammer et al., 1999) can create steep, upper slope and reef wall angles prone to failure (Hunt and Fitchen, 1999; Frost and Kerans, 2009, 2010) (Fig.2.1). Syndepositional shelf margin collapse, faulting, and fracturing may alter the evolution of carbonate platform architecture and stratigraphy through time (Yurewicz, 1976; Playford et al., 1984; Hurley, 1986; Hunt et al., 1995; Tinker, 1998; Hunt and Fitchen, 1999; Kerans and Tinker, 1999; Koša et al., 2003; Stanton Jr and Pray, 2004; Koša and Hunt, 2005; Carpenter et al., 2006; Collins et al., 2006; Narr et al., 2008; Frost and Kerans, 2009, 2010; Rush and Kerans, 2010; Hunt et al., 2012; Mathisen, 2014).

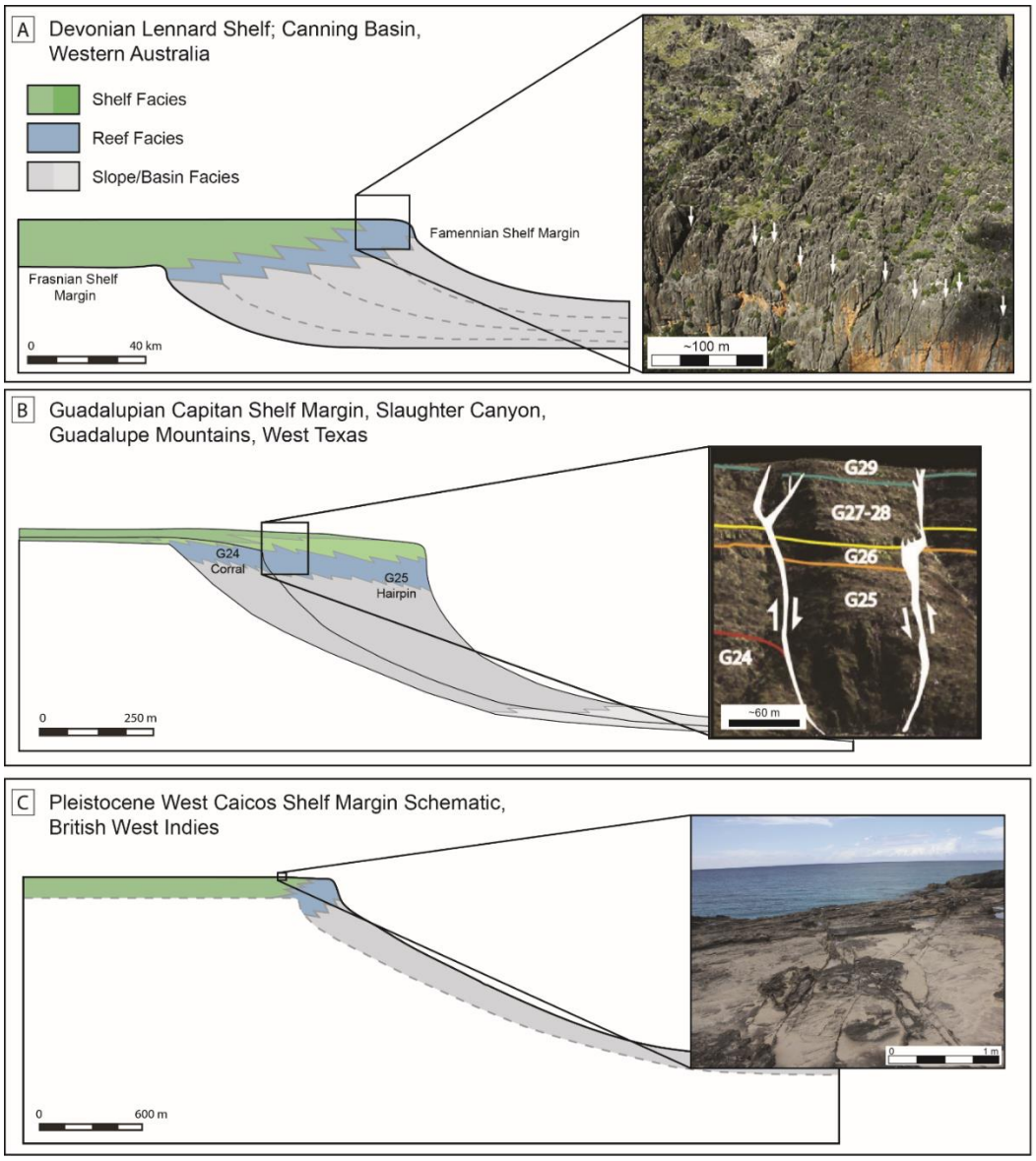

Figure 3.1. Examples (both modern and ancient) of syndepositional fractures in steep-walled carbonate platforms. (A) Large continuous, margin-parallel, syndepositional fractures (white arrows) occurring in Famennian reef and forereef of Windjana Gorge, Canning Basin (after Frost and Kerans, 2010). (B) Large syndepositional faults over terminal early Capitanian G24 shelf margin in Slaughter Canyon, Guadalupe Mountains, New Mexico (after Kerans et al. 2017 and Mathisen, 2014). (C) Margin-parallel and margin-normal early fractures on West Caicos intersect, highlighting the often irregular, anastomosing nature of fracture networks present on island. Note the relative scale of fractures compared to the Canning Basin and Capitan systems.

The Permian steep-rimmed carbonate shelf margin of the Guadalupe Mountains provides world-class outcrop exposures and type examples of syndepositional deformation (King, 1948; Stanton Jr and Pray, 2004). Large faults and open-mode fractures documented within McKittrick, Slaughter, and Rattlesnake Canyon represent syndepositional deformation (King, 1948; Hunt and Fitchen, 1999; Hunt et al., 2003; Stanton Jr and Pray, 2004; Koša and Hunt, 2005; Rush and Kerans, 2010; Hunt et al., 2012; Budd et al., 2013; Mathisen, 2014). At these locales, deformation is often centralized over the antecedent shelf margin and at the shelf edge (Hunt and Fitchen, 1999; Koša and Hunt, 2005; Frost and Kerans, 2009, 2010; Mathisen, 2014). The faults and fractures are often filled with skeletal carbonate and/or siliciclastic sediments and marine cements, indicating their syndepositional origin (i.e. neptunian dikes), and have been documented to be long-lived fluid flow conduits (Hunt et al., 2002; Koša et al., 2003; Stanton Jr and Pray, 2004; Carpenter et al., 2006; Narr et al., 2008; Frost et al., 2012; Budd et al., 2013; Mathisen, 2014; Simon, 2014).

Multiple mechanisms have been proposed as drivers of syndepostional deformation in steep-rimmed carbonate platforms including differential compaction (Hunt et al., 1995; Saller, 1996; Hunt and Fitchen, 1999; Rusciadelli and Di Simone, 2007; Frost and Kerans, 2009) sea-level change (Rusciadelli et al., 2003), geometry and antecedent topography (Hunt et al., 2003; Koša and Hunt, 2005; Frost and Kerans, 2010; Harman, 2011), and heterogeneous rock properties (Nolting et al., 2017b). While the proposed processes likely contribute to or partially control early deformation, one cannot quantify the effect from each mechanism on deformation without the use of physics-based geomechanical models.

Furthermore, you cannot quantify the relevant parameters to each process without numerical models. For example, it is unknown how much compaction of slope and basinal deposits is necessary to initiate deformation at the shelf edge. Nor can one quantify how much change in pore pressure due to sea-level variations is required to effect the development of deformation. Similarly, evaluations of the stress state and kinematics of a carbonate platform under gravitational loading and conditions that facilitate over-steepening remain largely speculated.

Numerical models have been previously employed to aid in identifying the controls on early deformation, but is not common. Early work by Rusciadelli et al. (2003) has suggested that movement along an active fault is the most likely trigger for large-scale platform margin collapse. Later work by Resor and Flodin (2010) identified compaction and slope geometry related to variable progradation/aggradation (P/A) ratio as a potential driver on syndepositional deformation. We build upon this understanding using numerical models that allow for the development of discrete failures under gravitational loading and over-steepening conditions.

The relationship between changes in platform geometry and syndepositional deformation has not been explicitly investigated. We hypothesize that platform geometry is a primary control on the development of syndepositional deformation in carbonate platforms. We use numerical models with an inelastic failure criteria that permits the development of fractures and faults, allowing for realistic simulation of brittle syndepositional deformation under the sole application of gravity. Our numerical modeling results suggest that geometry governs the stress distributions for any given carbonate

platform system. Carbonate platforms with steep upper slopes and reef walls are more likely to fail than their shallowly dipping counterparts. Failure caused by over-steepening and gravitational instability at the shelf edge is related to the region of most concentrated tensile stress state that is dictated by platform geometry.

GEOMECHANICAL NUMERICAL MODELS

We use 2D finite-discrete element software, ELFEN® (Rockfield, 2010) to investigate and isolate the effects that variations in the geometry of carbonate platforms have on the development of syndepositional faults, fractures, and collapse. Numerical models use a hybrid finite/discrete element method for analysis that is based on a quasi-static Lagrangian finite element formulation. ELFEN was chosen because it appropriately handles brittle deformation, is capable of modeling large scale domains (100-1000's of meters), and utilizes adaptive remeshing. Remeshing occurs when the deformations of individual elements exceeds a strain threshold. This preserves the deformation of the system as a whole without compromising the integrity of the model computations. An unstructured triangular mesh (grid) is used, where each element is 30 meters across. Variable mesh sizes were used to test sensitivity of the model to changes in mesh and the development of deformation, varying mesh size from 5 to 100 meters across. 30 meter element size was chosen because it captures deformation features while keeping computation time to a minimum. A triangular mesh is used because it enables fracturing and faulting within ELFEN. We chose the size of an element based on the size of the overall

modeled domain, the distribution of rock properties, and the need to keep computation time to a minimum while still producing meaningful model results.

We use an inelastic constitutive law combined with continuum and discontinuum analysis methods that allow for the development of discrete failure(s) and dissipation and interaction of stress(s) following failure. In a sedimentary basin, where stress conditions are uniaxial, the lateral stresses are compressive (Fig. 3.2A). However, the lateral stress conditions in a steep-walled carbonate platform do not represent uniaxial lateral stress conditions (Fig. 3.2A). This is because of the lack of lateral confinement. As a result, the least principal stress decreases and can become tensile (negative) (Fig. 3.2A). To appropriately predict tensile failure, the Mohr-Coulomb with a Rankine rotating crack modification constitutive law is used (Klerck et al., 2004). The traditional Mohr-Coulomb constitutive law is not capable of capturing tensile failure, even if it accounts for cohesional strength, because the Mohr's circle will always reach the shear failure envelope (Fig. 3.2B) before reaching the tensile strength of the rock. Using the Rankine rotating crack modification allows for tensile failure by the presence of a tensile corner (Fig. 3.2C), where failure is dependent on tensile strength (T_o) and the fracture energy (G_f). The tensile strength for the given material is located within the negative quadrant of the Mohr diagram (Fig. 3.2C), where negative effective stress values indicate tension and positive indicate compression. This constitutive law was chosen because it permits the development of brittle, tensile fractures and normal faults which is commonly how syndepositional deformation is expressed in carbonate platforms. In addition to brittle tensile failure and

their associated processes, the constitutive law considers the kinematics of the system as a whole.

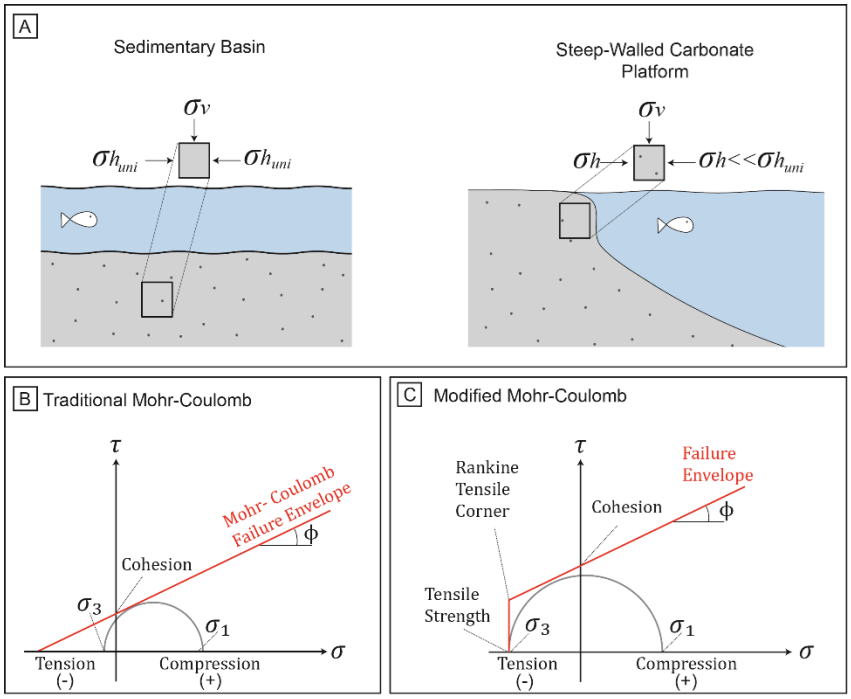

Figure 3.2. A) Stress conditions of a sedimentary basin and a steep-walled carbonate platform. A tensile stress state is likely to develop in a steep-walled carbonate platform at the shelf edge due to the lack of lateral confinement that allows volume of rock to get mobilized towards the open ocean. B) Traditional Mohr-Coulomb failure criterion with cohesion, where failure in shear occurs when the Mohr's circle reaches the shear failure envelope before ever reaching the tensile strength of the rock. C) Mohr-Coulomb with Rankine Rotating crack modification illustration. The tensile quadrant represents negative effective stress, while the compression region represent positive effective stress values. Tensile failure occurs when the least principal stress (σ_3), reaches the tensile strength of the material.

The three carbonate platforms used in this study were chosen to represent end-member geometries, based on Adams and Schlager's (2000) study of carbonate submarine slope curvature and were chosen to represent end-member carbonate shelf margin systems

(both recent and ancient), from ramps with shallow dips (>2°) to steeply-rimmed margins with vertical reef walls. Using the nomenclature of Adams and Schlager: Tabacco Cay, Belize represents a mixed planar/concave curvature shelf geometry; Amellago ramp, Morocco represents a sigmoidal geometry; and the Capitan profile (G25) represents a purely concave up curvature scenario. The Belize carbonate margin is characterized by a vertical, planar reef wall with a sharp transition to a concave slope (Fig. 3.3A) (James and Ginsburg, 1979b).. The Jurassic Amellago is characterized by shallow slope angles, more representative of a carbonate ramp depositional setting. For this profile, the platform top slowly grades in to a low angle slope, transitioning to a planar basin (Fig. 3.3C) (Pierre et al., 2010). The Capitan profile of the Guadalupe Mountains is characterized by a steep, vertical reef wall that gently transitions into a concave up slope (Fig. 3.3B). The Capitan profile (G25) is based on Kerans et al. (2017) stratigraphic architecture for the Guadalupe Mountains. The Amellago ramp is used to illustrate the effect from platform geometry on deformation. Each geometry is input into ELFEN is modeled with a one-to-one scale.

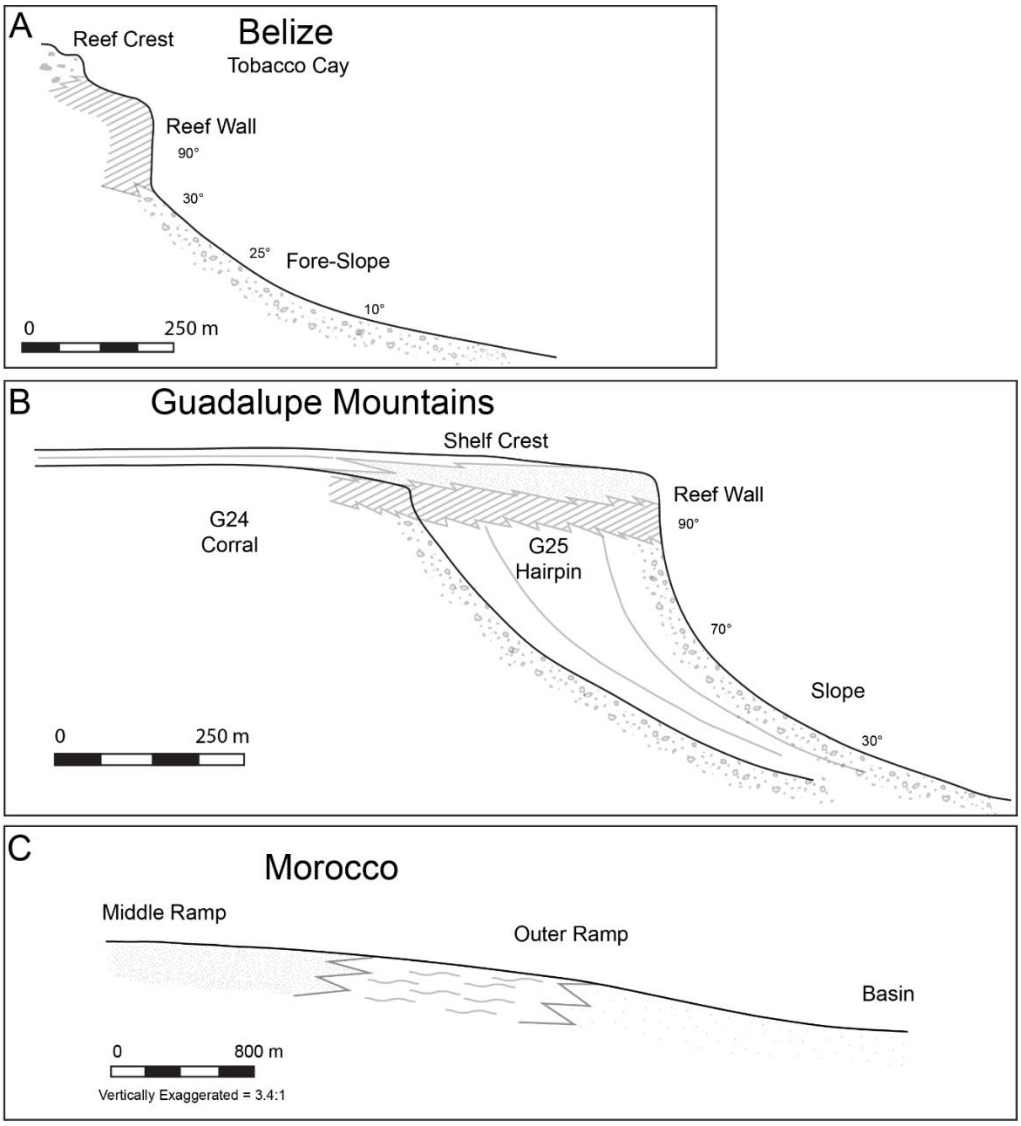

Figure 3.3. Line drawings of the geometries used in the numerical models after Adams and Schlagers (2000) slope curvatures classification scheme. A) Tobacco Cay Belize is characterized by a relatively flat platform interior and shelf edge has two steps and a vertical reef wall (after James and Ginsburg (1979b)). The Reef wall sharply transitions into a high angle slope and represents the mixed planar and concave up scenario. B) The Capitan profile of the Guadalupe Mountains, has a flat to low-angle seaward dipping platform top. The shelf edge is characterized by a vertical reef wall that transitions into high angle slopes. The profile represents the concave up scenario after Adam's and Schlager (2000). Geometry after Kerans et al. (2017). C) The Amellago ramp represents the sigmoidal geometry, after Pierre et al. (2010). The geometry is modeled after the Am 1 sequence.

All geometries were modeled with the same boundary conditions to isolate and test the effect of geometry on the development of syndepositional deformation. Each model was set up to simulate conditions under gravity. The application of gravity over a single time steps leads to computational instability where fractures develop as a byproduct of the energies associated with the applied load and are not realistic. Therefore we applied gravity incrementally over a specified number of time-steps within the model to allow the models to reach equilibrium and maintain computation stability throughout the duration of the model run. A bumper was also used around the edge of each model to maintain computational stability and to help reduce and dampen the inertial affects from the application of gravity (Fig. 3.4). The bumper is specified as a no slip boundary, constraining the model in the X &Y direction. During initialization, in general, the maximum principal stress is vertical and the minimum principal stress is horizontal. However, at near surface conditions along shelf margin and slope, the maximum principal stress is parallel to topographic expression with least principal stress perpendicular to it. The effective stress ratio of minimum to maximum principal effective stress is 0.7. The analyses are drained. Pore pressure is applied to the top of the models, simulating the presence of seawater at the shelf edge. Pore pressure is hydrostatic throughout the model.

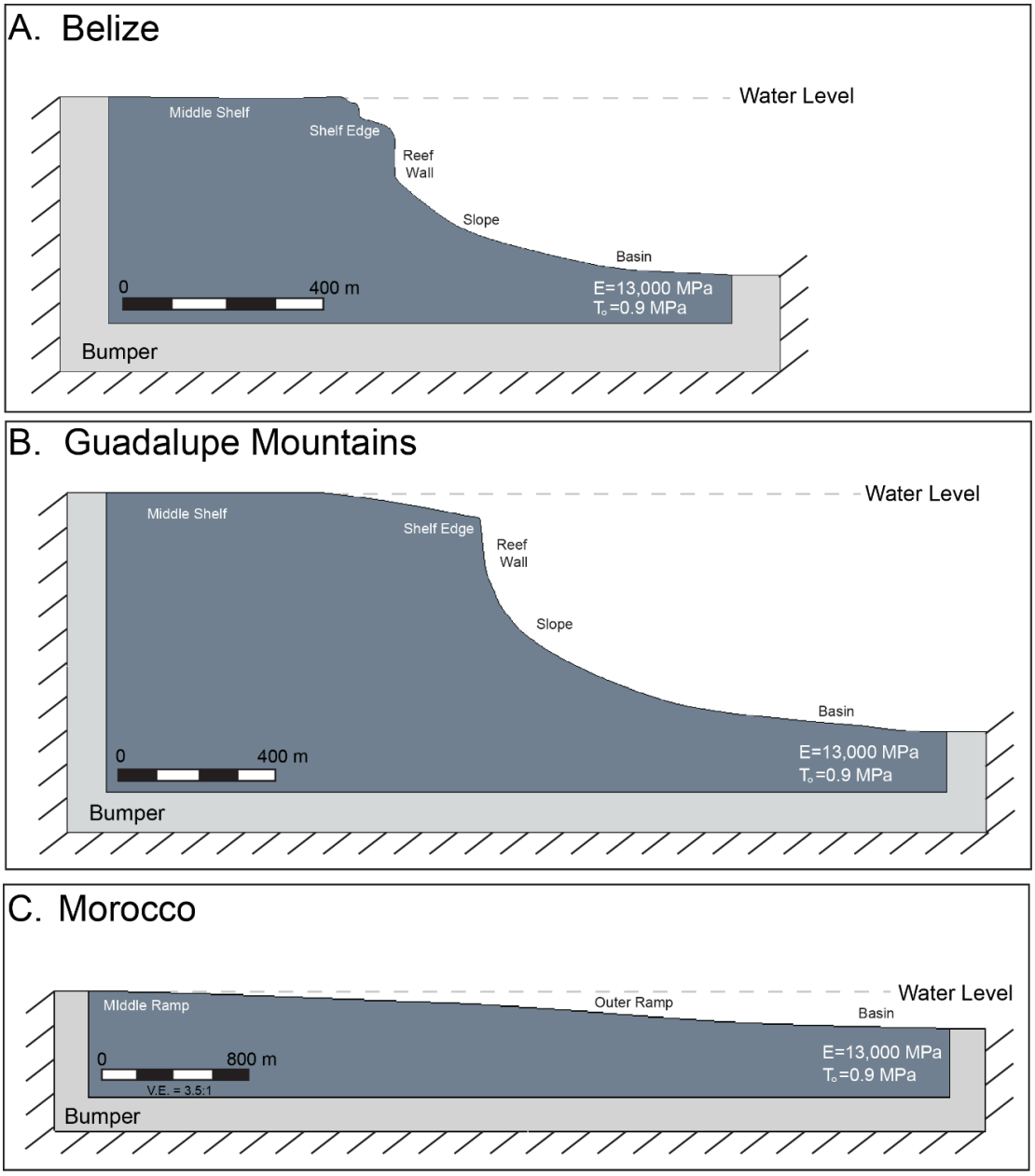

Figure 3.4. Three carbonate platform geometries use within ELFEN. Each model has the same boundary conditions to isolate the affects from geometry on deformation. Models are constrained in the X and Y direction. Hydrostatic pore pressure is applied to the top of each model and does not change with time. Each model has the same material properties that are distributed homogeneously (i.e. is not depth dependent). A) Tobacco Cay numerical model geometry. B) The Capitan profile model geometry. C) Amellago ramp numerical model geometry, vertically exaggerated 3.5 times for the illustration's purpose, modeled at a scale of 1:1.

Sensitivity modeling was used to test the effects of platform geometry on deformation and to understand the development of deformation within the numerical models. The sensitivity modeling included variations of slope angle and rock properties to determine their effect on the development of deformation under the sole application of gravity. Our early model work demonstrated that slopes above 60° angle are prone to the development of deformation. Additionally, the models are most sensitive to changes in Young's modulus and tensile strength with regards to the development of fractures and faults. The results of this early sensitivity modeling drove our choices of platform geometry and appropriate rock properties for investigating the effects of shelf profile morphology on the development of early deformation.

Rock properties used to populate each model are empirically-derived field and laboratory measurements taken on samples collected from the Pleistocene island of West Caicos, B.W.I. (Table 3.1) (Nolting et al., 2017b). These rock properties were chosen because they best represent the properties of a steep-rimmed carbonate shelf margin system close to the time of deposition, prior to major overprint from burial, compaction, uplift, and/or diagenesis. West Caicos is a useful steep-walled carbonate platform analog, as the western side of the island characterized by a steep-walled margin. The island's stratigraphic relationships, ages of the various deposits, and facies distributions are rigorously constrained (Lloyd et al., 1987; Wanless and Dravis, 1989; Simo et al., 2008; Kerans et al., 2016). While there is extreme heterogeneity and juxtaposition of rock properties on all carbonate platforms, with West Caicos being no exception, we used a single set of rock properties to test the effects of shelf margin morphology on the development of

deformation. Using a single set of rock properties (i.e. no facies dependence) distributed homogenously enabled faster computation times, improved ease of meshing and remeshing, and the isolation of controls related to deformation from platform geometry rather than facies relationships. We chose to utilize rock properties associated with a West Caicos Pleistocene grainstone, which is characterized by an intermediate Young's modulus and a low tensile strength (Table 3.1). Pleistocene grainstone rock properties are weaker compared to those of reefal deposits on West Caicos (Nolting et al., 2017b) and permit deformation to develop under the sole application of gravity. This allows us to isolate the effects of platform geometry on the development of early deformation in the absence of compaction and external perturbations (e.g. regional tectonics).

Parameter	Unit	Value
Young's Modulus, E	MPa	13,221
Poisson's Ratio, ν	-	0.3
Cohesion, C_o	MPa	3.0
Friction Angle	°	37.0
Tensile Strength, T_o	MPa	0.9
Fracture Energy, G_f	MPa*m	$1.32e^{-6}$
Fracture Toughness, K_{ic}	MPa*$\sqrt{m}$	$1.31e^{-1}$
Porosity, ϕ	%	34
Grain Density	Kg/m^3	2,710

Table 3.1. Input Material Parameters for Modified Mohr-Coulomb Model

There are several key assumptions made with regards to the three different model scenarios, including: (1) rock properties do not change with depth or time, (2) there is no diagenesis or fluid flow present, and (3) there is no deposition of sediments.

RESULTS

In the following section we present numerical modeling results for the three geometries. Results highlight the evolution of the least principal stress distributions, displacement vectors, and orientation of the maximum and minimum stresses. Results detailing the stress distributions through time are contoured by least principal stress magnitude (MPa), following geologic convention, where positive stress values indicate compression and negative stress values indicate tension. Locations with the most negative (tensile) stress magnitudes are most likely to develop open-mode (Mode I) fractures and normal faults.

Tobacco Cay, Belize

The surface expression is mirrored by the stress distributions (contours) for the Tobacco Cay, Belize steep-walled carbonate platform (Fig. 3.5A), where results highlight that the least principal stress distributions are affected by the platform geometry. The reef wall at Tobacco Cay is characterized by a notch that sharply transitions into the slope, which is reflected by the least principal stress contours. The platform interior and shelf edge experience a tensile stress state, as shown by the warm colors, which indicate themost negative values. With continued gradual application of gravity, tension in these regions intensifies. The accumulated displacement vectors point towards the basin (Fig. 3.5B). The vectors' magnitudes increase toward the shelf edge, illustrating increased displacement in this locale. Here the volume of rock at the shelf edge is moving down and away, towards

the basin. The development of fractures at the left-most edge of the model are a boundary effect from being constrained in the x and y direction.

At the completion of the model run (i.e. gravitational load is applied in full), discrete fractures have developed in the platform interior (Fig. 3.5C). Tensile fractures develop when the least principal stress magnitudes present in the model exceed the prescribed tensile strength of the material. This causes the development of open-mode tensile fractures, where they propagate in the vertical plane and open in the horizontal plane.

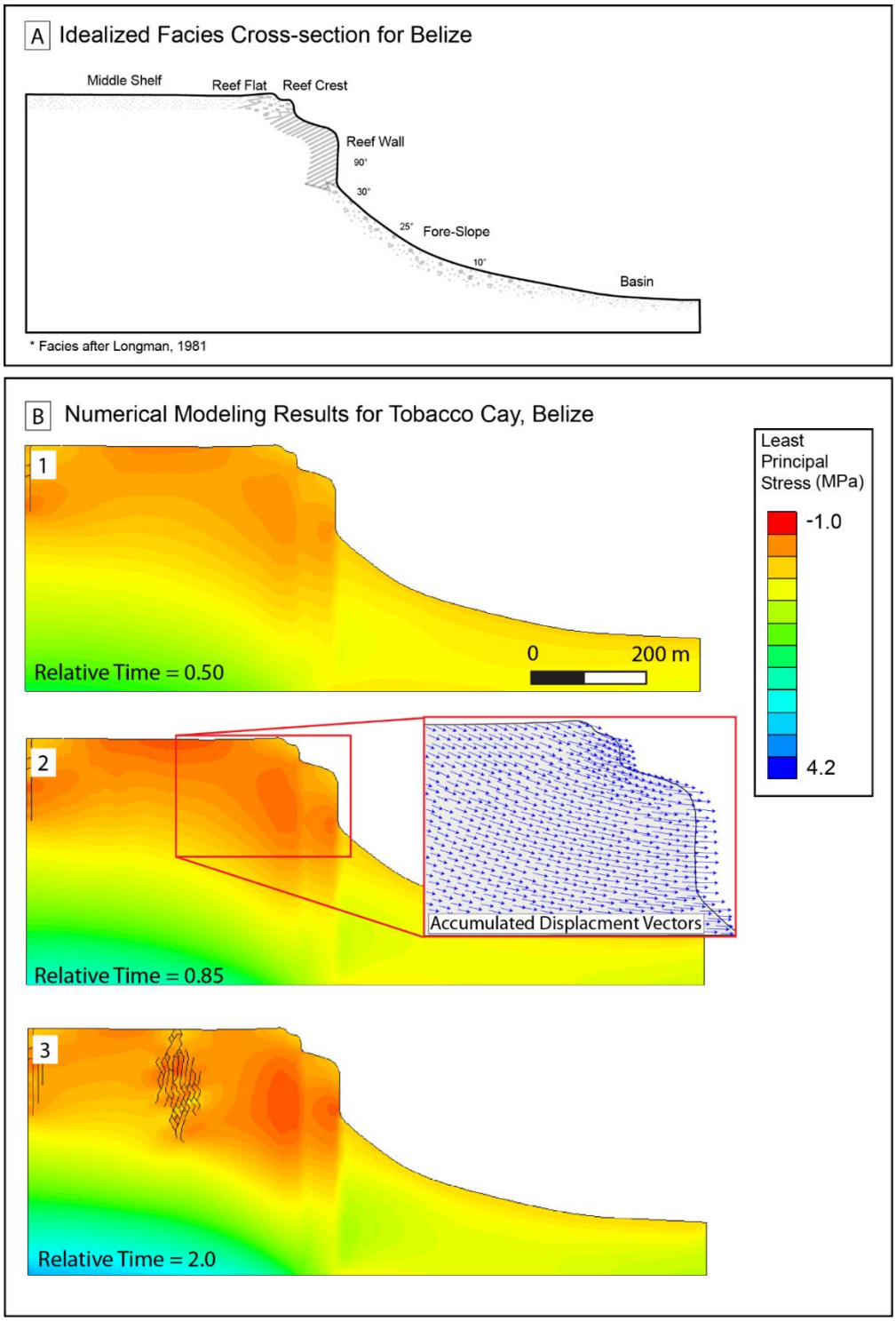
A Idealized Facies Cross-section for Belize
Middle Shelf
Reef Flat
Reef Crest
Reef Wall
90°
30°
25°
Fore-Slope
10°
Basin
* Facies after Longman, 1981
B Numerical Modeling Results for Tobacco Cay, Belize
Least Principal Stress (MPa)
-1.0
4.2
1
Relative Time = 0.50
0
200 m
2
Accumulated Displacment Vectors
Relative Time = 0.85
3
Relative Time = 2.0

Figure 3.5.

Figure 3.5. Numerical modeling results for Tobacco Cay Belize. A) Line drawing of the Tobacco Cay shelf margin profile with relevant facies distributions. B) Numerical modeling results where a tensile stress state has developed at the shelf edge and platform interior. B.1) The relative intensity of the tensile stress state is increasing. The accumulated displacement vectors at the platform margin highlight the volume of rock at the shelf edge is moving down and away, towards the basin. B.2) upon completion of the model run, the tensile strength of the material is exceeded in the platform interior and fracturing occurs. Fracture on the far left of the model are a model artifact dude to being constrained in that location.

Capitan Profile, Guadalupe Mountains, West Texas

Similar to the numerical models of Tobacco Cay, the models representing the Capitan profile (G25 high frequency sequence) geometry show regions of tensile stress state (negative least principal stress values) in the platform interior and shelf edge/reef wall (Fig. 3.6A). These regions continue to intensify with the gradual application of gravity (Fig. 3.6B). The stress distributions at the shelf edge mirror the topographic expression for the Capitan profile, where the model sharply transitions from regions under tension (warm contour colors) at the platform interior and shelf edge/ reef wall to regions under compression (cool contour colors) at the slope and basin. The orientation and relative magnitudes of the maximum and minimum principal stresses at, and directly below, the reef wall, indicate that this locale is under a tensile stress state in which the principal maximum stress is oriented in the vertical plane and the minimum is oriented in the horizontal plane. However, the transition into the slope yields a change in the stress state (compression) and stress orientation (parallel to the slope's surface expression). On the left-most edge of the model fractures have developed as a byproduct of the model being constrained in the x and y.

Fractures develop within the model as the tensile strength of the material is exceeded by the least principal stress values. They are located just below the reef wall at a 225 m depth (Fig. 3.6C). These fractures are open-mode, tensile fractures that propagate parallel to the maximum principal stress, and open in the perpendicular direction. This is consistent with the orientation of the maximum and minimum stress orientation (Fig. 3.6B). These fractures developed at depth and propagated up to the surface at the reef wall.

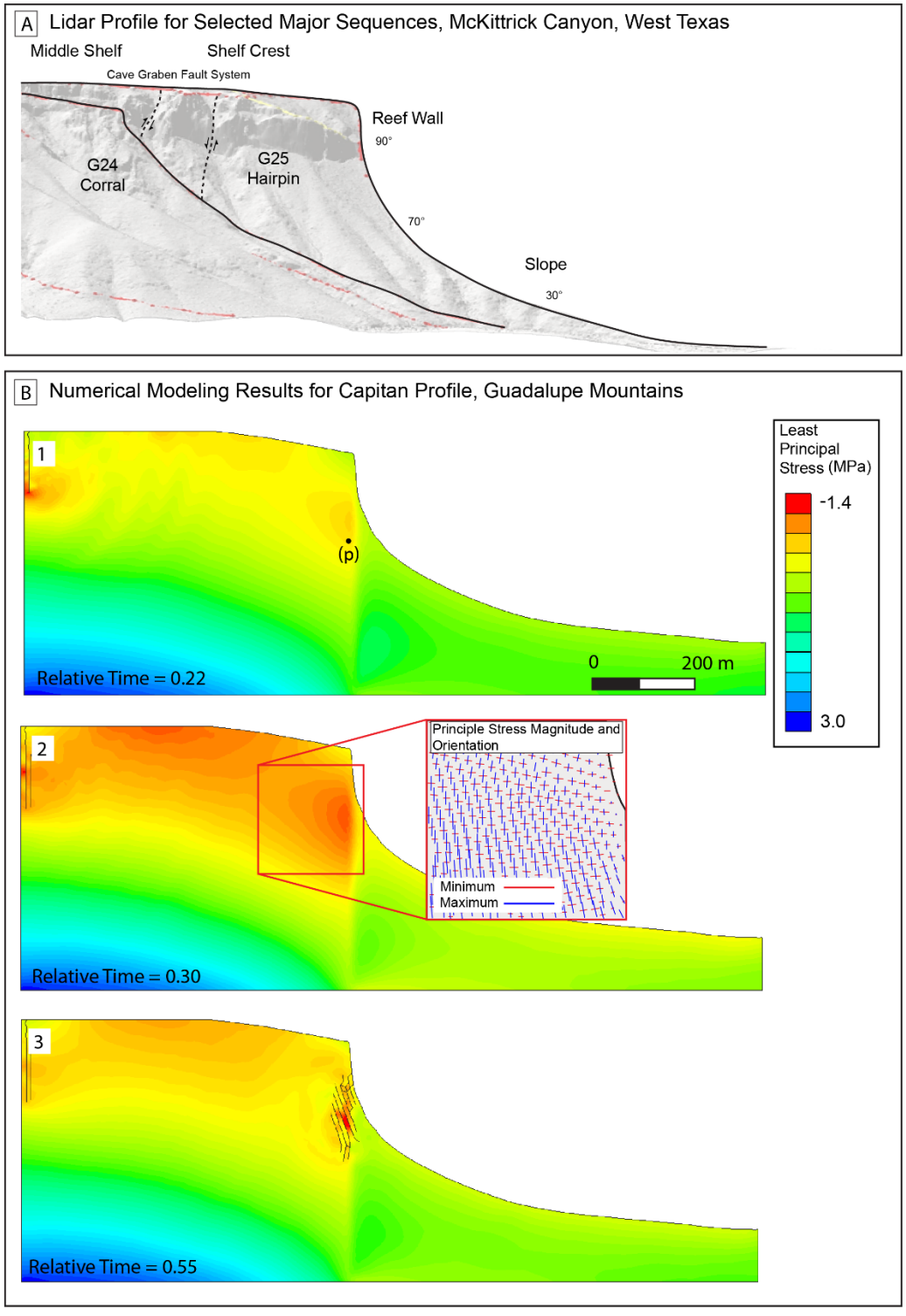
A Lidar Profile for Selected Major Sequences, McKittrick Canyon, West Texas
Middle Shelf
Shelf Crest
Cave Graben Fault System
Reef Wall
90°
G24
Corral
G25
Hairpin
70°
Slope
30°
B Numerical Modeling Results for Capitan Profile, Guadalupe Mountains
Least
Principal
Stress (MPa)
-1.4
3.0
1
(p)
0
200 m
Relative Time = 0.22
2
Principle Stress Magnitude and
Orientation
Minimum
Maximum
Relative Time = 0.30
3
Relative Time = 0.55

Figure 3.6

Figure 3.6. Numerical modeling results for the Guadalupian Capitan profile of the Guadalupe Mountains, West Texas. A) Lidar profile for the G24 and G25 high frequency sequences, McKittrick Canyon, Guadalupe Mountains, West Texas. The presence of the syndepositional Cave Graben Fault System is highlighted. B.1) Upon application of gravity, the platform margin and interior are experiencing a tensile stress state. Point (a) indicates the location of the stress path plot (Figure 2.8). B.2) As gravity is continued to be applied, the shelf edge experiences more negative least principal stress values (i.e. tensile stress state). The orientation of the minimum and maximum stress magnitudes and orientations highlight the shelf margin is likely to fail with the development of vertical fractures that open parallel to the minimum stress direction. B.3) Upon completion of the model run, discrete fractures have developed at the shelf edge and propagate parallel to the maximum stress direction.

Amellago Ramp, Morocco

The numerical modeling results for the Amellago ramp depict a fairly even distribution of least principal stress from the top down (Fig. 3.7). The shallowly dipping carbonate platform experiences regions under tension (negative least principal stress magnitudes) at the surface and quickly transitions into a compressional state (positive least principal stress magnitudes) with depth. The least principal stress values never exceed the tensile strength of the material, therefore no fractures develop.

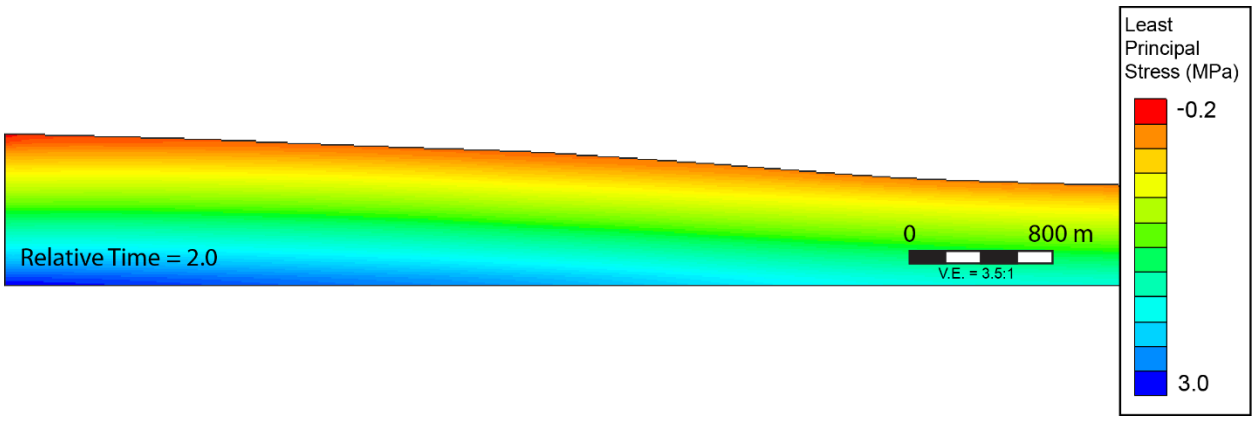

Figure 3.7. Numerical modeling results for The Amellago ramp. Results depict a relatively even distributions of stress across the platform. Vertically exaggerated for illustrations purpose, modeled at a scale of 1:1.

DISCUSSION

Our model results suggest that carbonate platforms characterized by steep, near-vertical reef walls experience tensile, open-mode fracture development while shallowly dipping carbonate platforms (i.e. carbonate ramps) rarely develop any syndepositional deformation features. Our numerical models of carbonate platforms that exhibit high relief with a vertical to near vertical reef wall (Fig. 3.5 & 3.6) have the following in common:

(1) a region at the shelf edge with an elevated tensile stress state; (2) a higher tensile stress state region in the platform interior; and (3) the largest accumulated displacements at the platform margin. Based on our models, these two regions are most likely to deform and develop fractures. These results can be used as a general guideline to predict areas where syndepositional deformation is likely to occur in steep-walled carbonate platforms. In contrast, the Amellago ramp model experiences an even distributions of stress across the low angle ramp with no deformation developed indicating that syndepositional deformation is likely negligible in carbonate ramp systems.

Stress State Controlled by Carbonate Platform Geometry

The three scenarios presented here emphasize the importance of the role that carbonate platform geometry plays in the occurrence of early deformation associated purely with gravitational forces. The comparison between model results of the Amellago ramp (Fig. 3.7) with Tobacco Cay, Belize (Fig. 3.5) or the Capitan profile (Fig. 3.6) shows a striking contrast in the regions prone to early deformation. The Amellago ramp exhibits a shallowly dipping (<2°) slope. The shallowly dipping slope allows the carbonate platform to equilibrate to gravity, i.e. uniform stress conditions. The shallowly dipping slopes are well below the angle of repose for sediments, and thus are gravitationally stable. In contrast, Tobacco Cay and the Capitan profile for the Hairpin high frequency sequence have steep, high-angle slopes and near-vertical reef walls that exceed the angle of repose for loose sediment and are prone to over steepening and gravitational instability. In the Tobacco Cay model, fractures develop in the middle of the shelf in the Tobacco Cay model

(Fig. 3.5B) where the tensile strength of the material has been exceeded by the least principle stress. Similarly, tensile fractures developed at the shelf edge in the Capitan profile after the tensile strength of the material was exceeded by the least principle stress under the sole application of gravity.

The development of fractures in both of these scenarios is best explained by the stress state of the system which is affected by the platform geometry (Fig. 3.2A). In a steep-walled carbonate platform, the volume of rock is able to move outwards towards the basin upon the application of gravity, because there is no lateral confinement (non-uniaxial stress conditions; Fig. 3.2A). As a result, the least principal stress decreases, and can become negative (tensile stress), leading to opening of tensile cracks and gravitational instability. In contrast, a shallowly dipping ramp, such as that depicted here with the Amellago system, provides a fair amount of lateral confinement. Thus, lateral extension is limited and a tensile stress state never develops. The stress conditions for the Amellago ramp are more similar to the stress state for a tectonically stable basin, where stress conditions are uniaxial (Fig. 3.2A).

Stress state and failure behind a steep-walled carbonate platform can be illuminated by plotting the normal and shear stress through time via Mohr's circles for individual time steps throughout the model duration (Fig. 3.8) for point (p) (Fig. 3.6B). The first Mohr's circle, with corresponding pinnacle point A (relative time 0.1) illustrates the model as it is being loaded via gravity, prior to any failure. The positive maximum principal stress represents the increase of the lithostatic load, whereas the negative (tensile) least principal

stress results from the lateral deformation of the rock towards the basin (Fig. 3.2; 3.5B). Moving from Mohr's circle A to B, there is a small increase in maximum principal stress magnitude (gravity increase), and a more significant decrease in least principal stress (lateral extension). This leads to an increase in the diameter of the Mohr's circle, which represents the shear stress component. Hence, the path A to B represents how stresses develop in the system leading up to tensile failure. However, the rock does not fail at point (p) yet. A fracture opens at a different area of the model, causing stress re-distribution and moving the stress state of (p) to Mohr Circle C. As the domain is continued to be loaded via gravity, the previous pattern is repeated: the maximum stress increases and the minimum decreases to higher tensile values (C to D). Eventually, the least principal stress becomes equal to the tensile failure strength, and a crack opens at (a) (D; red Mohr Circle). The fracture opening causes stress redistribution and moves the stress state to E.

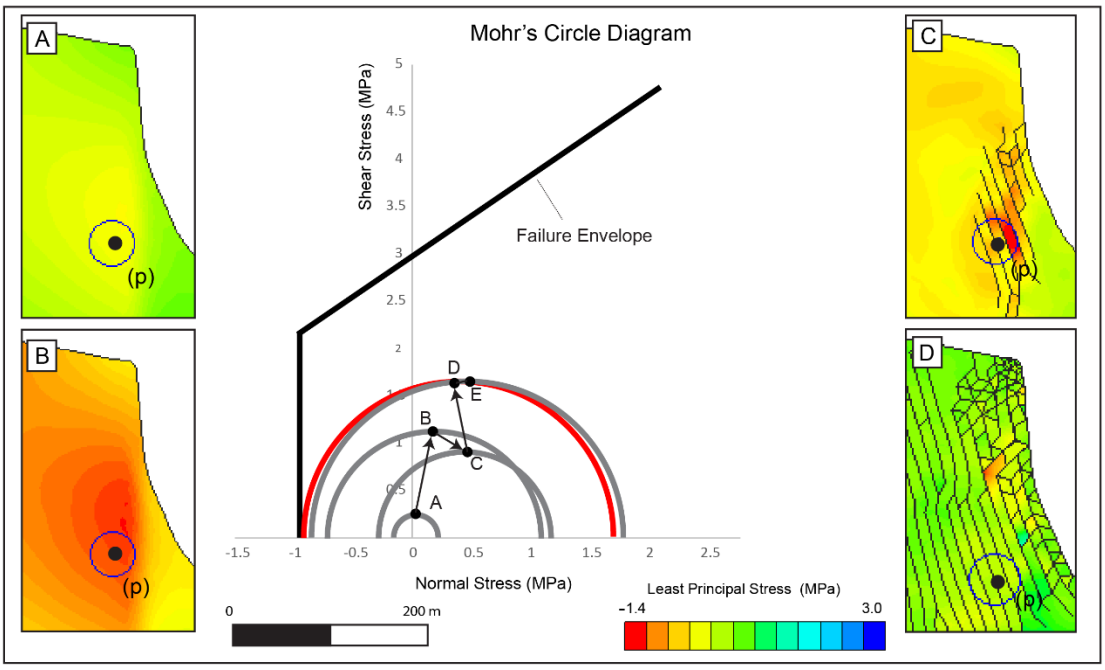

Figure 3.8. Mohr's circles for time steps throughout the duration of the model with corresponding ELFEN plots of the least principal stress. The smallest circle "A" represents the system upon initialization, prior to any failure. Corresponding to inset A. B) details the least principal stress contours for the shelf edge and is prior to any failure. Here Mohr's circle "B" is experiencing a large decrease in least principal stress, with a small increase in the normal stress component; hence an increase in the shear component. Mohr's circle "C" and inset C represent tensile failure at a different point within the shelf edge. This failure causes stress redistribution that moves the Mohr Circle to the right. Upon continuation of the application of gravity, the least principal stress for Mohr's circle "D" reaches the tensile failure envelope and fracturing occurs. This failure causes stress redistribution that moves the Mohr Circle to the right ("E"). Mohr's circle "E" is post failure at the shelf edge, where the shear stress component is maintained and the normal stresses increase.

Additionally, the stress state of the system can be investigated by tracking how mean and differential (shear) stresses change over the geologic history (stress path plot; Fig. 3.9) for point (p) at the shelf edge (Fig. 3.6A). A stress path plots the pinnacle of the

Mohr circle representing the stress state at any time during the history of the system (e.g., points A-E in Figure 3.9 correspond to the pinnacle points on the individual Mohr's circles in Figure 3.8). As the gravitational load is initially applied, the mean stress of point (p) at the shelf edge is in compression (point A in Fig. 3.9). Point B represents the system prior to failure at the shelf edge, showing the significant increase in shear (diameter of the Mohr circle in Fig. 3.8). Following failure elsewhere in the system and subsequent stress redistribution, the differential stress decreases and the mean stress increases (point C). Upon the continuation of the application of the gravitational load, the differential stress increases (points D & E). This stress path illustrates that the mean stress for point (a) remains compressive. In addition, even though the point experiences tensile failure (at time D), it is clear from the stress path plot (Fig. 3.9) that at any point during the model duration shear stresses remain much lower than the Mohr-Coulomb shear failure envelope.

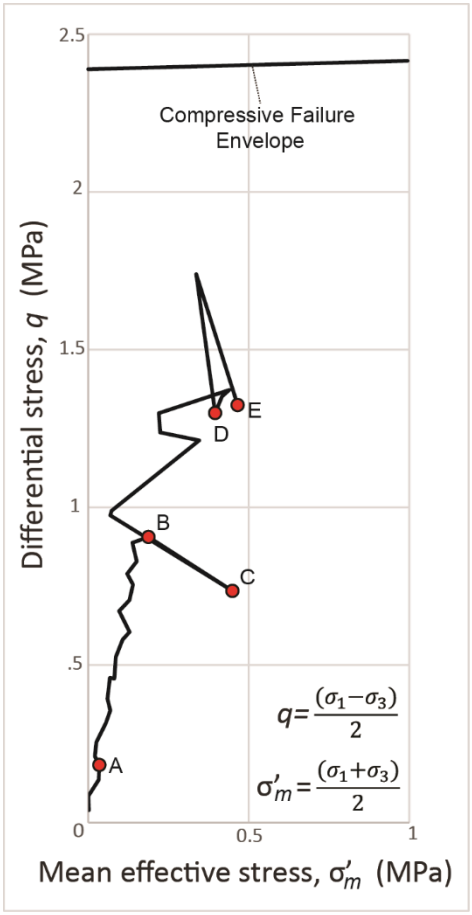

Figure 3.9. Capitan profile model: change in mean stress and differential stress with time (stress path) for point (p) in Figure 3.6 at the platform margin. The decrease in least principal stress (Fig. 3.8) increases significantly the differential stress from point A to point B (i.e. a larger Mohr Circle diameter), while the mean stress remains in compression. Opening of fractures elsewhere in the shelf causes decrease in shear and increase in mean stress (B to C). Continuation of gravitational loading causes decrease in least principal stress and increase in maximum principal, resulting in higher differential stress (C to D, E). Point D represents the instance of tensile failure for material point (p). Post failure stress redistribution leads to stress state E where the differential stress component remains constant and mean effective stress increases slightly. Note that the mean stress remains compressional throughout the process and differential stress remains lower than the shear strength.

Predicting Deformation: Examples from the Guadalupe Mountains

Syndepositional fractures and faults have been widely documented in the Capitan system of the Guadalupe Mountains as an important control on stratigraphic architecture and platform growth patterns through time (Hunt et al., 2002; Koša and Hunt, 2005; Rush and Kerans, 2010; Hunt et al., 2012; Mathisen, 2014; Smith and Kerans, 2017). Syndepositional, margin-parallel fractures and faults have been documented throughout outcrops in the Guadalupe Mountains (King, 1948). The faults are typically steeply dipping, have significant offset, and are associated with growth strata (Hunt et al., 2002; Koša and Hunt, 2005; Mathisen, 2014). The majority of faults and fractures in the Capitan profile are centralized within close proximity to the shelf edge with only minor faulting present in the platform interior (Hunt et al., 1995; Tinker, 1998; Hunt and Fitchen, 1999; Hunt et al., 2002; Rush and Kerans, 2010; Mathisen, 2014), a distribution that closely matches our numerically modeled predictions. Much of the previous work done in the Guadalupe Mountains interpreted differential compaction of basinal sediments to be a first order control on the development of syndepositional deformation (Hunt et al., 1995; Hunt et al., 1996; Saller, 1996; Hunt and Fitchen, 1999; Longley, 1999; Hunt et al., 2002; Koša and Hunt, 2005; Rush and Kerans, 2010). However, this work demonstrates that syndepositional deformation can develop in the absence of compaction. The two zones of deformation (Fig.3.6B) materialize solely as a byproduct of the lack of confining stress while equilibrating the model to gravitational forces, emphasizing that open-mode fractures and normal faults documented in steep-walled carbonate platforms are likely syndepositional/synsedimentary in origin.

Modification by gravitational processes is a significantly underappreciated driver of platform architecture. Steep-walled carbonate platform margins under tension are commonly modified by collapse processes from the lack of lateral confinement in the basinward direction, facilitating the development of vertical to sub-vertical reef walls. The development of a vertical reef wall is often marked by a foreslope that is composed of reef blocks and talus deposits, suggesting they are continually modified by repeated collapse (Enos and Moore, 1983; Grammer et al., 1993a; Kerans and Tinker, 1999). Gravitational processes are critical to the development and maintenance of a vertical to sub-vertical reef wall in steep-walled carbonate platform systems. Repeated gravitational failure of the shelf margin is an intrinsic process controlling platform development and facies distribution.

Limitations of Numerical Modeling

While our numerical models have aided in evaluating the control that carbonate platform geometry has on the development of early deformation, there are several limitations to our approach. These models utilize a single set of rock properties that do not change with time or depth, which enabled us to isolate the effects of platform geometry on deformation. However, this simplification does not accurately capture the heterogeneities in facies and rock properties in carbonates platforms. It also does not allow one to ascertain how changes in rock type and juxtaposition of facies with different rock properties may affect the development of deformation.

The use of 2D cross-sections for the three carbonate platforms within the numerical models limits our ability to capture along-strike variability with regards to shelf margin

geometry and deformation. The large scale of our models also prevents capture of the small-scale details present in carbonate platforms, such as wave cut notches and slight changes in topography. The use of the modified Mohr-Coulomb constitutive law allows us to accurately capture tensile and shear brittle failure, but does not simulate compaction or ductile-related deformation. These simplifications are made to test and isolate the effects of changes in platform geometry upon deformation and to keep computation time to a minimum, but must be considered when interpreting the modeling results.

CONCLUSIONS

The effects of variations in platform geometry upon the development of syndepositional deformation was investigated with finite element numerical inelastic models of three carbonate platform profiles. Our model results yield insights into the effects that carbonate platform geometry have on the development of early deformation and can be used as a guideline to predict areas where deformation is likely to occur. Carbonate platforms characterized by vertical reef walls are predisposed to failure under tensile stress state Where the manifestation of a near-vertical to vertical reef wall combined with the lack of lateral confining stress facilitates the development of these tensile regions, which are susceptible to failure. A tensile stress state and subsequent fracturing develop under the sole application of gravity with no additional loading or burial. This highlights the synsedimentary origin of deformation, demonstrating that syndepositional deformation can and likely does develop in the absence of differential compaction. These results suggest that carbonate platforms that have a vertical to near-vertical reef wall and steep angle slopes

are routinely modified by syndepositional deformation. We emphasize that zones of tensile stress state and ensuing brittle, tensile failure are fundamental elements of steep-walled carbonate platform systems.

Chapter 4: Effect of Variable Progradation to Aggradation Ratio and Facies Partitioning on the Development of Syndepositional Deformation: Insights From Numerical Modeling

INTRODUCTION

Syndepositional deformation is widely recognized in steep-walled carbonate platforms worldwide including, but not limited to, the Devonian of Western Australia, (Playford et al., 1984; Kerans, 1985; Hurley, 1986; Frost and Kerans, 2009, 2010) the Carboniferous of Spain and Kazakhstan (Porta et al., 2004; Carpenter et al., 2006; Collins et al., 2006; Narr et al., 2008) ,the Permian of New Mexico and West Texas (Hunt et al., 1995; Hunt et al., 1996; Hunt and Fitchen, 1999; Hunt et al., 2002; Koša and Hunt, 2005; Resor and Flodin, 2010; Rush and Kerans, 2010; Frost et al., 2012; Hunt et al., 2012), the Triassic of Italy (Berra, 2012), and the Quaternary of the Bahamas and British West Indies (Wanless and Dravis, 1989; Grammer et al., 1993a; Aby, 1994; Guidry et al., 2007). Frame-building biota and associated early marine cementation at the platform edge can develop and maintain vertical to sub vertical reef walls and steep upper slope angles (Ginsburg, 1957; Shinn, 1969; Ginsburg and James, 1974; Land and Moore, 1977; Read, 1985; Grammer et al., 1999; Pomar, 2001). As a consequence of the high relief and the brittle nature of reef and upper slope facies in these settings, syndepositional fractures and faults are common.

Syndepositional fractures generally develop as large, vertically and laterally extensive open mode (Mode I) tensile fractures (i.e. Neptunian dikes) and normal faults, that develop parallel to the shelf margin (Fig. 4.1) (Hunt et al., 2003; Frost and Kerans, 2010), with documented fracture apertures up to 2 m (Frost and Kerans, 2010). These deformation features develop prior to significant burial and are commonly unrelated to regional tectonic drivers (Koša et al., 2003; Frost and Kerans, 2009, 2010; Resor and Flodin, 2010; Berra, 2012). These early formed fractures are intrinsic in steep-walled carbonate platforms systems, often affecting platform architecture evolution and geometry (Kerans and Tinker, 1999; Frost and Kerans, 2009, 2010; Rush and Kerans, 2010). Commonly, they are associated with fracture fill and diagenetic halos in the rock record, indicating that open fractures act as conduits for early and late fluid flow (Kerans, 1985; Whitaker et al., 1997; Hunt et al., 2002; Stanton and Pray, 2004; Frost et al., 2012; Budd et al., 2013; Mathisen, 2014; Simon, 2014) and can significantly affect carbonate reservoir quality (Carpenter et al., 2006; Collins et al., 2006; Narr et al., 2008; Ronchi et al., 2010).

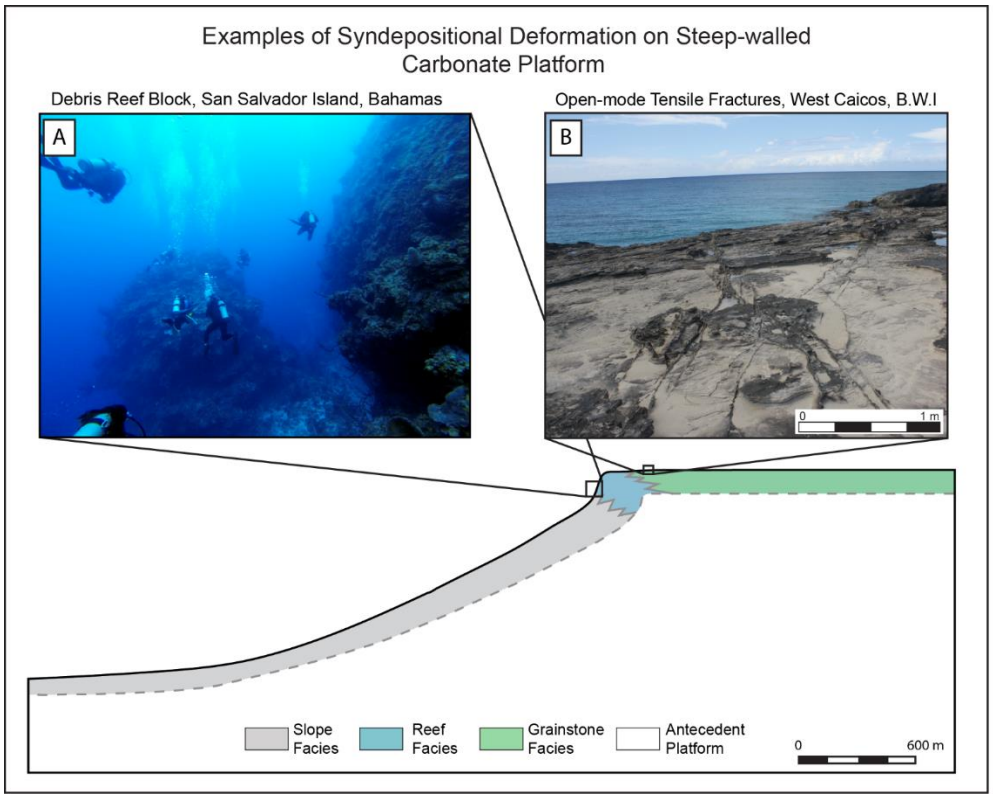

Figure 4.1 Syndepositional deformation examples from the Quaternary with relative location on schematic carbonate platform of each deformation feature. A) Examples of a modern spalled reef debris block off the steep-walled western margin of San Salvador Island, Bahamas. B) Margin parallel, open-mode syndepositional fractures on the Island of West Caicos, B.W.I.

Despite the prevalence and importance of syndepositional deformation features in steep-walled carbonate platform systems, the controls behind their development and distribution are still poorly understood. These processes are poorly understood because the scale over which they happen, the prevalence for their continued deformation and alteration through time, and the difficulty identifying individual mechanisms and their byproducts is challenging. Previous work has highlighted the relationship between stratigraphic architecture and syndepositional fractures, documenting high concentrations of fractures centralized at the shelf-edge (Playford et al., 1984; Frost and Kerans, 2009, 2010; Rush

and Kerans, 2010; Harman, 2011; Mathisen, 2014). While there have been many proposed drivers behind the development of syndepositional deformation, differential compaction of mud-rich basinal sediments is one of the most commonly proposed mechanisms (Hunt et al., 1996; Hunt et al., 1995; Hunt and Fitchen, 1999; Hunt et al., 2002; Koša and Hunt, 2005; Longley, 1999; Rush and Kerans, 2010; Saller, 1996). However, very little work has been done to exactly pinpoint the exact mechanisms driving the development of syndepositional deformation. Here, we examine the effect of variable progradation/aggradation (P/A) ratios and facies partitioning upon the development of syndepositional deformation in steep-walled carbonate platforms. We hypothesize that P/A ratio and facies partitioning are first order controls on the development of syndepositional deformation. Forward numerical modeling techniques are used to simulate these two controls and associated processes, facilitating better analysis of specific patterns of syndepositional deformation that develop as a result.

PREVIOUS NUMERICAL MODELING EFFORTS

There have been multiple incursions into numerical modeling of syndepositional deformation and their associated processes. Work identifying potential drivers on the development of syndepositional deformation documented in the Miaella Carbonate platform of the central Apennines Italy was carried out by Rusciadelli et al. (2003; 2007). Using 2D numerical models, Rusciadelli et al. (2003) identified earthquake swarms from active faulting as the likely mechanism triggering large scale platform margin collapse. Variations in static sea-level were unable to initiate large scale margin collapse, but may

predispose carbonate platform systems to later deformation. Resor and Flodin (2010) constructed 2D elastic numerical models to test the effect of variable P/A ratio on the likelihood of development of syndepositional deformation. Their model results suggested that deformation is most likely to occur in the platform interior due to differential subsidence while likely deformation at the shelf edge was indicated by positive tensile stress state. They highlight model results from a scenario that is highly progradational (P/A = 10), which best resembles the stratal geometries and deformation of the Permian Capitan depositional system of the Guadalupe Mountains, West Texas.

More recently, work by Nolting et al. (2017a) identified platform geometry as a first order control on the development of syndepositional deformation in carbonate platform systems using 2D numerical modeling. Model results suggest carbonate platforms that have a vertical to sub vertical reef wall develop significant syndepositional deformation at the shelf edge in the form of discrete, open mode fractures. This deformation is attributed to a tensile stress state that develops due to the platform geometry and from the lack of a lithostatic confining stress in the seaward direction leading to gravitational instability. However, the relationship between the development of discrete failures and changes in platform P/A ratio and facies partitioning has not been explicitly investigated.

GEOMECHANICAL MODELS

Four models were constructed using ELFEN®, a finite-discrete element numerical modeling software (Rockfield, 2010). Quasi-static Lagrangian formulation and adaptive

remeshing were used in each model. When deformation is substantial and distorts individual elements, the model automatically remeshes. This allows for the realistic simulation and evolution of deformation while maintaining the integrity of the model calculations. The first set of models evaluated the effects of changes in P/A ratio on the development of syndepositional deformation. The second set of models investigated facies partitioning with respect to rock property heterogeneity and its link to syndepositional deformation.

We employed an inelastic constitutive law (failure criteria) which supports both continuum and discontinuum analysis methods. This permits interactions of stresses through time and dissipation of stresses following the development of discrete failure(s). A modified Mohr-Coulomb constitutive law with a Rankine tensile corner was chosen because it supports brittle, tensile failure, the most common expression of syndepositional deformation in outcrop. Tensile, open mode failure occurs within the models when the tensile strength (T_o) of the prescribed material is exceeded by the least principal stress (σ_3). The modification by the Rankine corner allows tensile failure to be accurately captured within the models while considering the stress state of the system as a whole.

A stepwise model was utilized to apply gravity gradually over a specified number of time steps in order to ensure that the model remained computationally stable and able to reach equilibrium. Model conditions were set up to simulate a normal faulting stress state, with gravity representing the maximum (vertical) principal stress during initialization. The *in situ* confining stresses represent the least principal stress and were assigned as 0.7 of the gravitational load. A pore pressure gradient was applied to all models with a zero datum at

the top of the model, and increasing with increased depth. Pore pressure was held constant through the duration of all models. All simulations represent drained conditions. A bumper was used in each model to help dampen and absorb the inertial effects present from the application of gravity. It was used around the edges and the bottom of the model and was constrained in the X and Y direction. A triangular mesh, ranging in size from 5 to 30 meters, was used in all of the models. The finer mesh was used in locations most susceptible to deformation, grading into larger mesh. This distribution of mesh sizes was chosen because it helps maintain reasonable computation times, while allowing small scale features to be captured within the models. In the facies models, a mesh density region with 2 m elements is used around the platform margin to capture fracturing and reduce computation time.

All scenarios used a geometry modeled after the steep-walled margin on the west side of West Caicos Island, British West Indies (Fig. 4.2). The initial geometry was constructed using a combination of bathymetry data, sounding points, and field observations (noaa.com). P/A ratios were constrained with data from the Permian Capitan system of the Guadalupe Mountains, West Texas (Kerans and Tinker, 1999). Because syndepositional deformation is defined by deformation occurring contemporaneously with or shortly after deposition, we employed rock properties collected from various facies preserved on the Pleistocene island of West Caicos, B.W.I. These rock properties closely represent a lithified analog that has undergone little to no burial and is relatively free from late diagenetic overprint. In the first set of models, a single set of rock properties was used for the underlying antecedent topography, with a different, second set used for the overlying sequence (Fig. 4.2) (Table 4.1). The rock properties were distributed

homogenously within the two domains. The progradation scenario utilized a P/A ratio of 8 (Fig. 4.2A), while the aggradational scenario utilized a P/A ratio of 0.2 (Fig. 4.2B). In the second set of models, which used the same geometry and P/A ratios as the previous models, the antecedent shelf margin was assigned one homogenously distributed set of rock properties and the overlying sequence was broken down into typical facies tracts with corresponding rock properties (Fig. 4.2C) (Table 4.2). The contact between facies is a sharp contact with no inter-fingering of rock types, such thatreef facies are juxtaposed with platform top and slope facies. The contact between the underlying platform and the overlying sequence was designated as a surface that was permitted to slip (i.e. layer parallel slip), with a coefficient of friction of 0.7 and cohesion of 7 MPa.

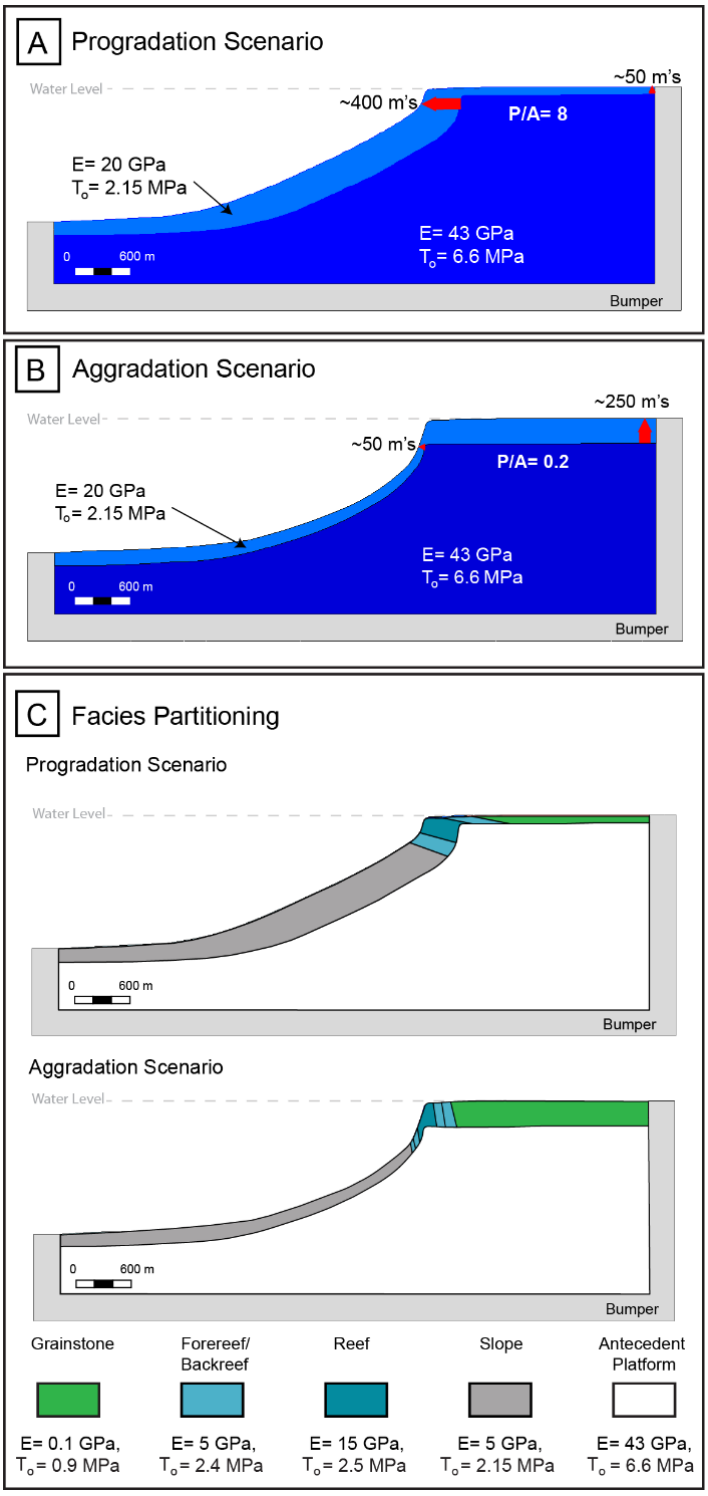
A
Progradation Scenario
Water Level
~50 m's
~400 m's
P/A= 8
E= 20 GPa
T$_o$= 2.15 MPa
E= 43 GPa
T$_o$= 6.6 MPa
0
600 m
Bumper
B
Aggradation Scenario
Water Level
~250 m's
~50 m's
P/A= 0.2
E= 20 GPa
T$_o$= 2.15 MPa
E= 43 GPa
T$_o$= 6.6 MPa
0
600 m
Bumper
C
Facies Partitioning
Progradation Scenario
Water Level
0
600 m
Bumper
Aggradation Scenario
Water Level
0
600 m
Bumper
Grainstone
Forereef/ Backreef
Reef
Slope
Antecedent Platform
E= 0.1 GPa, T$_o$= 0.9 MPa
E= 5 GPa, T$_o$= 2.4 MPa
E= 15 GPa, T$_o$= 2.5 MPa
E= 5 GPa, T$_o$= 2.15 MPa
E= 43 GPa, T$_o$= 6.6 MPa

Figure 4.2

Figure 4.2. Model set-up for the numerical models, including variable P/A ratio and facies tracts. (A) Steep-walled carbonate platform geometry used in numerical model. Antecedent platform has a single set of rock properties distributed homogeneously throughout (Table 1.) The overlying sequence, which progrades 400 meters and aggrades only 50 meters (P/A = 8) has a single set of rock properties (different from the underlying platform) (Table 1.) Pore pressure is applied to the top of the domain and changes with depth. (B) Aggradation numerical modeling scenario, where the overlying sequence aggrades 250 meters and progrades only 50 (P/A = 0.2). The rock properties and their distribution are the same as in the previous model. Pore pressure gradient is applied to the top of the mode. (C) Input geometries (same as previous) and facies tracts location. Rock properties for the given facies tracts are detailed in Table 2. Within with facies tract, the rock properties are distributed homogeneously (i.e. no inter-fingering). Pore pressure is applied to the top of each model and does not change with time but does vary with depth. No vertical exaggeration present in any of the geometries and their subsequent numerical models.

Parameter		Second Sequence	Antecedent Platform
	Unit	Value	Value
Young's Modulus, E	MPa	13,221	32,940
Poisson's Ratio, ν	-	0.30	0.25
Cohesion, C_o	MPa	3.0	22
Friction Angle	°	37.0	35
Tensile Strength, T_o	MPa	0.9	6.6
Fracture Energy, G_f	MPa*m	$1.32e^{-6}$	$2.14e^{-5}$
Fracture Toughness, K_{ic}	MPa*$\sqrt{m}$	$1.31e^{-1}$	$9.59e^{-1}$

Table 4.1. Rock Properties used in first set of numerical models

Parameter		Antecedent Platform	Grainstone	Forereef/ Backreef	Reef	Slope
	Unit	Value	Value	Value	Value	Value
Young's Modulus, E	MPa	32,940	100	5,000	15,000	5,000
Poisson's Ratio, ν	-	0.25	0.30	0.27	0.26	0.27
Cohesion, C_o	MPa	22	3.0	7	40	7
Friction Angle	°	35	37.0	37	37	37
Tensile Strength, T_o	MPa	6.6	0.9	2.25	2.5	2.15
Fracture Energy, G_f	MPa*m	$2.14e^{-5}$	$1.32e^{-6}$	$4.44e^{-6}$	$1.39e^{-5}$	$4.44e^{-6}$
Fracture Toughness, K_{ic}	MPa*$\sqrt{m}$	$9.59e^{-1}$	$1.31e^{-1}$	$4.5e^{-1}$	$7.27e^{-1}$	$4.5e^{-1}$

Table 4.2. Rock Properties used in numerical models with variable P/A ratio and facies tracts

RESULTS

In the following section we present results for the variable P/A ratio and facies partitioning model scenarios. Results are contoured by least principal stress distributions. Following geologic convention, negative values indicate tension and positive values indicate compression. Locales with the most negative stress values are likely to fail in

tension through the development of open-mode fractures and normal faults. Orientations of the principal stresses are designated with arrows, where red arrows indicate the magnitude and orientation of the least principal stress and blue arrows indicate the magnitude and orientation of the maximum principal stress.

Progradation vs. Aggradation Scenarios

Progradation (P/A = 8)

Upon the gradual application of gravity (at time step 0.60), a tensile stress state has developed at the shelf edge, in both the antecedent platform and the overlying sequence (Fig. 4.3). An additional tensile stress state has developed in the platform interior at the interface between the overlying sequence and the underlying topography (Fig. 4.3A). As time progresses the tensile strength of the material is exceeded in the overlying sequence and discrete fractures occur at the shelf edge (Fig. 4.3B). The orientations of the principal stresses vectors at the shelf edge show that the stress's orientation mirrors the topographic expression of the shelf margin. Fractures develop where the principal stresses are predominately tensile. The accumulated displacement vectors (arrow length is proportional to the amount of accumulated displacement), highlight basinward displacement of the rock volume at the shelf edge. The magnitude of the accumulated displacement vectors increases at the shelf edge, illustrating increased displacements at the shelf edge in comparison to the platform interior.

The completed model exhibits localized discrete fractures at the shelf edge (Fig. 4.3C). Fractures have occurred in the weaker overlying sequence and have propagated

downward into the underlying platform. This location on the platform has the most tensile least principal stress values, which result in the development of open-mode tensile fractures. Here, the fractures propagate primarily in the vertical plane, oriented parallel to the maximum principal stress direction, and open in the horizontal plane, parallel to the least principal stress.

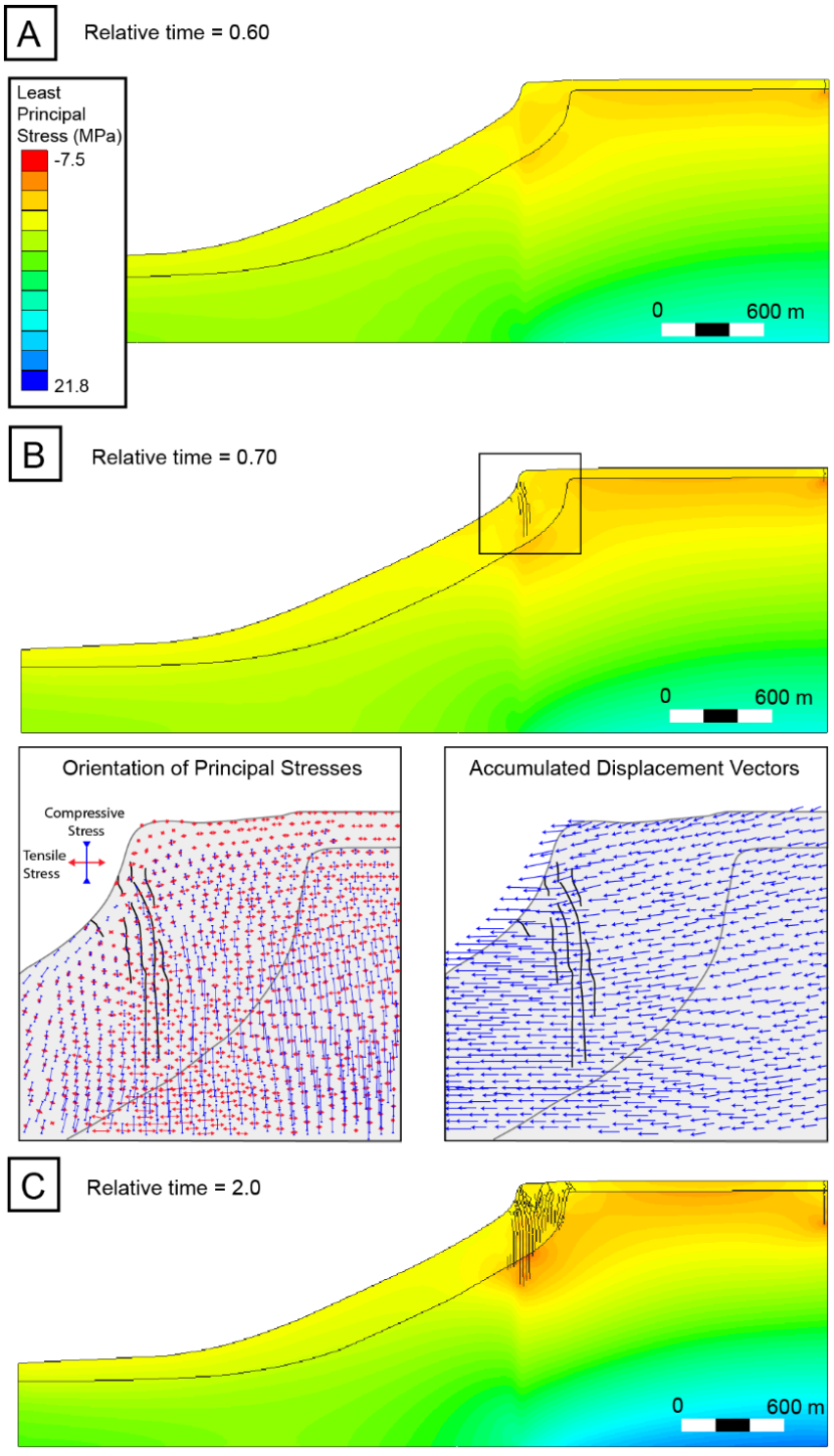
A
Relative time = 0.60
Least Principal Stress (MPa)
-7.5
21.8
0
600 m
B
Relative time = 0.70
0
600 m
Orientation of Principal Stresses
Compressive Stress
Tensile Stress
Accumulated Displacement Vectors
C
Relative time = 2.0
0
600 m

Figure 4.3

Figure 4.3. Numerical modeling results for the progradational model scenario. (A) As gravity is gradually applied, a tensile stress state (designated by the hot colors) develops in front of the antecedent shelf margin, where the over burden column is the thickest. A tensile stress state also develops in the platform interior at the boundary between the underlying platform and overlying sequence. (B) With continued application of gravity, fractures develop in front of the underlying platform margin, in the thickest section of overburden. The principal stresses orientation and magnitude highlight that much of the surface of the second sequence is in tension, where the fractures are developing parallel to the maximum principal stress orientation. The accumulated displacement vectors highlight that the greatest amount of relative displacement has occurred at the shelf edge, where the volume of rock is moving basinward. (C) Upon completion of the model run, a high concentration of fractures have developed in front of the underlying platform margin, propagating towards the free surface and down into the antecedent platforms slope.

Aggradation (P/A = 0.2)

At relative time step 0.67, a tensile stress state has developed at the shelf edge of the underlying antecedent shelf margin (Fig. 4.4). The least principal stress contours mirror the topographic expression of the antecedent shelf margin (Fig. 4.4A). As the platform continues to be loaded via gravity, the tensile strength of the material is exceeded and discrete fractures develop in the platform interior (Fig. 4.3B). The fractures develop at the surface and propagate down until encountering the antecedent platform, which represents a mechanical stratigraphy boundary. Inspection of the orientation of principal stresses and the accumulated displacement vectors at the shelf edge depict a tensile stress state (Fig. 4.4B inset). However, no fracturing has occurred because neither the tensile strength of the antecedent margin nor the overlying sequence has been exceeded. Accumulated displacement vectors exhibit the greatest amount of displacement at the shelf edge. Longest arrows occur at the shelf edge, where the volume of rock is moving basinward. Surface conditions at the shelf edge are in tension as indicated by the principal stress orientations and magnitudes.

Upon completion of the numerical model, discrete fractures have developed across the platform interior and at the shelf edge in the overlying, weaker sequence (Fig. 4.4C). The fractures that develop in these locations are open-mode tensile fractures propagating parallel to the maximum principal stress and opening parallel to the minimum principal stress. The tensile strength of the underlying antecedent shelf margin is never exceeded and therefore never fractures. In this scenario, fractures develop at the surface and

propagate downward until the mechanical stratigraphy boundary of the underlying platform is encountered, where fracture propagation is arrested.

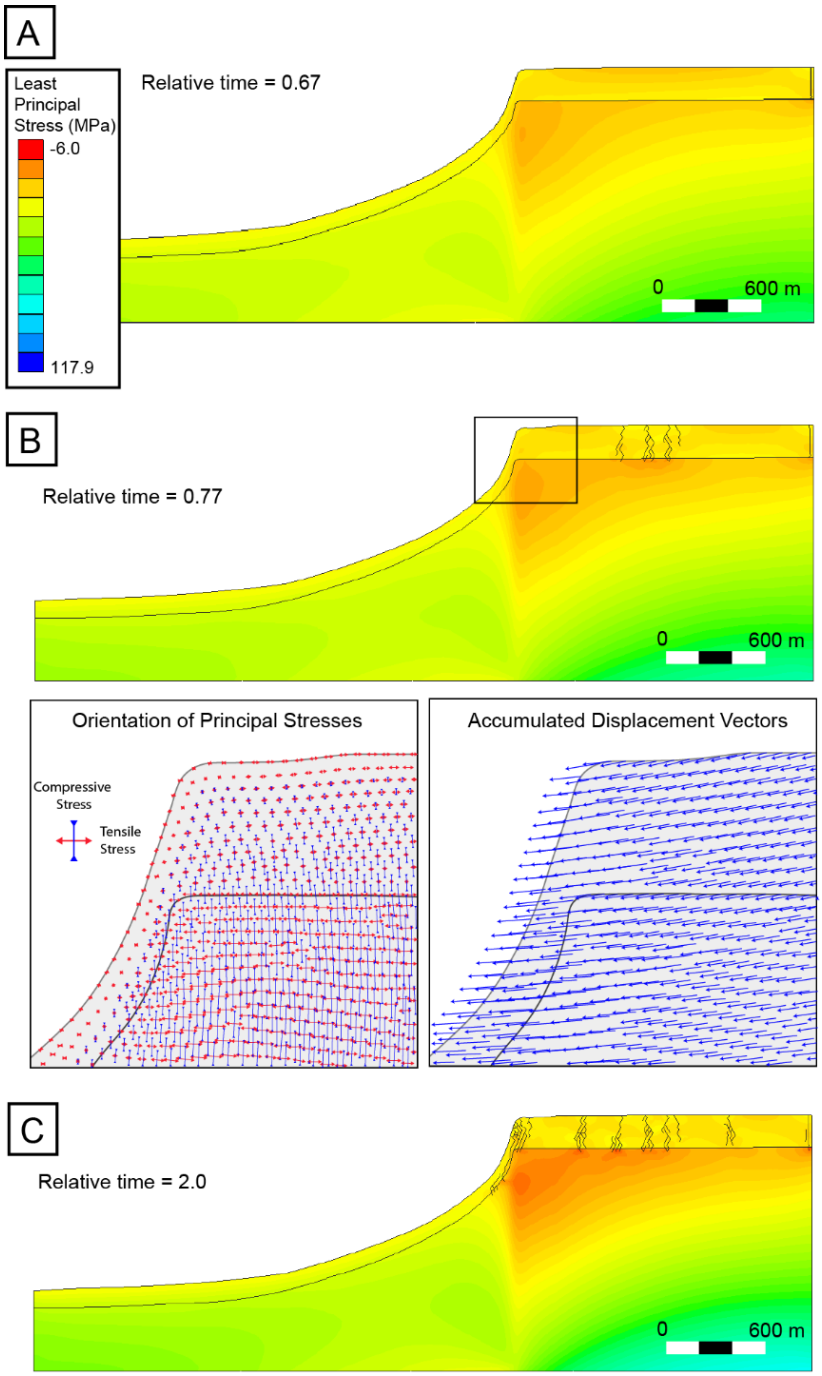

Figure 4.4.

Figure 4.4. Numerical modeling results for the aggradation scenario (P/A = 0.2). (A) as gravity is slowly applied, a tensile stress state develops in the shelf edge of the underlying platform. (B) The magnitudes of the least principal stress value in the antecedent's shelf edge continues to become more negative with the continued application of gravity. Despite the tensile stress state developing in the underlying shelf margin, the tensile strength of the overlying sequences is exceeded in the platform interior and discrete fractures develop that propagate in the vertical plane. The orientation and the relative magnitude of the principal stresses, as well as the accumulated displacement vectors display a trend similar to the highly progradational model. Where the surface conditions and the platform margin are in a tensile stress state. Additionally, the platform margin has the greatest amount of accumulated displacement. (C) Fractures have developed all across the platform top and at the shelf edge by the end of the model run. While a tensile stress state is still present at the shelf margin of the underlying platform.

Facies Modeling

In the model that is highly progradational (P/A = 8), a high concentration of fractures have developed in the reef facies at the shelf edge in front of the antecedent shelf margin where the overburden column is thickest (Fig. 4.5A). This location also corresponds to an increase in Young's modulus (proxy for brittleness), facilitating failure. The fractures initiate at the boundary between the underlying antecedent topography and the overlying sequence and propagate up to the free surface and down into the higher-strength underlying shelf margin. The facies tracts work as mechanical stratigraphy boundaries and retard fracturing in areas of low Young's modulus (i.e. the slope and platform interior).

Inspection of the orientation and relative magnitude of the principal stresses demonstrates that a tensile stress state exists at the shelf edge. This corresponds with the locations of discrete fractures. Additionally, the orientation of the principal stresses at near-surface conditions mirrors the topographic expression. The fractures that develop on the left side of the model are a boundary effect caused by constraining the displacement at the edge of the model.

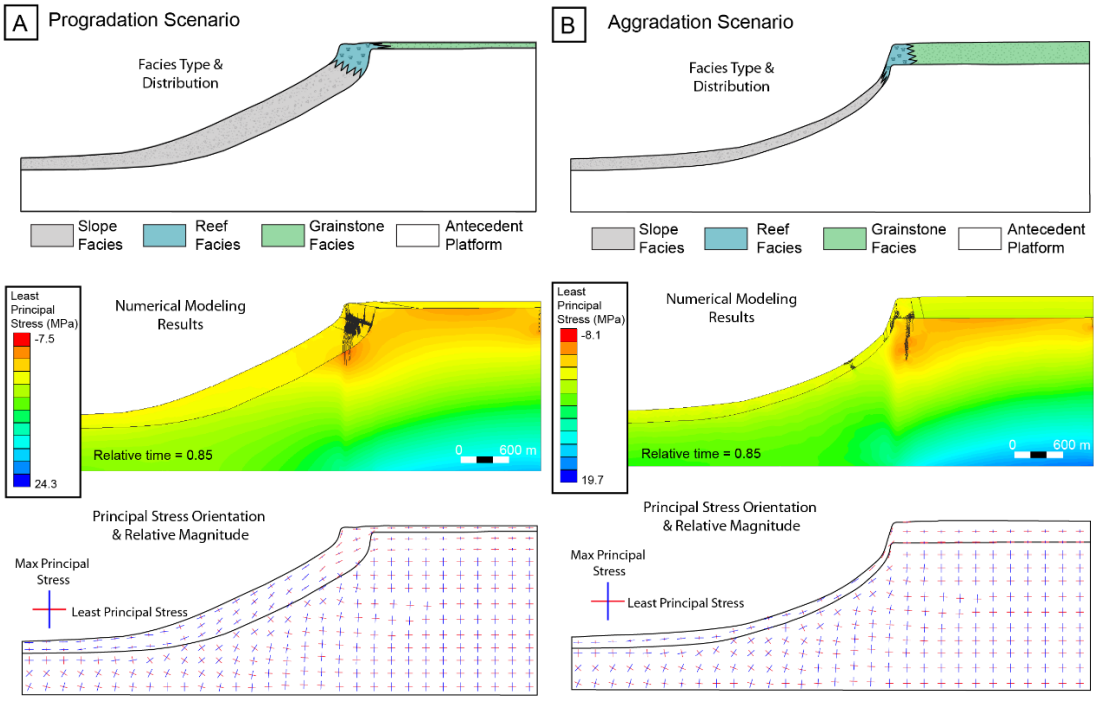

Figure 4.5. Modeling results for both the highly progradational and aggradational scenarios with the addition of facies tracts. (A) Results for progradational case with facies tracts, contoured by least principal stress. Fractures are centralized in front of the antecedent shelf margin. The presence of facies tracts work as mechanical stratigraphy boundaries where fracturing is retarded in facies with low Young's Modulus. Orientations and magnitude of the principal stresses highlight that, where the overburden column is thickest in the overlying sequence corresponds to a stress state that is dominated by tension. (B) Model results for aggradational case with facies tracts, contoured by least principal stress. Discrete fractures have developed on top of the antecedent shelf edge within the reef facies and propagate down into the underlying platform. Fractures that have developed mid-wag in the slope are a model artifact and caused by sharp changes in mesh sizes. The platform top and shelf edge of the second sequence is in a tensile stress state as depicted by the orientation and relative magnitude of the principal stresses.

The highly aggradational (P/A = 0.2) model differs from the highly progradational model in its fracturing locations (Fig. 4.5B). The discrete fractures have developed in reef strata, over the top of antecedent platform margin instead of in front of it. Fractures nucleate at the boundary between the underlying platform and the overlying sequence, exceeding

the tensile strength and propagating upward to the surface and down into the underlying platform. Fractures also develop in front of the antecedent shelf edge, and propagate in the overlying sequence up to the surface. Stress is dissipated upon initial fracturing, but once a fracture is formed, fractures continue to develop in that location. The fractures that develop mid-way down the slope in the overlying sequence are a model artifact and should not be considered realistic. These fractures are considered a model artifact because they do not occur from exceeding the tensile or shear strength of the material; they develop at the onset of the model and do not grow as the model continues. The development of these fractures is a byproduct of the differences in mesh size due to the density mesh region. The plot of the orientation and the relative magnitude of the principal stresses for the aggradational scenario demonstrates that the platform top and shelf edge are in a tensile stress state, while the slope and much of the underlying platform are dominated by compression (Fig. 4.5B). Here, the orientation of the principal stresses mirror not only the topographic expression of the carbonate platform but also the underlying antecedent topography. The orientation of the principal stresses dictates the direction in which fractures grow, with propagation parallel to the maximum principal stress (compression) and opening occurring in parallel to the least principal stress. This relationship is demonstrated by the orientation of the developed discrete fractures.

DISCUSSION

Our model results suggest that P/A ratio is a primary control on the location of syndepositional deformation, with facies tracts affecting the style of deformation and

propagation of fractures. Steep-walled/rimmed carbonate platforms that have a high P/A ratio will likely develop syndepositional fractures and faults in reef strata, localized in front of the antecedent platform margin (Fig. 4.3). A more strongly aggradational system with a low P/A ratio will experience more diffused deformation, present primarily in reef strata that directly overly the antecedent shelf margin (Fig. 4.4).

Effect of Variable P/A Ratio on the Development of Syndepositional Deformation

Prograding and aggrading platforms have the ability to develop high relief margins with hundreds of meters of relief between the platform top and the basin floor (Read, 1985). The P/A ratio for a given steep-walled carbonate platform not only affects the overall geometry, it affects the development of syndepositional deformation. The combination of an over steepened shelf margin (both in the underlying antecedent platform and the overlying sequence) and high rates of sedimentation results in a thickened overburden section during progradation, affecting the location and intensity of deformation (Mullins et al., 1986). Syndepositional deformation was found to be localized over the platform margin in a highly progradational systems (Hurley, 1986; Hunt and Fitchen, 1999; Koša and Hunt, 2005; Frost and Kerans, 2009, 2010).Collapse due to thickened overburden section associated with progradation has been attributed to catastrophic failure in steep-walled carbonate platforms (Crevello and Schlager, 1980; Mullins et al., 1986; George et al., 1995). In contrast, syndepositional deformation in a carbonate platform that is dominated by aggradation is typically more localized at the shelf edge, with a much smaller zone affected by deformation (Frost and Kerans, 2009, 2010).

The numerical modeling results of this study emphasize the importance of P/A ratio on the development of syndepositional deformation. The comparison between a system that is highly progradational (Fig. 4.6A) and a system that is dominated by aggradation (Fig. 4.6A) depicts a readily visible contrast in the development of deformation. A system that is dominated by aggradation experiences more diffused deformation than the system dominated by progradation. The thickest overburden column occurs on the platform top and serves to initiate failure, primarily in reefal strata, via loading. In contrast, a steep-walled carbonate platform that is dominated by progradation develops discrete fractures in front of the underlying antecedent shelf margin at the shelf edge. Work by Frost and Kerans (2009; 2010) in the Canning Basin of Western Australia has documented the difference in occurrence of syndepositional deformation between progradation and aggradational carbonate platform systems. Our numerical modeling results closely match their field observations, showing that the progradational system will experience a greater zone of deformation (Fig. 4.6A) than its aggradational counterpart (Fig. 4.6B).

The vertical to sub vertical reef wall of the underlying carbonate platform coupled with the thick overburden section of the overlying sequence facilitates failure by loading, over steepening, and gravitational instability in both scenarios. In both the progradational and aggradational scenarios, a tensile stress state has developed at the shelf edge, extending into the middle shelf, as indicated by the least principle stress magnitudes. This stress state is a byproduct of the lack of later confining stress in the seaward direction. The progradational scenario develops more widespread deformation because of the thickened overburden column, the low rock strength of the overlying sequence, and the proximity to

the open ocean where the lack of lateral confinement stress is likely greatest. The aggradational numerical modeling results experience more localized deformation centralized over the antecedent shelf margin. Here, deformation is controlled by the tensile stress state as well as the antecedent shelf margin and the location and thickness of the overburden column. Our models, which employ only gravitational loading, suggest that gravitational failure can occur in steep-walled carbonate platforms in the absence of differential compaction and external perturbations (i.e. movement along faults, tsunamis, earth quakes, sea-level fluctuations, etc.). Syndepositional deformation is an intrinsic process in carbonate platforms commonly altering platform architecture, geometry and facies distributions. The above results illustrate that P/A ratio is capable of directly controlling the intensity and location of syndepositional deformation.

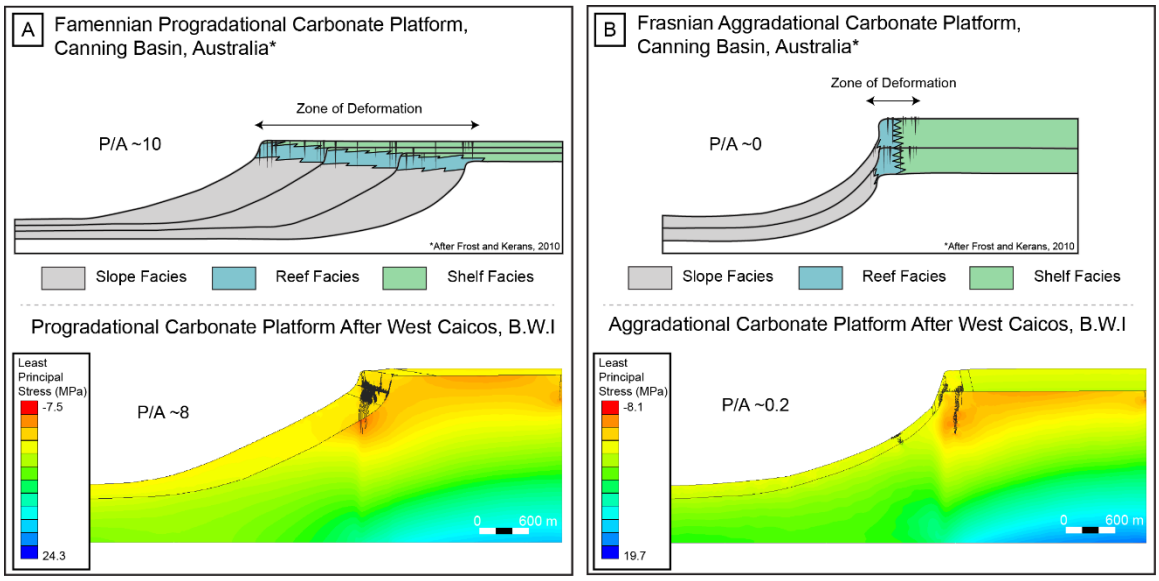

Figure 4.6. Documented outcrop expressions of syndepositional deformation in the Canning Basin, Western Australia compared with our numerical modeling results. A) The highly aggradational carbonate platform system experiences a wider swath of syndepositional deformation based on Frost and Kerans (2009; 2010) work. Our numerical model results closely match this documented example. B) Alternatively, the aggradational scenario experiences a much more localized zone of deformation, primarily centralized over the underlying antecedent shelf margin. Our numerical modeling results closely match this outcrop expression. *Modified after Frost and Kerans (2009)

Rock Property Heterogeneity Associated with Facies Tracts

The importance of steep-walled carbonate platform geometry, specifically the presence of a vertical reef wall, has been shown to be a first order control on the development of syndepositional deformation (Nolting et al., 2017a). The reef is susceptible to early lithification via early marine cementation (Land and Moore, 1977; Grammer et al., 1993a; Grammer et al., 1993b), which enables brittle failure. The early lithification of reef deposits in combination with the numerous depositional environments and resultant

variation in facies types causes significant rock property heterogeneity across the platform (Wilson, 1974; Read, 1985; Grotzinger, 1989; Wilson, 2012).

The juxtaposition of facies and their associated rock properties across the platform can create areas of high mechanical contrast (Nolting et al., 2017b). The contrast in mechanical behavior and rock properties at facies boundaries promotes zones that are susceptible to deformation. This is the case in the highly progradational scenario, where reef facies are directly juxtaposed over slope facies (Fig. 4.5A). Facies tracts also act as mechanical stratigraphy boundaries that have the ability to retard and/or enhance deformation (Di Naccio et al., 2005; Wennberg et al., 2006). This phenomenon is documented in our numerical model. Fractures within the models initiate most commonly in reef deposits in both the progradational and aggradational systems and propagate until they encounter a facies boundary. If the boundary they encounter is a contact with a facies that has a low Young's modulus, such as the platform interior, fractures are arrested. However, if a mechanical stratigraphy boundary is encountered with a moderate to high Young's modulus, the fractures propagate. While Young's modulus is important in governing the propagation of fractures that have already developed, tensile strength governs the actual development of fractures. Tensile strength between the individual facies tracts in the second, overlying sequence ranges from 0.9 to 2.5 MPa, with the reef exhibiting the greatest tensile strength. Our model results depict the reef facies having the greatest number of fractures due to the brittle nature of the rock properties, the presence of the vertical reef wall, and the proximity to the underlying antecedent shelf margin. The antecedent shelf margin exhibits the highest value for tensile strength at 6.6 MPa.

Fracturing occurs in the underlying platform margin as a byproduct of fractures that develop in the overlying sequence. A zone of inherited weakness develops as a byproduct of fracturing in the overlying sequence. Here, fractures continue to grow vertically along the established plane of weakness, fracturing the underlying antecedent shelf margin.

This work allows for a realistic representation of the mechanical stratigraphy boundaries (i.e. changes in facies type and their associated mechanical properties), which allows for observation of the impacts that mechanical stratigraphy boundaries have on the development and evolution of syndepositional deformation.

Comparison with Published Outcrop Examples

The manifestation of synsedimentary deformation within our models closely resembles published outcrop examples of syndepositional deformation in highly progradational systems. The Permian Capitan system of the Guadalupe Mountains is a type example for syndepositional deformation in outcrop. At least 13 syndepositional normal faults have been documented in Slaughter Canyon, Guadalupe Mountains, New Mexico (Hunt et al., 2003). During times of strong progradation, faulting is centralized along and in front of the antecedent shelf margin (Hunt and Fitchen, 1999; Hunt et al., 2003; Koša and Hunt, 2005; Mathisen, 2014). The style and location of deformation is not exclusive to Slaughter Canyon, as Rattlesnake Canyon and Walnut Canyon exhibit similar syndepositional features (Koša and Hunt, 2006). These documented examples of syndepositional deformation in highly progradational systems of the Guadalupe Mountains closely match our numerical modeling results.

This style of deformation is also documented in the Canning Basin of Western Australia (Playford, 1984; George et al., 1995; Frost and Kerans, 2009, 2010; Playton et al., 2010; Playton and Kerans, 2015a, b). Deformation is commonly centralized in front of the antecedent shelf edge in reef and forereef facies during progradational Famennian deposition (Frost and Kerans, 2010), which is consistent with our numerical modeling results (Fig. 4.6A) . Syndepositional fracturing is also present during the Frasnian when the system is dominated by aggradation. Here, fracturing is a byproduct of the early lithification of the reef and forereef strata and the proximity to the platform margin escarpment (Frost and Kerans, 2010) (Fig. 4.6B). During times of progradation, the vertical extent and apertures of fractures is greater than during times of aggradation (Frost and Kerans, 2009, 2010), which is again consistent with our numerical modeling results. Our model results also suggest that in absence of significant mechanical stratigraphy boundaries, increased overburden thickness leads to more vertically extensive fractures and increased zones affected by deformation.

CONCLUSIONS

Our modeling results highlight locations on steep-rimmed carbonate platforms that are likely to have syndepositional deformation features and can be used as a tool to predict fracturing occurrence when taking into account the P/A ratio of the carbonate system. Model results suggest that a highly progradational system will experience increased deformation within reef deposits at the shelf edge where the overburden column is thickest. A system that is dominated by aggradation will experience more diffused deformation at

the shelf edge and across the platform top, with the potential to fail down into an underlying antecedent shelf margin. Our model results mimic outcrop examples such as the Permian Capitan System, New Mexico and the Famennian of the Canning Basin, Western Australia. This suggests that P/A ratio is a first order control on syndepositional deformation, with facies types (mechanical stratigraphy boundaries) affecting the intensity and propagation of fractures. The ability of fractures to solely develop under the application of gravity and the stress associated with overburden highlight the syndepositional origin of deformation in steep-walled carbonate systems. We interpret these results as evidence that deformation from gravitational failure and over steepening is an intrinsic process in all steep-walled carbonate platform systems.

Chapter 5: Conclusions

Syndepositional deformation is a process intrinsic to steep-walled carbonate platforms worldwide. However, despite the recognition of syndepositional features steep-walled carbonate platform systems, the controls behind their development and distribution were poorly understood until now. A combination of outcrop based field work, laboratory analyses and numerical modeling assist in identifying primary and secondary controls on the development of syndepositional deformation in steep-walled carbonate shelf margin systems.

The lack of published data on mechanical rock properties of young, unburied carbonates necessitated their acquisition via field measurements and laboratory analyses from samples collected on West Caicos, B.W.I. This was an essential first step because it provided the foundation for the materials database used in the numerical models. West Caicos was chosen for sampling over an older system, such as the Guadalupian Capitan System, because the eustatic signal, stratigraphic relationships, ages, and diagenetic history are well constrained. The samples collected represent young, recently deposited carbonate rocks that have undergone little to no burial, closely mimicking the properties of carbonates at a time when syndepositional deformation would occur.

In addition to being used in the numerical models, the collected rock properties were used for identification of several key relationships between rock strength, age, and cementation due to near surface diagenesis. The presence and development of caliche crusts, which formed during subaerial exposure and subsequent cementation, generates increases in measured UCS values. Each stratigraphic package (related to each individual MIS event) on West Caicos is capped with a caliche surface. The top of each package shows increased rock strength, decreasing in the underlying sediments where cementation

from exposure is not as prevalent. Overall, there is an increase in UCS through time, where the MIS 9/11 deposits exhibit higher average UCS values than MIS 5e deposits. Additionally, reef facies, overall exhibit higher average UCS values than grain dominated facies.

Numerical models were used to identify controls on syndepositional deformation. Models results demonstrate that carbonate platform geometry and P/A ratio are first order controls on the development of syndepositional deformation. To a lesser extent, rock property heterogeneity and juxtaposition of facies with different rock properties are second order controls on deformation, affecting the distribution, intensity, and propagation of fracturing. Carbonate platform geometries that are characterized by high relief, vertical reef wall, regardless of P/A ratio and heterogeneities form rock property, are predisposed to failure under tensile stress state from a lack of lateral confinement. The manifestation of a near-vertical to vertical reef wall combined with the lack of confining stress towards the basin facilitates the development of these tensile regions, which create zones susceptible to failure. Model results also suggest that a system that is highly progradational will experience increased deformation within reef deposits at the shelf edge where the overburden column is thickest. A system that is dominated by aggradation will experience more diffused deformation at the shelf edge in reef deposits and across the platform top, with the potential to fracture down into an underlying antecedent shelf margin.

Much of the previous work done on characterization of syndepositional deformation speculates that differential compaction of basinal sediments is the primary mechanism responsible for syndepositional deformation. However, this work suggests otherwise. The ability of fractures to solely develop under the application of gravity in all model scenarios, with no compaction or external perturbations, highlights the likelihood of syndepositional origin of deformation in steep-walled carbonate systems. We interpret

these results as growing evidence that gravity driven deformation from loading and over steepening is an intrinsic process in all steep-walled carbonate platform systems.

This work has significant implications for future studies of shelf margin systems. This work highlights the effects from platform geometry, P/A ratio, and carbonate rock property heterogeneity, providing the foundation to identify areas that are susceptible to the development of syndepositional fractures and faults and their associated stress state. This work also details probabilistic locations on steep-walled carbonate platforms where deformation occurs and their associated process, that is possible pathways for hydrocarbon and early and late diagenetic fluid flow, where syndepositional fractures and faults have enhanced porosity and permeability.

References

Aby, S. B., 1994, Relation of bank-margin fractures to sea-level change, Exuma Islands, Bahamas: Geology, v. 22, no. 12, p. 1063-1066.

Adams, E. W., and Schlager, W., 2000, Basic types of submarine slope curvature: Journal of Sedimentary Research, v. 70, no. 4, p. 15.

Alonso-Zarza, A. M., and Wright, V., 2010, Calcretes: Developments in Sedimentology, v. 61, p. 225-267.

Anselmetti, F. S., and Eberli, G. P., 1993, Controls on sonic velocity in carbonates: Pure and Applied Geophysics, v. 141, no. 2-4, p. 287-323.

Anselmetti, F. S., and Eberli, G. P., 1999, The velocity-deviation log: a tool to predict pore type and permeability trends in carbonate drill holes from sonic and porosity or density logs: AAPG Bulletin, v. 83, no. 3, p. 450-466.

ASTM, 2014, Standard test method for determination of rock hardness by rebound hammer method- D5873-14, West Conshohocken, Pennsylvania, ASTM International, 1-6 p.:

Beach, D. K., 1982, Depositional and diagenetic history of Pliocene-Pleistocene carbonates of northwestern Great Bahama Bank; evolution of a carbonate platform [Ph.D Thesis]: University of Miami, 447 p.

Beach, D. K., 1995, Controls and effects of subaerial exposure on cementation and development of secondary porosity in the subsurface of Great Bahama Bank, v. Chapter 1, p. 1-33.

Berra, F., and Carminati, E., 2012, Differential compaction and early rock fracturing in high-relief carbonate platforms: numerical modelling of a Triassic case study (Esino Limestone, Central Southern Alps, Italy): Basin Research, v. 24, p. 598-614.

Bieniawski, Z., and Bernede, M., 1979a, Suggested methods for determining the uniaxial compressive strength and deformability of rock materials: Part 1. Suggested method for determining deformability of rock materials in uniaxial compression, International Journal of Rock Mechanics and Mining Sciences & Geomechanics Abstracts, Volume 16, Elsevier, p. 138-140.

Bieniawski, Z., and Bernede, M., 1979b, Suggested methods for determining the uniaxial compressive strength and deformability of rock materials: Part 2. Suggested method for determining deformability of rock materials in uniaxial compression, International Journal of Rock Mechanics and Mining Sciences & Geomechanics Abstracts, Volume 16, Elsevier, p. 138-140.

Budd, D. A., 2002, The relative roles of compaction and early cementation in the destruction of permeability in carbonate grainstones: a case study from the Paleogene of west-central Florida, USA: Journal of Sedimentary Research, v. 72, no. 1, p. 116-128.

Budd, D. A., Frost, E. L., Huntington, K. W., and Allwardt, P. F., 2013, Syndepositional deformation features in high-relief carbonate platforms: long-lived conduits for diagenetic fluids: Journal of Sedimentary Research, v. 83, no. 1, p. 12-36.

Carpenter, D. G., Guidry, S. A., Degraff, J. D., and Collins, J., Evolution of Tengiz rim/flank reservoir quality: new insights from systematic, integrated core fracture and diagenesis investigations (Abstract): American Association of Petroleum Geologists, *in* Proceedings Giant hydrocarbon reservoirs of the world: From rocks to reservoir characterization and modeling: AAPG Annual Meeting Abstract Volume2006, Volume 15, p. 18.

Chang, C., Zoback, M. D., and Khasksar, A., 2006, Empirical relations between rock strength and physical properties in sedimentary rocks: Journal of Petroleum Science and Engineering, v. 51, p. 223-237.

Collins, J. F., Kenter, J. A., Harris, P. M., Kuanysheva, G., and Steffen, D. F. K., 2006, Facies and reservoir-quality variations in the late Visean to Bashkirian outer platform, rim, and flank of the Tengiz buildup, Precaspian Basin, Kazakhstan: P. M. Harris and L. J.Weber, eds., Giant hydrocarbon reservoirs of the world: From rocks to reservoir characterization and modeling: AAPG Memoir 88/SEPM Special Publication, p. 55-95.

Coniglio, M., and Harrison, R. S., 1983, Facies and diagenesis of late Pleistocene carbonates from Big Pine Key, Florida: Bulletin of Canadian Petroleum Geology, v. 31, no. 3, p. 135-147.

Crevello, P. D., and Schlager, W., 1980, Carbonate debris sheets and turbidites, Exuma Sound, Bahamas: Journal of Sedimentary Research, v. 50, no. 4, p. 1121-1148.

Di Naccio, D., Boncio, P., Cirilli, S., Casaglia, F., Morettini, E., Lavecchia, G., and Brozzetti, F., 2005, Role of mechanical stratigraphy on fracture development in carbonate reservoirs: Insights from outcropping shallow water carbonates in the Umbria–Marche Apennines, Italy: Journal of Volcanology and Geothermal Research, v. 148, no. 1, p. 98-115.

Dolan, J. F., Mullins, H. T., and Wald, D. J., 1998, Active tectonics of the north-central Caribbean: Oblique collision, strain partitioning, and opposing subducted slabs: Geological Society of America Special Papers, v. 326, p. 1-61.

Dravis, J. J., 1996, Rapidity of freshwater calcite cementation—implications for carbonate diagenesis and sequence stratigraphy: Sedimentary Geology, v. 107, no. 1-2, p. 1-10.

Eberli, G. P., Baechle, G. T., Anselmetti, F. S., and Incze, M. L., 2003, Factors controlling elastic properties in carbonate sediments and rocks: The Leading Edge, v. 22, no. 7, p. 654-660.

Enos, P., and Moore, C. H., 1983, Fore-reef Slope Environment: Chapter 10: The American Association of Petroleum Geologist, p. 507-521.

Esteban, M., and Klappa, C. F., 1983, Subaerial exposure environment: carbonate depositional environments:: AAPG Memoir, v. 33, p. 1-54.

Frost, E. L., Budd, D. A., and Kerans, C., 2012, Syndepositional deformation in a high-relief carbonate platform and its effect on early fluid flow as revealed by dolomite patterns: Journal of Sedimentary Research, v. 82, no. 12, p. 913-932.

Frost, E. L., and Kerans, C., 2009, Platform-margin trajectory as a control on syndepositional fracture patterns, Canning Basin, Western Australia: Journal of Sedimentary Research, v. 79, no. 2, p. 44-55.

Frost, E. L., and Kerans, C., 2010, Controls on syndepositional fracture patterns, Devonian reef complexes, Canning Basin, Western Australia: Journal of Structural Geology, v. 32, no. 9, p. 1231-1249.

Gavish, E., and Friedman, G. M., 1969, Progressive diagenesis in Quaternary to Late Tertiary carbonate sediments: sequence and time scale: Journal of Sedimentary Research, v. 39, no. 3, p. 980-1006.

George, A. D., Playford, P. E., and Powell, C. M., 1995, Platform-margin collapse during Famennian reef evolution, Canning Basin, Western Australia: Geology, v. 23, no. 8, p. 691-694.

Ginsburg, R. N., 1957, Early diagenesis and lithification of shallow-water carbonate sediments in south Florida: SEPM Special Publication, p. 80-98.

Ginsburg, R. N., and James, N. P., 1974, Holocene carbonate sediments of continental shelves, Springer.

Goldhammer, R., 1997, Compaction and decompaction algorithms for sedimentary carbonates: Journal of Sedimentary Research, v. 67, no. 1, p. 26-35.

Grammer, G. M., Crescini, C. M., McNeill, D. F., and Taylor, L. H., 1999, Quantifying rates of syndepositional marine cementation in deeper platform environments—new insight into a fundamental process: Journal of Sedimentary Research, v. 69, no. 1, p. 202-207.

Grammer, G. M., Ginsburg, R. N., and Harris, P. M., 1993a, Timing of Deposition, Diagenesis, and Failure of Steep Carbonate Slopes in Response to a High-Amplitude/High-Frequency Fluctuation in Sea-Level, Tongue of the Ocean, Bahamas: Chapter 4, p. 107-131.

Grammer, G. M., Ginsburg, R. N., Swart, P. K., McNeill, D. F., Jull, A. T., and Prezbindowski, D. R., 1993b, Rapid growth rates of syndepositional marine aragonite cements in steep marginal slope deposits, Bahamas and Belize: Journal of Sedimentary Research, v. 63, no. 5, p. 983-989.

Grotzinger, J. P., 1989, Facies and evolution of Precambrian carbonate depositional systems: emergence of the modern platform archetype: Contorls on Carbonate Platform and Basin Development, SEPM Special Publication, no. 44, p. 79-106.

Guidry, S. A., Grasmueck, M., Carpenter, D. G., Gombos Jr, A. M., Bachtel, S. L., and Viggiano, D. A., 2007, Karst and early fracture networks in carbonates, Turks and Caicos Islands, British West Indies: Journal of Sedimentary Research, v. 77, no. 6, p. 508-524.

Harman, C. A., 2011, Quantified facies distributions and sequence geometry of the Yates Formation, Slaughter Canyon, New Mexico [Unpublished masters thesis]: University of Texas at Austin, 137 p.

Harrison, R., 1975, Porosity in Pleistocene grainstones from Barbados: some preliminary observations: Bulletin of Canadian Petroleum Geology, v. 23, no. 3, p. 383-392.

Harrison, R., 1977, Caliche profiles: indicators of near-surface subaerial diagenesis, Barbados, West Indies: Bulletin of Canadian Petroleum Geology, v. 25, no. 1, p. 123-173.

Harrison, R. S., and Steinen, R. P., 1978, Subaerial crusts, caliche profiles, and breccia horizons: comparison of some Holocene and Mississippian exposure surfaces, Barbados and Kentucky: Geological Society of America Bulletin, v. 89, no. 3, p. 385-396.

Hatzor, Y., and Palchik, V., 1997, The influence of grain size and porosity on crack initiation stress and critical flaw length in dolomites: International Journal of Rock Mechanics and Mining Sciences, v. 34, no. 5, p. 805-816.

Hearty, P. J., 2002, Revision of the late Pleistocene stratigraphy of Bermuda: Sedimentary Geology, v. 153, no. 1, p. 1-21.

Hugman, R. I., and Friedman, M., 1979, Effects of texture and composition on mechanical behavior of experimentally deformed carbonate rocks: AAPG Bulletin, v. 63, no. 9, p. 1478-1489.

Humphrey, J. D., and Kimbell, T. N., 1990, Sedimentology and Sequence Stratigraphy of Upper Pleistocene Carbonates of Southeastern Barbados, West Indies (1): AAPG Bulletin, v. 74, no. 11, p. 1671-1684.

Hunt, D., Allsop, T., and Swarbrick, R. E., 1996, Compaction as a primary control on the architecture and development of depositional sequences: conceptual framework, applications and implications: Geological Society, London, Special Publications, v. 104, no. 1, p. 321-345.

Hunt, D., Fitchen, W., Swarbrick, R., and Allsop, T., 1995, Differential compaction as a primary control of sequence architecture and development in the Permian Basin: geological significance and potential as a hydrocarbon exploration model: West Texas Geological Society, p. 83-104.

Hunt, D., and Fitchen, W. M., 1999, Compaction and the dynamics of carbonate-platform development: insights from the Permian Delaware and Midland basins, Southeast New Mexico and West Texas, USA: Society for Sedimentary Geology, Advances in Carbonate Sequence Stratigraphy Application to Reservoirs Outcrops and Models SEPM Special Publication, no. 63, p. 75-106.

Hunt, D., Resor, P., Simo, J., Blendiger, W., and Labrana, G., 2012, Syndepositional faulting, sedimentation, and paleokarst development within the Permian Capitan platform, Guadalupe Mountains, NM: Digital Geospatial Context for, p. 89-99.

Hunt, D. W., Fitchen, W. M., and Kosa, E., 2002, Syndepositional deformation of the Permian Capitan reef carbonate platform, Guadalupe Mountains, New Mexico, USA: Sedimentary geology, v. 154, no. 3, p. 89-126.

Hunt, D. W., Fitchen, W. M., and Kosa, E., 2003, Syndepositional deformation of the Permian Capitan reef carbonate platform, Guadalupe Mountains, New Mexico, USA: Sedimentary Geology, v. 154, no. 3, p. 89-126.

Hurley, N., 1986, Geology of the Oscar Range Devonian reef complex: Canning Basin, Western Australia [Ph. D. thesis]: Ann Arbor, University of Michigan.

Iannello, C., Hughes, T., Derewetzky, A. N., Hillock, P., Tremblay, M., McKerron, A., Parker, R. S., Gibbons, S., and Bachtel, S., 2006, Pleistocene and Holocene stratigraphic studies, Caicos Platform, British West Indies: AAPG Search and Discovery.

Incze, M. L., 1998, Petrophysical properties of shallow-water carbonates in modern depositional and shallow subsurface environments [Ph.D Thesis]: Univeristy of Miami, 405 p.

Jaeger, J. C., Cook, N. G. W., and Zimmerman, R. W., 2007, Fundamentals of rock mechanics Malden Massachusetts, Wiley-Blackwell, 488 p.:

James, N., and Ginsburg, R., 1979b, The seaward margin of Belize barrier and atoll reefs International Association of Sedimentologists, Special Publication 3, p. 191.

James, N. P., 1972, Holocene and Pleistocene calcareous crust (caliche) profiles: criteria for subaerial exposure: Journal of Sedimentary Research, v. 42, no. 4, p. 817-836.

James, N. P., and Choquette, P. W., 1984, Diagenesis 9. Limestones-the meteoric diagenetic environment: Geoscience Canada, v. 11, no. 4, p. 161-194.

James, N. P., Ginsburg, R. N., Marszalek, D. S., and Choquette, P. W., 1976, Facies and fabric specificity of early subsea cements in shallow Belize (British Honduras) reefs: Journal of Sedimentary Research, v. 46, no. 3, p. 523-544.

Jones, B., 1988, The influence of plants and micro-organisms on diagenesis in caliche: example from the Pleistocene Ironshore Formation on Cayman Brac, British West Indies: Bulletin of Canadian Petroleum Geology, v. 36, no. 2, p. 191-201.

Jones, G. D., Braun, E., Brown, R., van Gaalen, G., Gaswirth, S., Holzwarth, W., Houser, P., Lee, A., Longo, J., and Markello, J., 2008, An Investigation of Early Diagenesis in from Isolated Carbonate Platform: Caicos Platform, British West Indies: Holocene and Pleistocene Carbonates of the Caicos Platform, British West Indies, SEPM Core Wowrkshop 22, p. 177-194.

Jones, G. D., and Xiao, Y., 2006, Geothermal convection in the Tengiz carbonate platform, Kazakhstan: Reactive transport models of diagenesis and reservoir quality: AAPG bulletin, v. 90, no. 8, p. 1251-1272.

Kerans, C., 1985, Petrology of Devonian and Carboniferous Carbonates of the Canning and Bonaparte Basins:: Westen Australia Mining and Petroleum Research Institute, Report 12, p. 223.

Kerans, C., and Tinker, S. W., 1999, Extrinsic stratigraphic controls on development of the Capitan reef complex: Society of Sedimentary Geology, SEPM Special Publication, no. 65, p. 15-36.

Kerans, C., Zahm, C., Bachtel, S., Lambert, J., Danger, N., and Nolting, A., 2016, Stratigraphic evolution of an icehouse strandplain system — West Caicos, B.W.I., AAPG ACE: Calgary, AAPG Search and Discovery.

Kerans, C., Zahm, C., Garcia-Fresca, B., and Harris, P. M., 2017, Guadalupe Mountains, West Texas and New Mexico: Key excursions: AAPG Bulletin, v. 101, no. 4, p. 465-474.

Kindler, P., and Hearty, P. J., 1996, Carbonate petrography as an indicator of climate and sea-level changes: new data from Bahamian Quaternary units: Sedimentology, v. 43, no. 2, p. 381-399.

King, P. B., 1948, Geology of the southern Guadalupe Mountains, Texas, US Government Professional Paper P-2015, 183 p.:

Koša, E., Hunt, D., Fitchen, W. M., Bockel-Rebelle, M.-O., and Roberts, G., 2003, The heterogeneity of paleocavern systems developed along syndepositional fault zones: the Upper Permian Capitan Platform, Guadalupe Mountains, USA, in Ahr, W.M., Harris, P.M., Morgan, W.A., and Somerville, I.D., eds., Permo-Carboniferous Carbonate Platforms and Reefs: SEPM, p. 291-322.

Koša, E., and Hunt, D. W., 2005, Growth of syndepositional faults in carbonate strata: Upper Permian Capitan platform, New Mexico, USA: Journal of Structural Geology, v. 27, no. 6, p. 1069-1094.

Koša, E., and Hunt, D. W., 2006, The effect of syndepositional deformation within the Upper Permian Capitan Platform on the speleogenesis and geomorphology of the Guadalupe Mountains, New Mexico, USA: Geomorphology, v. 78, no. 3, p. 279-308.

Kowalski, W. C., 1966, The interdependence between the strength and voids ratio of limestones and marls in connection with their water saturating and anisotropy, 1st ISRM Congress: Lisbon, Portugal, International Society for Rock Mechanics, p. 1-2.

Land, L. S., 1970, Phreatic versus vadose meteoric diagenesis of limestones: evidence from a fossil water table: Sedimentology, v. 14, no. 3-4, p. 175-185.

Land, L. S., and Moore, C. H., 1977, Deep forereef and upper island slope, North Jamaica: modern and ancient reefs: AAPG, v. Special Volumes, SG 4: Reefs and related carbonates-ecology and sedimentology, p. 53-65.

Land, L. S., T MACKENZIE, F., and Gould, S. J., 1967, Pleistocene history of Bermuda: Geological Society of America Bulletin, v. 78, no. 8, p. 993-1006.

Li, R., and Jones, B., 2014, Calcareous crusts on exposed Pleistocene limestones: a case study from Grand Cayman, British West Indies: Sedimentary Geology, v. 299, p. 88-105.

Lloyd, R., Perkins, R., and Kerr, S., 1987, Beach and shoreface ooid deposition on shallow interior banks, Turks and Caicos Islands, British West Indies: Journal of Sedimentary Petrology, v. 57, no. 6, p. 976-982.

Longley, A. J., 1999, Differential compaction and its effects on the outer shelf of the Permian Capitan Reef Complex, Guadalupe Mountains, New Mexico: Geologic Framework of the Capitan Reef, SEPM Special Publication, no. 65, p. 85-105.

Mathisen, M. G., 2014, Spatial and temporal evolution of the cave graben fault system, Guadalupe Mountains , New Mexico [Unpublished Masters Thesis]: University of Texas at Austin, 121 p.

Matthews, R., 1968, Carbonate diagenesis: equilibration of sedimentary mineralogy to the subaerial environment; coral cap of Barbados, West Indies: Journal of Sedimentary Research, v. 38, no. 4, p. 1110-1119.

Matthews, R., 1974, A process approach to diagenesis of reefs and reef associated limestones.

Moh'd, B. K., 2009, Compressive strength of vuggy oolitic limestones as a function of their porosity and sound propagation: Jordan J Earth Environ Sci, v. 2, no. 1, p. 18-25.

Mullins, H. T., Breen, N., Dolan, J., Wellner, R. W., Petruccione, J. L., Gaylord, M., Andersen, B., Melillo, A. J., Jurgens, A. D., and Orange, D., 1992, Carbonate platforms along the southeast Bahamas-Hispaniola collision zone: Marine Geology, v. 105, no. 1-4, p. 169-209.

Mullins, H. T., Gardulski, A. F., and Mine, A. C., 1986, Catastrophic collapse of the west Florida carbonate platform margin: Geology, v. 14, no. 2, p. 167-170.

Narr, W., Fischer, D., Harris, P. M. M., Heidrick, T., Robertson, B., and Payrazyan, K., 2008, Understanding and predicting fractures at Tengiz—a giant, naturally fractured reservoir in the Caspian Basin of Kazakhstan: AAPG Search and Discovery article 20057.

Nolting, A., Zahm, C., and Kerans, C., 2017a, Synsedimentary deformation in steep-walled carbonate margins: insights from numerical modeling of carbonate platforms in the recent and ancient rock record.: Marine Geology, *In Review*.

Nolting, A., Zahm, C., Kerans, C., and Bachtel, S., 2017b, Early-formed rock strength heterogeneity in Pleistocene carbontes: significance of early near-surface diagenesis, Journal of Sedimentary Research, p. *in review*.

Palchik, V., 1999, Influence of porosity and elastic modulus on uniaxial compressive strength in soft brittle porous sandstones: Rock Mechanics and Rock Engineering, v. 32, no. 4, p. 303-309.

Palchik, V., and Hatzor, Y., 2004, The influence of porosity on tensile and compressive strength of porous chalks: Rock Mechanics and Rock Engineering, v. 37, no. 4, p. 331-341.

Pierre, A., Durlet, C., Razin, P., and Chellaï, E. H., 2010, Spatial and temporal distribution of ooids along a Jurassic carbonate ramp: Amellago outcrop transect, High-Atlas, Morocco: Geological Society, London, Special Publications, v. 329, no. 1, p. 65-88.

Pierson, B. J., and Shinn, E. A., 1985, Cement distribution and carbonate mineral stabilization in Pleistocene limestones of Hogsty Reef, Bahamas: Society of Sedimentary Geology, v. SP36, p. 153-168.

Playford, P. E., 1984, Platform-margin and marginal-slope relationships in Devonian reef complexes of the Canning Basin, Geological Society of Australia Incorporated and Petroleum Exploration Society of Western Australia, v. 189-234, 214 p.:

Playford, P. E., Kerans, C., and Hurley, N. F., 1984, Platform-margin and marginal slope relationships and sedimentation in Devonian reef complexes of Canning basin, Western Australia: AAPG Bulletin, v. 68, no. 4, p. 516-517.

Playton, T., Janson, X., and Kerans, C., 2010, Carbonate slopes: Facies models, v. 4, p. 449-476.

Playton, T. E., and Kerans, C., 2015a, Late Devonian Carbonate Margins and Foreslopes of the Lennard Shelf, Canning Basin, Western Australia, Part A: Development During Backstepping and the Aggradation-To-Progradation Transition: Journal of Sedimentary Research, v. 85, no. 11, p. 1334-1361.

Playton, T. E., and Kerans, C., 2015b, Late Devonian Carbonate Margins and Foreslopes of the Lennard Shelf, Canning Basin, Western Australia, Part B: Development During Progradation and Across the Frasnian–Famennian Biotic Crisis: Journal of Sedimentary Research, v. 85, no. 11, p. 1362-1392.

Pomar, L., 2001, Types of carbonate platforms: a genetic approach: Basin Research, v. 13, no. 3, p. 313-334.

Porta, G. D., Kenter, J. A. M., and Bahamonde, J. R., 2004, Depositional facies and stratal geometry of an Upper carboniferous prograding and aggrading high-relief carbonate platform (Cantabrian Mountains, N. Spain): Sedimentology, v. 51, p. 29.

Read, J. F., 1985, Carbonate platform facies models: AAPG bulletin, v. 69, no. 1, p. 1-21.

Reeckman, S. A., and Gill, E., 1981, Rates of vadose diagenesis in Quaternary dune and shallow marine calcarenites, Warrnambool, Victoria, Australia: Sedimentary Geology, v. 30, no. 3, p. 157-172.

Reeves, C. C., 1976, Caliche: origin, classification, morphology and uses, Tex, Estacado 1-233 p.:

Resor, P. G., and Flodin, E. A., 2010, Forward modeling synsedimentary deformation associated with a prograding steep-sloped carbonate margin: Journal of Structural Geology, v. 32, no. 9, p. 1187-1200.

Rockfield, 2010, ELFEN Forward modelring user manual, Swansea, United Kingdom, Rockfield, 824 p.:

Ronchi, P., Ortenzi, A., Borromeo, O., Claps, M., and Zempolich, W. G., 2010, Depositional setting and diagenetic processes and their impact on the reservoir quality in the late Visean–Bashkirian Kashagan carbonate platform (Pre-Caspian Basin, Kazakhstan): AAPG bulletin, v. 94, no. 9, p. 1313-1348.

Rossinsky, V. J., and Wanless, H. R., 1992, Topographic and vegetative controls on calcrete formation, Turks and Caicos Islands, British West Indies: Journal of Sedimentary Research, v. 62, no. 1, p. 84-98.

Rusciadelli, G., and Di Simone, S., 2007, Differential compaction as a control on depositional architectures across the Maiella carbonate platform margin (central Apennines, Italy): Sedimentary Geology, v. 196, no. 1, p. 133-155.

Rusciadelli, G., Sciarra, N., and Mangifesta, M., 2003, 2D modelling of large-scale platform margin collapses along an ancient carbonate platform edge (Maiella Mt., Central Apennines, Italy): geological model and conceptual framework: Palaeogeography, Palaeoclimatology, Palaeoecology, v. 200, no. 1, p. 245-262.

Rush, J., and Kerans, C., 2010, Stratigraphic response across a structurally dynamic shelf: the latest Guadalupian composite sequence at Walnut Canyon, New Mexico, USA: Journal of Sedimentary Research, v. 80, no. 9, p. 808-828.

Sachpazis, C. I., 1990, Correlating Schmidt hardness with compressive strength and Youngs modulus of carbonate rocks: Bulletin of the International Association of Engineering Geology, v. 42, p. 75-84.

Saller, A. H., 1996, Differential compaction and basinward tilting of the prograding Capitan reef complex, Permian, west Texas and southeast New Mexico, USA: Sedimentary Geology, v. 101, no. 1-2, p. 21-30.

Schmoker, J. W., and Halley, R. B., 1982, Carbonate porosity versus depth: a predictable relation for south Florida: AAPG bulletin, v. 66, no. 12, p. 2561-2570.

Sealey, N. E., 2006, Bahamian landscapes, Oxford, Macmillan-Caribbean, 1-184 p.:

Shinn, E. A., 1969, Submarine lithification of Holocene carbonate sediments in the Persian Gulf: Sedimentology, v. 12, no. 1-2, p. 109-144.

Simo, J. T., Guidry, S. A., Iannello, C., Rankey, G., Harris, C. E., Guarin, H., Ruf, A., Hughes, T., Derewetzky, A. N., and Parker, R. S., 2008, Holocene-Pleistocene geology of a transect of from isolated carbonate platform, NW Caicos Platform, British West Indies: *in* Morgan, W.A, and Harris P.M eds., Workshop on developing models and analogs for isloated carbonate platforms—Holocene and Pleistocene carbonates of Caicos platform, British West Indies: SEPM Core Workshop, v. 22, p. 111-118.

Simon, R. E., 2014, Syndepositional fault control on dolomitization of a steep-walled carbonate platform margin, Yates Formation, Rattlesnake Canyon, New Mexico [Masters Thesis]: University of Texas at Austin, 137 p.

Smith, B. P., and Kerans, C., 2017, Interpreting Stratal Architecture in Shelf-top Carbonate Systems: An Example from the Seven Rivers Formation, McKittrick Canyon, New Mexico: Journal of Sedimentary Research, p. *In-review*.

Stanton Jr, R. J., and Pray, L. C., 2004, Skeletal-carbonate Neptunian dikes of the Capitan Reef: Permian, Guadalupe Mountains, Texas, USA: Journal of Sedimentary Research, v. 74, no. 6, p. 805-816.

Stanton, R. J., and Pray, L. C., 2004, Skeletal-Carbonate Neptunian Dikes of the Capitan Reef: Permian, Guadalupe Mountains, Texas, USA: Journal of Sedimentary Research, v. 74, no. 6, p. 805-816.

Steinen, R. P., 1974, Phreatic and vadose diagenetic modification of Pleistocene limestone: petrographic observations from subsurface of Barbados, West Indies: AAPG bulletin, v. 58, no. 6, p. 1008-1024.

Steinen, R. P., and Matthews, R. K., 1973, Phreatic vs. vadose diagenesis: stratigraphy and mineralogy of a cored borehole on Barbados, WI: Journal of Sedimentary Research, v. 43, no. 4, p. 1012-1020.

Tinker, S. W., 1998, Shelf-to-basin facies distributions and sequence stratigraphy of a steep-rimmed carbonate margin: Capitan depositional system, McKittrick Canyon, New Mexico and Texas: Journal of Sedimentary Research, v. 68, no. 6, p. 1146-1174.

Tuğrul, A., 2004, The effect of weathering on pore geometry and compressive strength of selected rock types from Turkey: Engineering Geology, v. 75, no. 3, p. 215-227.

Tuğrul, A., and Zarif, I., 2000, Engineering aspects of limestone weathering in Istanbul, Turkey: Bulletin of Engineering Geology and the Environment, v. 58, no. 3, p. 191-206.

Waelbroeck, C., Labeyrie, L., Michel, E., Duplessy, J. C., McManus, J. F., Lambeck, K., Balbon, E., and Labracherie, M., 2002, Sea-level and deep water temperature changes derived from benthic foraminifera isotopic records: Quaternary Science Reviews, v. 21, p. 295-305.

Walls, R. A., Harris, W. B., and Nunan, W., 1975, Calcareous crust (caliche) profiles and early subaerial exposure of Carboniferous carbonates, northeastern Kentucky: Sedimentology, v. 22, no. 3, p. 417-440.

Waltz, M., 1988, The evolution of shallowing-upwards reef to oolite sequences at the leeward margin of Caicos Platform: BWI [unpublished MS, thesis]: University of Miami.

Wanless, H. R., and Dravis, J. J., 1989, Carbonate environments and sequences of the Caicos Platform, Florida, 28th International Geological Congress guidebook T374, American Geophyscial Union, 75 p.:

Wennberg, O., Svånå, T., Azizzadeh, M., Aqrawi, A., Brockbank, P., Lyslo, K., and Ogilvie, S., 2006, Fracture intensity vs. mechanical stratigraphy in platform top carbonates: the Aquitanian of the Asmari Formation, Khaviz Anticline, Zagros, SW Iran: Petroleum Geoscience, v. 12, no. 3, p. 235-246.

Whitaker, F., Smart, P., Hague, Y., Waltham, D., and Bosence, D., 1997, Coupled two-dimensional diagenetic and sedimentological modeling of carbonate platform evolution: Geology, v. 25, no. 2, p. 175-178.

Wilson, J. L., 1974, Characteristics of carbonate-platform margins: AAPG Bulletin, v. 58, no. 5, p. 810-824.

Wilson, J. L., 2012, Carbonate facies in geologic history, Springer Science & Business Media.

Wright, V. P., 1994, Paleosols in shallow marine carbonate sequences: Earth-Science Reviews, v. 35, no. 4, p. 367-395.

Yurewicz, D. A., 1976, Sedimentology, paleoecology, and diagenesis of the massive facies of the lower and middle Capitan limestone(Permian), Guadalupe Mountains, New Mexico and West Texas [Ph.D Thesis]: University of Wisconsin, 296 p.

Zahm, C. K., 2015, Structural components of West Caicos, *in* Personal Communication with Nolting, A., ed.: Austin.

Zhou, J., and Chafetz, H. S., 2009, Biogenic caliches in Texas: the role of organisms and effect of climate: Sedimentary Geology, v. 222, no. 3, p. 207-225.